PREPARATION AND CHARACTERIZATION OF MODIFIED LEAD ZIRCONATE TITANATE CERAMICS

A
Thesis submitted for the
Award of degree of

Doctor of Philosophy

By

PRATIBHA
(*Reg. No. 90712502*)

to

School of Physics and Materials Science
Thapar University
Patiala-147004

APRIL - 2011

Dedicated

To

My Family

CERTIFICATE

This is to certify that the thesis entitled **"Preparation and Characterization of Modified Lead Zirconate Titanate Ceramics"** which is being submitted by **Ms. Pratibha** in fulfillment of the requirement for the award of degree of Doctor of Philosophy to Thapar University, Patiala, is a record of candidate's own work carried out by her under our supervision and guidance. The matter presented in this thesis has not been submitted in part or full for the award of any degree in any other University or Institute.

Supervisors

.....

Dr. Chandra Prakash
Directorate of ER&IPR, DRDO
DRDO Bhawan, New Delhi-110105
(Adjunct Professor, Thapar University, Patiala-147004)

.....

Dr. J.K. Juneja
Department of Physics
Hindu PG College, Sonepat-131001

.....

Prof. K.K. Raina
School of Physics and Materials Science
Thapar University, Patiala-147004

ACKNOWLEDGEMENT

I wish to express my deepest and sincere gratitude to my supervisor ***Dr. Chandra Prakash****, DRDO, New Delhi, for his detailed and exquisitely written scientific papers on PZT ceramics. Without the guidance of his previous work, much of what accomplished in this thesis would not have been possible. He is a great mentor as his level of commitment in guiding his students towards research is exceptional. I express my sincere gratitude to my supervisor* ***Dr. J. K. Juneja****, for his continuous support and advice in my research efforts. It is really difficult to express in words my indebtedness to him for everything he has done for me. I express my heartfelt gratitude to my supervisor* ***Dr. K. K. Raina****, besides expanding my breadth of ferroelectric knowledge, has made working at Thapar University, a true pleasure.*

I am obliged to ***Dr. Jyoti Juneja****, Principal, G.V.M. Girls College, Sonepat, for providing excellent research facilities and working atmosphere in Electroceramic Research Laboratory (ERL), G.V.M. Girls College, Sonepat. I thank* ***Dr. Sangeeta Singh****, G.V.M. Girls College, Sonepat for her valued inputs and continual patience in resolving my problems whatsoever.*

I must acknowledge ***Dr. Abhijit Mukherjee****, Director Thapar University, Patiala, for granting me the permission to register for Ph.D. programme in his meritorious institute. I would like to recognize the contribution of* ***Dr. Kulbir Singh****, Head SPMS, Thapar University, Patiala, for his persistent help in overcoming the bureaucracy issues that would have impeded completion of my Ph. D. work. I also appreciate the time and efforts of* ***Dr. O. P. Pandey,*** *Faculty SPMS, devoted in analyzing my research work.*

I acknowledge the co-operation of ***Dr. R. P. Pant****, National Physical Laboratory, New Delhi for permitting in recording XRD patterns for this study. Thanks to* ***Prof. Mushahid Hussain*** *and research scholar* ***Avshish Kumar****, Jamia Millia Islamia, New Delhi, for providing facilities for SEM measurements. I thank* ***Mr. Purshotam****, Thapar University Patiala, for carrying out SEM measurements. It is my pleasure to thank* ***Dr. Ratnamala Chatterji****, IIT Delhi, for her kind permission to undertake piezoelectric measurements related to this work. I acknowledge the contribution of research scholar* ***Abhishek Pathak****, IIT Delhi and* ***Dr. Vinod Chahar*** *for helping me in every capacity they could.*

I would also like to express my appreciation to the my ERL group including ***Parveen Kumar, Renu Dahiya, Rekha Gandhi*** *and* ***Deepti*** *for extending daily help in performing experiments and for their sincere friendship. I thank* ***Mr. Dushyant Kumar****, Lab Assistnat (ERL) for providing his help round the clock in lab. I thank my friends* ***Ravi Shukla, Neeraj Sharma*** *and all lab members in Material Research Lab, Thapar University, Patiala for their co-operation in every manner.*

*Finally, I would like to thank my Mummy, Papa and brother for their continual love and unconditional support. I would like to extend special thanks to my in-laws family for their persistent moral support, encouragement and their forbearance of my hectic schedule in completing my research work. I thank my husband, **Gaurav**, for his unstinted support and love without which it would have not been possible for me to complete my work in time.*

*The financial support in the form of research fellowship through the **Defence Research and Development Organisation** (D.R.D.O.), Ministry of Defence is greatly acknowledged.*

Pratibha
(PRATIBHA)

ABSTRACT

The ceramics are classified as high performance ceramics, structural ceramics, construction ceramics, industrial ceramics, engineering ceramics, functional ceramics, electrical ceramics, cutting ceramics and medical ceramics depending on their properties. The area of interest in the present work is the electronic ceramics, which are highly specialized class of materials, termed as electroceramics. The lead zirconate titanate (PZT) is the most widely used ferroelectric ceramic. The Ti^{4+} ions in $PbTiO_3$ can be partially substituted by Zr^{4+} with a molar ratio x to form a binary system (solid solution) with the following chemical formula $Pb(Zr_xTi_{1-x})O_3$. It also belongs to the perovskite type ferroelectrics. In this solution, Zr^{4+} and Ti^{4+} occupy at B site cation positions is random. PZT compositions possess the advantageous combination of properties of high electromechanical coupling coefficient, relatively high curie temperature (T_c), wide range of dielectric constants, capability to form solid-solutions with many different compositions and easy poling. PZT is especially attractive for a number of device applications. Wide range of physical properties can be obtained by variation of Zr/Ti ratio, particularly in so-called morphotropic phase boundary (MPB) region at Zr/Ti ratio 52/48. PZT (52/48) has both rhombohedral and tetragonal ferroelectric phases. The extraordinary ability of PZT at the MPB to re-orient its polarization allows it to retain a large remanent polarization. Moreover, the activity of 3 non-180° domain walls creates a large extrinsic contribution to its piezoelectric response.

PZT ceramics are generally used with a dopant or a modifier to optimize and improve their basic properties for specific applications. These modifiers create various types of defects in the crystal structure which results in significant changes in domain structures and electromechanical properties. Three general types of modifiers are isovalent additives, such as Sr^{2+}/Ba^{2+} replacing Pb^{2+} or Sn^{4+} replacing (Zr^{4+},Ti^{4+}) are the ones in which the substituting ion has same valency and has approximately the same size as of the replaced ion, the donors, such as La^{3+}/Sm^{3+} replacing Pb^{2+} or, Nb^{5+} replacing (Zr^{4+},Ti^{4+}) and acceptors, such as Na^{+}/K^{+} replacing Pb^{2+} or Fe^{3+}/Mn^{2+} replacing (Zr^{4+}, Ti^{4+}). In general, with the amount of dopant content, the compositional modification (doping) by single dopant leads the unstable electrical properties with drastic variations for the PZT ceramics. Soft and hard PZT ceramics are respectively donor- and acceptor-doped PZT, which are commercially available and widely employed in various

applications. The complex doping of two or more elements is expected to combine the properties of donor doped and/or acceptor doped PZT, which could exhibit better stability or improved piezoelectric and dielectric properties than those of the single element doped PZT. In view of above facts, rare- earth ions softeners (La^{3+}, Sm^{3+}) at A site and hardener-softener (Fe^{3+}, Nb^{5+}) and isovalent (Mn^{4+}) substituents at B site have been selected for investigating the structural, dielectric, ferroelectric and piezoelectric properties in PZT (60/40). In the present work the following compositional series were prepared by conventional solid state route.

1. $Pb_{1-x}Sm_x(Zr_{0.60}Ti_{0.40})_{0.98}Fe_{0.01}Nb_{0.01}O_3$ (where x = 0, 0.0025, 0.0050, 0.0075, 0.01, 0.02, 0.04, 0.06, 0.08) (PSZFNT-Series A)
2. $Pb_{1-x}La_x(Zr_{0.60}Ti_{0.40})_{0.98}Fe_{0.01}Nb_{0.01}O_3$ (where x = 0, 0.0025, 0.0050, 0.0075, 0.01, 0.02, 0.04, 0.06, 0.08) (PLZFNT -Series B)
3. $Pb(Zr_{0.60}Ti_{0.40})_{0.98-x}Fe_{0.01}Nb_{0.01}Mn_xO_3$ (where x = 0, 0.005, 0.010, 0.015, 0.02) (PZFMNT-Series C)

The research work carried out for the Ph.D. thesis has been divided in 5 chapters as summarized below:

In **Chapter I**, we describe a brief review of the research and development work that has been carried out recently in solid ferroelectric materials in general and lead zirconate titanate in particular. The aim of carrying out the present work including the criteria of selection of various compositions, here in studied, scope of these investigations have also been discussed. **Chapter II** deals with methods of sample preparation and characterization techniques used for studying physical and electrical properties (like structural, dielectric, ferroelectric and piezoelectric) of modified lead zirconate titanate ceramics (PZFNT). The ceramics samples were prepared in bulk form. For preparation of the samples, conventional solid state reaction route was used. The details of experimental techniques, various characterization equipments and their working details are summarized in this chapter. The optimization of sintering temperature is also discussed. **Chapter III** concerns with study of structural and microstructural properties of the La, Sm and Mn substituted modified PZT compositional series. The experimental density, lattice parameters, relative density and grain size variation of doped compositions is compared with those of undoped PZFNT. In **Chapter IV** dielectric, ferroelectric and piezoelectric properties of the series have been studied in detail. The dielectric constant (ε) and loss

(*tanδ*) have been investigated over a wide frequency (100 Hz–100 kHz) and temperature (30^oC - 500^oC) range. The effect of substituents (viz; La, Sm and Mn) on the curie temperature, dielectric constant and loss have also been studied. The remanant polarization, spontaneous polarization and coercive field variation with amount of La, Sm and Mn substitution is investigated in detail by hysteresis behaviour. The temperature dependence of hysteresis behavior is also studied. The piezoelectric coefficient (d_{33}) and electromechanical coupling coefficient (k_p) is measured at room temperature. The dielectric constant, remanant polarization and piezoelectric coefficient enhances with La and Sm substitution while manganese substitution reduces dielectric, ferroelectric and piezoelectric parameters. In **Chapter V** we conclude our work with future work recommendations. The suitability of the composition to give desired properties is highlighted which can be explored for various device applications.

LIST OF PUBLICATIONS

International Journals (thesis):

1. Dielectric Studies of Samarium Modified (Pb)(Zr, Ti, Fe, Nb)O_3 Ceramic System,
   PRATIBHA SINGH, SANGEETA SINGH, J. K. JUNEJA, CHANDRA PRAKASH, K. K. RAINA, ***Modern Physics Letters B*** **23** [11] (2009) 1437-1442.

2. Effect of Samarium Substitution on Dielectric Properties of (Pb)(Zr, Ti, Fe, Nb)O_3 Type Ceramic System,
   PRATIBHA SINGH, SANGEETA SINGH, J. K. JUNEJA, CHANDRA PRAKASH
   Ceramics International **35** (2009) 3335-3338.

3. Synthesis and Ferroelectric Properties of La-Substituted PZFNT,
   PRATIBHA SINGH, SANGEETA SINGH, J. K. JUNEJA, CHANDRA PRAKASH, K. K. RAINA, VINOD CHAHAR, R. P. PANT, ***Physica B*** **405** (2010) 10-14.

4. Effects of Samarium doping on the ferroelectric properties of modified lead zirconate titanate ceramics,
   PRATIBHA SINGH, SANGEETA SINGH, J.K. JUNEJA, K.K RAINA, R.P. PANT, CHANDRA PRAKASH
   Integrated Ferroelectrics **122** (2010) 23-30.

5. Sintering Temperature Effect on Modified Lead Zirconate Titanate Bulk Ceramics
   PRATIBHA SINGH, SANGEETA SINGH, J.K. JUNEJA, CHANDRA PRAKASH, K.K. RAINA
   American Institute of Physics (Accepted).

6. Ferroelectric Hysteresis in Mn-Substituted Modified Lead Zirconate Titanate Ceramics,
   PRATIBHA SINGH, SANGEETA SINGH, J. K. JUNEJA, CHANDRA PRAKASH, K.K. RAINA (To be Communicated).

7. Influence of Lanthanum Substitution on Dielectric Response of Modified Lead Zirconate Titanates,
   PRATIBHA SINGH, SANGEETA SINGH, J. K. JUNEJA, CHANDRA PRAKASH, K. K. RAINA (To be communicated).

Other publications in Journals (not included in thesis):

8. Effect of Two-Stage Sintering on Dielectric and Ferroelectric Properties of $Ba_{0.80}Pb_{0.20}TiO_3$ Ceramics,
   PARVEEN KUMAR, **PRATIBHA SINGH**, SANGEETA SINGH, J.K. JUNEJA, CHANDRA PRAKASH AND K.K. RAINA
   Ferroelectric Letters **36** (2009) 92-101.

9. Improved Properties of $BaTiO_3$ Ceramics Prepared by Ultrasonic Mixing,
   PARVEEN KUMAR, **PRATIBHA SINGH**, SANGEETA SINGH, J.K. JUNEJA, CHANDRA PRAKASH AND K.K. RAINA
   Integrated Ferroelectrics **122** (2010) 114-118.

10. Study on Microwave Processed PZT-Ni-Zn Ferrite Magneto-Electric Composites,
REKHA RANI, **PRATIBHA SINGH**, SANGEETA SINGH, J.K. JUNEJA, K.K. RAINA, CHANDRA PRAKASH
Bulletin of Material Science (Communicated).

International Conferences/Workshops:

11. Effect of Zirconium Substitution on Structural and Dielectric Properties of $Ba_{0.80}Pb_{0.20}TiO_3$ Ceramics,
PARVEEN KUMAR, **PRATIBHA SINGH**, SANGEETA SINGH, J.K. JUNEJA, CHANDRA PRAKASH, K.K. RAINA
(International Conference on Electroceramics, 13-17 December-2009, Delhi University, New Delhi).

12. Study of Ferroelectric Hysteresis in Mn-Substituted Modified Lead Zirconate Titanate (60/40),
PRATIBHA SINGH, SANGEETA SINGH, J.K. JUNEJA, K.K. RAINA, CHANDRA PRAKASH
(International Workshop & Symposium on the Synthesis and characterization of Glass/Glass-ceramics (IWSSCGGC-2010), 7-10 July 2010, Centre for Materials for Electronic Technology (CMET), Pune).

National Conferences/Workshops:

1. Structural and Ferroelectric Properties of Samarium Substituted PZTFN,
PRATIBHA SINGH, SANGEETA SINGH, J.K. JUNEJA, K.K. RAINA, CHANDRA PRAKASH
(National Seminar on Electroceramics, November 05-06, 2007, GVM Girls College, Sonepat, Haryana).

2. Dielectric Behaviour of Samarium Substituted Modified PZT,
PRATIBHA SINGH, SANGEETA SINGH, J.K. JUNEJA, K.K. RAINA, CHANDRA PRAKASH
(Recent Advances in Innovative Materials (RAIM), February 16-17, 2008, National Institute of Technology, Hamirpur, HP).

3. Dielectric Behaviour of Lanthanum Substituted PZT,
PRATIBHA SINGH, SANGEETA SINGH, J.K. JUNEJA, K.K. RAINA, CHANDRA PRAKASH
(National Seminar on Ferroelectric Devices (NSFD), Nov. 2008, Thapar University, Patiala, Punjab).

4. Effect of Lanthanum doping on ferroelectric and dielectric properties of modified PZT,
PRATIBHA SINGH, SANGEETA SINGH, J.K. JUNEJA, CHANDRA PRAKASH, K.K. RAINA
(National Conference on Photonics & Materials Science, Oct 24-25, 2008, Guru Jambheshwar University of Science & Technology, Hisar).

5. Dielectric Properties of Samarium Modified PZFNT Ceramics,
   PRATIBHA SINGH, SANGEETA SINGH, J.K. JUNEJA, CHANDRA PRAKASH, K.K. RAINA
   (National Conf on Emerging Perspectives and Sustainable Developments in Physics, Nov. 18-19, 2009, DAV College, Abohar Punjab).

TABLE OF CONTENTS

		Page No.
Certificate		i
Acknowledgement		ii
Abstract		iv
List of Publications		vii
CHAPTER I	**Introduction**	
1.1.	**Background**	(I)-1
1.2.	**Ferroelectric Ceramics**	(I)-2
1.3.	**Domain Walls and Hysteresis Behaviour**	(I)-4
1.4.	**Dielectric Properties**	(I)-7
	1.4.1. Dipolar Polarization (Orientational Polarization)	(I)-7
	1.4.2. Ionic Polarizablity	(I)-8
	1.4.3. Electronic Polarizability	(I)-8
	1.4.4. Interfacial Polarizability/Space Charge Polarizability	(I)-9
	1.4.5. Dielectric Constant (ε_r)	(I)-9
	1.4.6. Dielectric Loss (tanδ)	(I)-10
	1.4.7. Phase Transition Temperature/Curie Temperature (T_c)	(I)-10
1.5.	**Poling**	(I)-13
1.6.	**Piezoelectricity**	(I)-14
	1.6.1. Mechanism	(I)-15
	1.6.2. Piezoelectric Parameters	(I)-15
	1.6.2.1. Piezoelectric Charge Coefficient (d)	(I)-16
	1.6.2.2. Hydrostatic Charge Coefficient (g)	(I)-16
	1.6.2.3. Piezoelectric Voltage Coefficient (d_h)	(I)-16
	1.6.2.4. Hydrostatic Voltage Coefficient (g_h)	(I)-17
	1.6.2.5. Electromechanical Coupling Factor (k)	(I)-17
1.7.	**Ferroelectrics for Commercial Applications**	(I)-18
	1.7.1. Capacitors	(I)-18
	1.7.2. Tunable Dielectrics	(I)-19
	1.7.3. Opto-Electronic Devices	(I)-19

1.7.4. Piezoelectric Applications (I)-19
1.7.5. Non-Volatile Memory (I)-20
1.8. **Perovskite Structure** (I)-20
1.8.1. Lead Zirconate Titanate (I)-22
1.9. **Background of the proposal** (I)-26
1.10. **Proposed Objectives of the Present Work** (I)-32
References (I)-35

CHAPTER II Material Synthesis & Characterization Techniques

2.1. **Introduction** (II)-1
2.2. **Material Synthesis: Solid State Route** (II)-2
2.2.1. Ball Miliing and Drying (II)-4
2.2.2 Calcination (II)-5
2.2.3. Shaping (II)-6
2.2.4. Sintering (II)-7
2.3. **Characterization Techniques** (II)-9
2.3.1. Phase Identification (II)-9
2.3.2. Microstructure Analysis (II)-11
2.3.3. Density (II)-12
2.3.4. Electroding and Poling (II)-13
2.3.5. Hysteresis Measurement (II)-13
2.3.6. Dielectric Measurements (II)-14
2.3.7. Piezoelectric Coefficient Measurement (II)-15
2.3.7.1. Piezoelectric Charge Coefficient (d_{33}) (II)-15
2.3.7.2. Electromechanical Coupling Coefficient (k_p) (II)-16
2.4. **Pb(Zr,Ti, Fe, Nb)O_3 System: Processing Parameters and Optimization of Sintering Temperature** (II)-17
References (II)-25

CHAPTER III Structural & Microstructural Properties of Substituted Pb(Zr,Ti,Fe,Nb)O_3 System

3.1. **Introduction** (III)-1
3.2. **Structural properties of Substituted PZFNT compositions** (III)-1
3.2.1. Structural Analysis of Sm-Substituted PZFNT Ceramics (III)-1
3.2.2. Structural Analysis of La-Substituted PZFNT Ceramics (III)-4

3.2.3. Structural Analysis of Mn-Substituted PZFNT Ceramics (III)-5
3.3. **Density Measurements of Substituted PZFNT compositions** (III)-7
3.4. **Microstructural Analysis of Substituted PZFNT compositions** (III)-9
References (III)-16

CHAPTER IV Dielectric, Ferroelectric & Piezoelectric Properties of Substituted $Pb(Zr,Ti,Fe,Nb)O_3$ System

4.1. **Introduction** (IV)-1
4.2. **Dielectric properties of Substituted modified PZT** (IV)-3
4.2.1. Room Temperature Variation of ε and $tan\delta$ with Frequency (IV)-4
4.2.2. Variation of ε and $tan\delta$ with Temperature (IV)-5
4.3. **Ferroelectric Properties of Substituted Modified PZFNT** (IV)-21
4.3.1. Room Temperature Hysteresis Behaviour (IV)-21
4.3.2. Hysteresis Behaviour versus Temperature (IV)-29
4.4. **Piezoelectric properties of substituted modified PZFNT** (IV)-38
References (IV)-40

CHAPTER V Conclusions & Recommendations for Future Work

5.1. **Conclusions** (V)-1
5.2. **Recommendations for Future Work** (V)-3

LIST OF FIGURES

		PAGE NO.
CHAPTER I	**Introduction**	
Fig.1.1.	(a). Surface charge and depolarizing field (E_d) associated with spontaneous polarization (P_s) (b). Formation of 180^o domains to minimize electrostatic energy	(I)-5
Fig.1.2.	A schematic diagram representing 180^o and 90^o domain walls	(I)-5
Fig.1.3.	P-E loop for a ferroelectric material indicating the remanent polarization (P_r), saturation polarization (P_s), and coercive field (E_c)	(I)-6
Fig.1.4.	Different polarization mechanisms; (a) Electronic polarization, (b) Ionic polarization, (c) Dipolar polarization and (d)Space charge/ Interfacial polarization	(I)-8
Fig.1.5.	Frequency range of different polarization mechanisms	(I)-9
Fig.1.6.	Temperature dependence of the dielectric permittivity (ε′) and spontaneous polarization P_s for (a) a first-order, (b) a second-order ferroelectric and (c) a relaxor ferroelectric	(I)-12
Fig.1.7.	Poling steps in a ferroelectric material	(I)-14
Fig.1.8.	Notation of axis for a poled piezoelectric element	(I)-16
Fig.1.9.	The (a) cubic (b) tetragonally distorted perovskite crystal cells with up and (c) down polarized B atoms	(I)-21
Fig.1.10.	Phase diagram of the $PbZrO_3$ / $PbTiO_3$ solid solution system (modified)	(I)-23
CHAPTER II	**Material Synthesis & Characterization Techniques**	
Fig.2.1.	A flow chart depicting the conventional solid state route for bulk modified PZT samples	(II)-3
Fig.2.2.	Conventional Ball mill	(II)-4
Fig.2.3.	Programmable furnace for calcination and sintering	(II)-5
Fig.2.4.	Uniaxial pressing	(II)-6
Fig.2.5.	Hydraulic press for uniaxial pressing	(II)-7
Fig.2.6.	Time-Temperature sintering profile for modified PZT	(II)-8
Fig.2.7.	Bragg's law for reflection	(II)-10
Fig.2.8.	The schematic diagram for Bragg's diffraction	(II)-11
Fig.2.9.	Poling setup	(II)-13
Fig.2.10.	P-E hysteresis loop tracer	(II)-14
Fig. 2.11.	LCR meter for dielectric measurements	(II)-15
Fig. 2.12.	Piezo d meter	(II)-16
Fig. 2.13.	Bulk densities of PZFNT sample as a function of sintering Temperatures	(II)-19
Fig 2.14.	XRD patterens of PZFNT samples at different sintering Temperatures	(II)-19
Fig. 2.15.	SEM micrographs of PZFNT ceramics sintered at at different Temperatures	(II)-20
Fig. 2.16.	P-E hysteresis curves of modified PZT samples at (a) 1150^oC (b) 1200^oC (c) 1250^oC (d) 1300^oC (e) Comparison of PE loop at different sintering temperatures	(II)-22

Fig. 2.17. Room temperature variation of dielectric constant and loss with frequency at different sintering temperatures (II)-23

CHAPTER III Structural & Microstructural Properties of Substituted $Pb(Zr,Ti,Fe,Nb)O_3$ System

Fig.3.1. (a) X-ray diffraction patterns of the Series A (PSZFNT) samples with different amount of Sm substitution (b) shifts in (002), (200) and (c) (112), (211) peaks in 2θ ranges of (42-48^o) and (52-58^o) (III)-2
Fig.3.2. Variation in lattice parameters (a, c) with Sm content (x = 0-0.08) (III)-3
Fig.3.3. (a) X-ray diffraction patterns of the Series B (PLZFNT) samples with different amount of La substitution (b) shifts in (002), (200) and (c) (112), (211) peaks in 2θ ranges of (42-48^o) and (52-58^o) (III)-4
Fig.3.4. Variation in lattice parameters (a, c) with amount of La (x = 0-0.08) (III)-5
Fig.3.5. (a) X-ray diffraction patterns of the Series C (PZFMNT) samples with different amount of Mn substitution (b) shifts in (200) and (c) (112), (211) peaks in 2θ ranges of (42-48^o) and (52-58^o) (III)-6
Fig.3.6. Scanning electron micrographs of fractured surface of Series A samples for x=0-0.08 (III)-11
Fig.3.7. Scanning electron micrographs of fractured surfaces of Series B samples for x=0-0.08 (III)-13
Fig.3.8. Scanning electron micrographs of fractured surface of Mn-substituted PZFMNT samples (III)-15

CHAPTER IV Dielectric, Ferroelectric & Piezoelectric Properties of Substituted $Pb(Zr,Ti,Fe,Nb)O_3$ System

Fig. 4.1. Variation of (a) and (b) dielectric constant (ε_{RT}), (c) and (d) loss tangent ($\tan\delta_{RT}$) of Series A as a function of frequency at room temperature (IV)-8
Fig. 4.2. Variation of (a) and (b) dielectric constant (ε_{RT}), (c) and (d) loss tangent ($\tan\delta_{RT}$) of Series B as a function of frequency at room temperature (IV)-9
Fig. 4.3. Room temperature variation of (a) dielectric constant (ε_{RT}) (b) loss tangent ($\tan\delta_{RT}$) of Series C as a function of frequency (IV)-10
Fig. 4.4 Variation of dielectric constant (ε) and loss tangent (tanδ) with temperature for Series A (Sm-substituted PZFNT) samples at different frequencies (IV)-11
Fig. 4.5 Variation of dielectric constant (ε) and loss tangent (tanδ) with temperature for Series B (La-substituted PZFNT) samples at different frequencies (IV)-15
Fig. 4.6. Variation of dielectric dielectric constant (ε) and loss tangent (tanδ) with temperature for Series C (Mn-substituted PZFMNT) samples at different frequencies (IV)-18
Fig. 4.7. Hysteresis curves of Series A compositions at different maximum electric fields (IV)-23
Fig. 4.8. Hysteresis curves of Series B samples at different maximum electric fields (IV)-26
Fig. 4.9. Hysteresis loops of Series C compositions at different maximum electric fields. (IV)-28

Fig. 4.10. Hysteresis loops of Series A ceramics for varying concentrations of Sm as a function of temperature (IV)-30
Fig. 4.11. Temperature dependence of (a) P_r (b) E_c of Series A samples (IV)-32
Fig. 4.12. Hysteresis loops of Series B ceramics for varying concentrations of La as a function of temperature (IV)-33
Fig. 4.13. Temperature dependence of (a) P_r and (b) E_c of Series B samples (IV)-35
Fig. 4.14. Temperature dependence of hysteresis behavior of Series C samples (IV)-36
Fig. 4.15 Temperature dependence of (a) P_r and (b) E_c for Series C samples (IV)-37
Fig. 4.16. Typical admittance spectra for the calculation of k_p for PZFNT (x=0) sample (IV)-39

LIST OF TABLES

		PAGE NO.
CHAPTER I	**Introduction**	
Table 1.1.	Comparison of effect of doping on various properties of soft, hard and relaxor PZT ferroelectrics	(I)-25
CHAPTER II	**Material Synthesis & Characterization Techniques**	
Table 2.1.	Variation of grain size, ferroelectric, room temperature dielectric and piezoelectric parameters with sintering temperature	(II)-21
CHAPTER III	**Structural & Microstructural Properties of Substituted $Pb(Zr,Ti,Fe,Nb)O_3$ System**	
Table 3.1.	Lattice parameters of Series A (PSZFNT) samples	(III)-3
Table 3.2.	Lattice parameters of Series B (PLZFNT) samples	(III)-5
Table 3.3.	Lattice parameters of Series C (PZFMNT) samples	(III)-7
Table 3.4.	Variation of experimental (d_{ex}), theoretical (d_{th}) and relative density (d_{rel}) with substituent amount in PZFNT	(III)-8
Table 3.5.	Variation of grain size with substitution in PZFNT compositions	(III)-10
CHAPTER IV	**Dielectric, Ferroelectric & Piezoelectric Properties of Substituted $Pb(Zr,Ti,Fe,Nb)O_3$ System**	
Table.4.1.	Variation of dielectric parameters of Series A ceramics at different frequencies	IV-14
Table 4.2.	Variation of dielectric parameters of Series B ceramics at different frequencies	IV-14
Table 4.3.	Variation of dielectric parameters of Series C at different frequencies	IV-19
Table 4.4.	Variation of curie temperature (T_m) with amount of substitution (x) in PZFNT samples	IV-20
Table 4.5.	Variation of ferroelectric parameters of Series A samples	IV-25
Table 4.6.	Variation of ferroelectric parameters of Series B ceramics	IV-25
Table 4.7.	Variation of ferroelectric parameters of Series C ceramics	IV-25
Table 4.8.	Variation of piezo-coefficients in substituted modified PZT ceramics	IV-39

CHAPTER I

Introduction

This chapter deals with a brief introduction to the electronic ceramics which include dielectric, ferroelectric and piezoelectric materials. Ferroelectric materials, having perovskite structure, and its applications are discussed in detail. Current developments and recent trends in lead zirconate titanate (PZT) and substituted lead zirconate titanate are discussed here. The effects of substituents on properties of modified PZT are reviewed and the importance of $(Pb,Zr,Ti,Fe,Nb)O_3$ system which is the subject of investigation in the present thesis is discussed.

1.1. Background

Science tells us that we are on one planet among many, in one galaxy among many, in one solitary universe of incomprehensible size and complexity. At present, the material world is the only world we know. The social relationships and economic quality of life is largely defined by the world of material possessions that we live in. The most popular way of naming human era of early civilization is in terms of materials from which tools and weapons of our ancestors were made of. The “Stone Age”, “Bronze Age”, “Copper Age” and “Iron Age” have been traced as far back as 2.5 billion years when human civilization started till 1 B.C. The history of human civilization, to a certain degree, could be regarded as a history of materials evolution. The term "material" is used more narrowly to refer to substances or components with certain physical properties that are used as inputs to production or manufacturing. In this sense, materials are the parts required to make something else, from buildings and art to stars and computers. In material science, rather than discovering materials and exploiting their properties, the aim is instead to understand materials so that new materials with the desired properties can be developed.

The materials can be classified into metals, ceramics and glasses, polymers, composites and semiconductors depending on their properties, range of applications, technological progress and potential use in industries. These engineering materials encompass wide range of applicability and usage in various emerging fields of modern times but ceramics are the ones that are admired for their mechanical, chemical and thermal stability, their unique electrical, optical and magnetic properties that have become of utmost importance in many key technologies including energy conversion and storage, automation, electronics and communications. These materials find applications in our daily lives ranging from electronic components, environment sensors, gas ignitors, ultrasonic cleaners to intrusion alarms etc. Ceramics are composed of randomly oriented crystallites (small crystals of less than 100 μm or 10^{-2} cm average diameter) intimately bonded together to form a solid. Although the crystallites do possess an ordered internal structure just as single crystal do, their random orientation produced during the high temperature sintering or coalescing operation causes the ceramic to have an overall isotropic (equal in all directions) character in

regard to its properties. The isotopic character can be modified if desired, by special techniques employed during the sintering operation or after cooling to room temperature [1].

Ceramics are classified as high performance ceramics, structural ceramics, construction ceramics, industrial ceramics, engineering ceramics, functional ceramics, electrical ceramics, cutting ceramics and medical ceramics depending on their properties. It is the combination of traditional ruggedness of conventional ceramics and the exceptional functionality of selected electroceramic materials that make them particularly attractive as smart materials. The area of interest in the present work is the electronic ceramics, which are highly specialized class of materials, also termed as electroceramics. Their properties are predominantly controlled by their composition in addition to processing conditions and complexities of shape. Various types of electroceramics include insulators, capacitors, ferrites, PTC's, ferroelectrics, pyroelectrics, piezoelectrics and electro-optic ceramics [2].

1.2. Ferroelectric Ceramics

Ferroelectric ceramics are commonly described as non-centrosymmetric polycrystalline materials containing an electrically re-orientable spontaneous polarization at equilibrium. The spontaneous polarization of such materials disappears at certain temperature called curie temperature.

The first experimental observation of ferroelectricity was made in 1920 when Joseph Valasek in 1921 discovered that the polarization of Rochelle salt ($KNaC_4H_4O_6 \bullet 4H_2O$) reverses with the application of an external electric field [3]. It was first produced in France in 1665 for medicinal use by pharmacist Elie Seignette. Consequently, the term Seignette-electricity has also been used to describe ferroelectricity [4, 5]. Initially, ease in preparation of single crystals of Rochelle salt rendered it interesting to study, but its water solubility made it technologically unattractive [5]. The first technological breakthrough in ferroelectricity came with the discovery of barium titanate ($BaTiO_3$) as a high-k dielectric material during the Second World War [6-9]. The relative dielectric constant of this ceramic was reported to be at least 1100, which was enormous compared to the permittivity of ~100 for the previously reported Rutile. $BaTiO_3$ was identified as being ferroelectric perovskite substance [10, 11] as its pseudocubic (tetragonal) nature at room temperature made it to possess spontaneous polarization [12, 13]. It was realized that if a ferroelectric

polycrystalline ceramic is poled (held at an electric field greater than the coercive field at an elevated temperature), the dipoles in the isotropic ceramic can be aligned to form a unique polar axis that is electromechanically active [4]. Since its discovery in the 1940s, $BaTiO_3$ has been engineered to act as a temperature invariant, high permittivity, low dielectric loss material for high capacitance devices. However, for piezoelectric and ferroelectric applications, $BaTiO_3$ has been replaced by the family of lead zirconate titanate (PZT) solid solutions, which were first reported on by Jaffe et al. in 1954 [14].

Ferroelectricity in crystals can be explained on the basis of symmetry operations. It is found that symmetry operations can be combined in 32 different ways, resulting in 32 different crystal classes. Out of these 32, only 11 crystal classes have center of symmetry and 21 are non centro-symmetric. Further, out of the remaining 21 non centro-symmetric classes, only 20 show piezoelectricity. The remaining one non-centro symmetric class does not show any piezoelectric effect because of the combined effect of symmetry. Piezoelectricity is a material property that linearly relates applied stresses to induced dielectric displacements (direct piezoelectric effect) or applied electric fields to induced strains (converse piezoelectric effect). Hence piezoelectric effect is the phenomenon of creation of electric polarization on the application of external stress and vice-versa.

Out of 20 piezoelectric crystals only 10 possess spontaneous polarization. They are also known as pyroelectric crystals. Pyroelectric effect is the appearance of an electric charge at the surface of the material with change in ambient temperature. Further a current is generated when they are heated or cooled. The current generated due to generated electrical charge is called pyroelectric current. There are materials such as ZnO or GaN, with a unique polar axis but they are not ferroelectric. The final requirement, a switchable or "re-orientable" dipole, is required for ferroelectric response. There exists a subclass of pyroelectric materials, which have two or more orientation states of polarization in the absence of an electric field. The polarization in these materials can be switched from one state to other with the application of an electric field and thus are known as ferroelectric materials. Hence the non-centrosymmetric class is divided into piezoelectric and pyroelectric class. All ferroelectric crystals are piezoelectrics as well as pyroelectrics both. However, pyroelectrics are not necessarily ferroelectrics [15].

1.3. Domain Walls and Hysteresis Behaviour

Ferroelectrics may exhibit one or more ferroelectric (polar) phases that show a *domain structure* in which the individual domain states can be reoriented by an applied field. Domain structures are strongly dependent on the symmetry of the ferroelectric phase. As the changes occur in symmetry resulting in different domain configurations, the other properties of the material will also be influenced. In a ferroelectric crystal usually there are many domains (regions with uniform polarization). Within each individual domain, all the electric dipoles are aligned in the same direction. These domains in a crystal are separated by interfaces called *domain walls* [16]. As these walls differ from the perfect crystal, there is a certain amount of energy (W_{dw}; domain wall energy) associated with them, in addition to the elastic energy, W_e. From energy considerations, in real materials, domain patterns depend on many factors, including the existing defect structure and concentration, stress and electric history, boundary conditions, temperature relative to T_c, and even the history of crystal preparation [3, 16].

Fig. 1.1. depicts 180^o domain formation which minimizes the electrostatic energy of the system. Defects and internal stresses must be also considered for a crystal that exhibits piezoelectricity in the paraelectric state [17]. The presence of mechanical stress in a crystal results in the development of non-180^o domain walls configured to minimize the strain. The structure of a ferroelectric domain depends on the structure of the crystal. In a ferroelectric crystal, the variety of domain patterns and the number of types of domain walls depend on the number of orientations of the dipole moment when the spontaneous polarization occurs from the prototype phase. Onset of the spontaneous polarization at T_c, leads to the formation of a surface charge. These surface charges produce an electric field, called depolarizing field, E_d. The depolarizing field may be very strong of the order of several kV/cm, rendering the single domain state of the ferroelectric energetically unfavorable [3, 18]. The electrostatic energy associated with the depolarizing field may be minimized if the ferroelectric split into domains with oppositely oriented polarization and the depolarizing charge is compensated by electrical conduction through the material or by charges from the material surroundings.

Domain wall is typically classified by the angular difference between the spontaneous polarization directions of the two domains it separates. The walls, which separate domains

with oppositely oriented polarization, are called 180° walls and while those which separate regions with mutually perpendicular polarization, are called 90° walls [20].

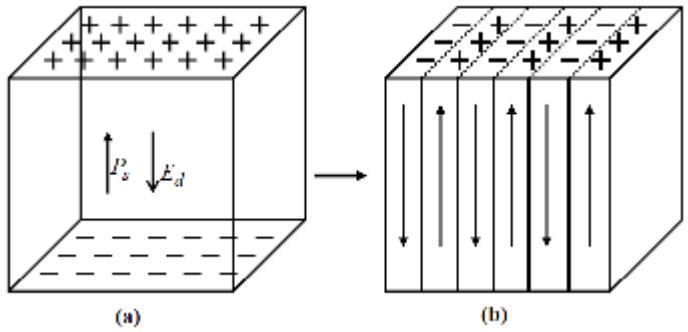

Fig. 1.1(a). Surface charge and depolarizing field (E_d) associated with spontaneous polarization (P_s); **(b).** Formation of 180° domains to minimize electrostatic energy [19].

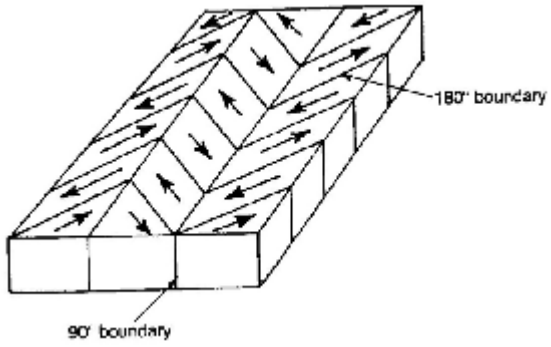

Fig. 1.2. A schematic diagram representing 180° and 90° domain walls [19].

Fig. 1.2. illustrates the 180° and 90° domain walls in perovskites. Besides 180° domain walls, tetragonally distorted perovskites can have 90° domain walls while rhombohedrally distorted perovskites can have 71° and 109° domain walls. 180° domain walls are capable of reducing the electrostatic energy associated with depolarizing field (E_d) while non-180° domain walls can relieve both electrostatic as well as elastic energies. Because non-180° domain walls separate domains with different spontaneous strain tensors, these walls are ferroelastic as well as ferroelectric. Due to their ferroelastic nature, the motion of non-180° domain walls contributes to the piezoelectric response of a ferroelectric (180° domain wall movement does not) [16].

A plot of polarization verses electric field, which is also known as hysteresis loop, is the most outstanding feature of ferroelectric ceramics. It describes the nonlinear polarization switching behavior as a function of field. *Fig. 1.3.* shows a typical hysteresis loop for a ferroelectric material demonstrating the schematic repartition of two partitions of states corresponding to different regions of the loop [21]. As the electric field strength is increased, the domain starts to align in the positive direction, giving rise to rapid increase in the polarization. At very high field levels, the polarization saturates. The polarization does not fall to zero when the external field is removed. At zero external fields, some of the domains remain aligned in the positive direction and hence the crystal will show a remanant polarization P_r. As the field is reversed, polarization is first reduced to zero and then, changes direction (sign) as the field produces saturation polarization (P_s) in the opposite direction, thereby resulting in a hysteresis loop.

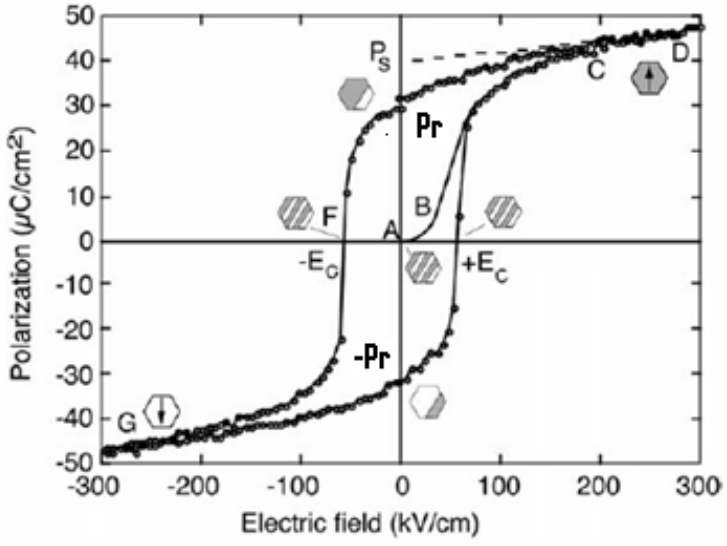

Fig 1.3. P-E loop for a ferroelectric material indicating the remanent polarization (P_r), saturation polarization (P_s), and coercive field (E_c). Hexagons with grey and white regions represent schematically repartition of two polarization states in the material [21].

The field at which the polarization is zero (changes sign) is known as the coercive field E_c. Poling consists of applying one-quarter of a hysteresis loop, leaving the material in a remanently polarized condition at P_r. On decreasing field strength, polarization decreases. When field is reduced to zero, some of the domains remain aligned in the positive direction

of the crystal and the polarization left is called remanant polarization (P_r). The extrapolation of the linear segment on this curve back to the polarization axis depicts spontaneous polarization, P_s [16]. The classic hysteresis loop shape is analogous to the magnetization response of a ferromagnet. Another similarity to ferromagnets is the transition temperature. Above transition temperature, denoted the curie point (T_c), ferroelectric materials transform to a higher symmetry paraelectric phase where no P-E loop is observed.

1.4. Dielectric Properties

Ferroelectric materials are very often termed as dielectrics. For various applications of ferroelectric materials, the dielectric constant (ε) and dielectric loss ($tan\delta$) are important practical parameters. The studies of the dielectric properties provide a great deal of information about the suitability of the material in various applications. Dielectric polarization of a material is dipole moment per unit volume and is defined as

$$P = \alpha E \qquad \text{.....(1.1)}$$

where P is the polarization of the material under an applied electric field E and α is the polarizability of the material. Generally, the overall polarizability, α, of a material is made up of four contributions:

$$\alpha = \alpha^d + \alpha^i + \alpha^e + \alpha^f \qquad \text{....(1.2)}$$

where α^d = Dipolar polarizability, α^i = Ionic polarizability, α^e = Electronic polarizability, and α^f = Interfacial polarizability These different polarizations are shown in *Fig. 1.4.* and are discussed as follows.

1.4.1. Dipolar Polarization (Orientational Polarization)

If the system is composed of heteronuclear molecules then the displacement of the individual atoms within a molecule may be such that the molecule itself has a permanent dipole moment and its magnitude doesn't change with the local field magnitude and this polarization is known as dipolar polarization. In zero fields, the permanent dipoles will be randomly oriented and the system has no net polarization, but an electric field will tend to align the dipoles and the material will acquire a net polarization, so it is also known as

orientational polarization. Due to the randomizing effect of the thermal vibrations this type of polarization is more effective at low temperatures and decreases with the increase in temperature. Dipolar polarization is frequency dependent, and active in low and microwave frequency range [22].

1.4.2. Ionic Polarizability

It originates with the displacement of ions in an electric field from the equilibrium positions. Displacement of an ion from an equilibrium position is equivalent to the placing of a fictitious dipole at the position with the ion in equilibrium. Although, positive and negative ions displace in opposite senses in an electric field, the induced moments all have the same sign. Ionic polarization is active in infrared frequency range

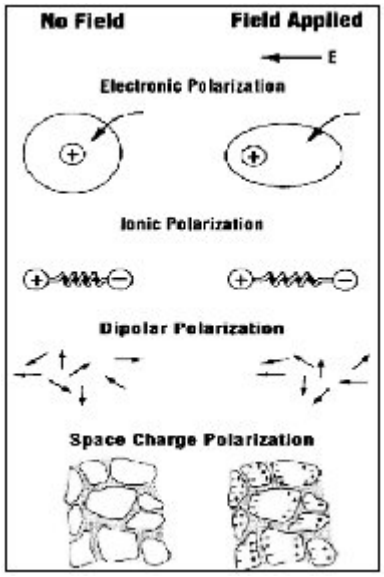

Fig. 1.4. Different polarization mechanisms; (a) Electronic polarization, (b) Ionic polarization, (c) Dipolar polarization and (d) Space charge/ Interfacial polarization.

1.4.3. Electronic Polarizability

It arises due to the relative displacement of the centers of the +ve charges with respect to the centre of the –ve charges of an atom or ion when subjected to an external electric field, E. It is operative in all dielectrics and is temperature independent. Electronic polarization is active in the optical (visible-ultraviolet) frequency range.

1.4.4. Interfacial/Space Charge Polarizability

In polycrystalline materials, the inter-grain boundaries are zones, where free charges interstitial ions, vacancies, injected electrons etc.) may accumulate and cause polarization of crystallites, which is known as interfacial polarization. The notion of interface polarization is related to separate surfaces between crystallites, which act as barriers to the motion of free charges from one crystallite to the other and is a characteristics of polycrystalline materials [23]. Interfacial polarization is prominent in microwave frequency range.

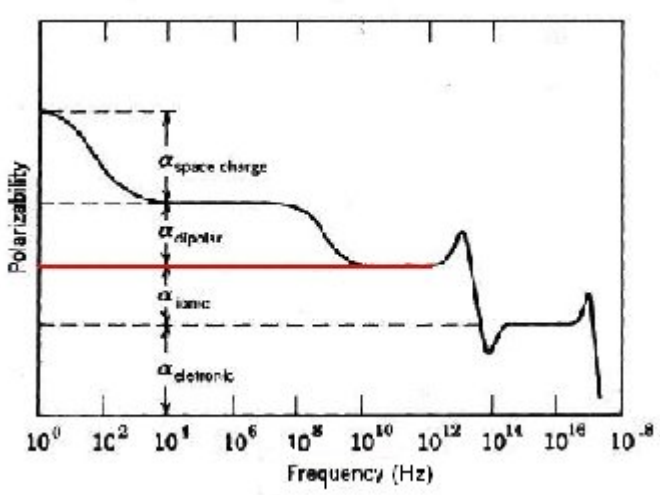

Fig. 1.5. Frequency range of different polarization mechanisms.

The electronic polarization is active in visible and ultraviolet frequency range. As the frequency for the absorption for the electrons of outer shells lies in this range shown in *Fig. 1.5*. At low frequency, this mechanism makes a constant contribution since the inertia of the electrons is negligible. On the other hand, the three mechanisms (dipolar, ionic and interfacial) are inhibited in the optical range due to the inertia of particles (in the case of ionic and dipolar polarization) and to the low mobility of carriers (for interfacial polarization).

1.4.5. Dielectric Constant (ε_r)

The dielectric constant (ε_r) of a material is the ratio between the charge stored on an electroded slab of material brought to a given voltage and the charge stored on a set of identical electrodes, separated by vacuum. It is defined as

$\varepsilon_r = 1+P / \varepsilon_o E$ ….. (1.3)

where ε_r = Dielectric constant

P = Induced dipole moment per unit volume under an applied electric field E

ε_o = Permittivity of the free space

For an alternating electric field, the dielectric constant can be written as

$\varepsilon_r = \varepsilon' - i\varepsilon''$ ….. (1.4)

where ε' is the real component of the dielectric constant, in phase with the applied field. ε'' is the imaginary component, 90^o out of phase with the applied field, caused by either resistive leakage or dielectric absorption. For normal substances, the value of ε_r is low, usually under 5 for organic materials and under 20 for most inorganic solids. Generally, ferroelectric ceramics have much higher ε_r, typically several hundred to several thousand [4].

1.4.6. Dielectric Loss (tanδ)

The charging current in an ideal dielectric leads the applied voltage by $\pi/2$ radians (90^o). However, in real dielectrics in addition to the charging current associated with the storage of electric charge by the dipoles, a loss current must also be considered. The loss current arises from the long-range migration of charges, e.g., dc ohmic conduction and the dissipation of energy associated with the rotation or oscillation of dipoles [4]. As the dielectric is not loss free, it is generally represented by a complex dielectric constant, defined in equation 1.4. The total current in the real dielectric is a complex quantity which leads the voltage by an angle (90^o-δ), where δ is called the loss angle. Dielectric loss (tanδ) also known as dissipation factor is defined as $tan\delta = \varepsilon''/\varepsilon'$. The inverse of the loss tangent, $Q = (1/tan\delta)$, is used as a figure of merit in high frequency applications.

1.4.7. Phase Transition Temperature/Curie Temperature (T_c)

Phase transition is a characteristic feature of all ferroelectric materials [24]. A ferroelectric phase change represents a special class of structural phase transition denoted by the appearance of a spontaneous polarization. Ferroelectric crystals are characterized by displacements of ions from their centro-symmetric positions. This displacement leads to a net dipole moment of the unit cell and to a spontaneous static polarization. With increasing

temperature this polarization decreases until, at the ferroelectric phase-transition temperature, the crystal undergoes a phase transition from the polarized ferroelectric phase to the non-polarized paraelectric phase. At this temperature, the static dielectric constant diverges.

Phase transitions (including ferroelectric transitions) are divided into first and second order Transition [15]. Most ferroelectric materials undergo a structural phase transitions from a high-temperature nonferroelectric (or paraelectric) phase into a low-temperature ferroelectric phase. The paraelectric phase may be piezoelectric or non-piezoelectric and is rarely polar. The symmetry of the ferroelectric phase is always lower than the symmetry of the paraelectric phase. Above the Curie point, T_c, the dielectric permittivity decreases with temperature according to Curie – Weiss law,

$$\varepsilon = \varepsilon_o + C/T - T_o \sim C/T - T_o \quad .....(1.5)$$

where C is the Curie constant, T_o ($T_o < T_c$) is the Curie -Weiss temperature. The transition into the first ferroelectric phase is called the Curie point. If there is more than one ferroelectric phase, the temperature at which the crystal transforms from one ferroelectric phase to another is called the transition temperature.

In case of first order phase transition, the first derivatives of the thermodynamic potential, such as spontaneous polarization and volume experience a sudden change. In first order phase transition $T_o < T_c$, the crystal does not show ferroelectricity. The second derivatives of the thermodynamic potential change during a second-order phase transition. These derivatives include the dielectric constant, dielectric susceptibility, specific heat, thermal-expansion coefficient, elastic modulus, piezoelectric modulus and so on. In case of second order phase transition $T_c = T_o$ which is depicted in *Fig. 1.6.* When the temperature is in the vicinity of the Curie point, thermodynamic properties (such as dielectric, elastic, optical, and thermal properties) of a ferroelectric crystal show anomalies and the structure of the crystal changes. For example, dielectric constant in most ferroelectric crystals has a very high value near their curie point. This phenomenon is usually called the 'dielectric anomaly'. In most ferroelectrics, the temperature dependence of the dielectric constant above the Curie point (in the paraelectric region) can be described fairly accurately by a simple law called Curie-Weiss law. This anomaly exhibited in the dielectric behaviour of a material [26] with variation in

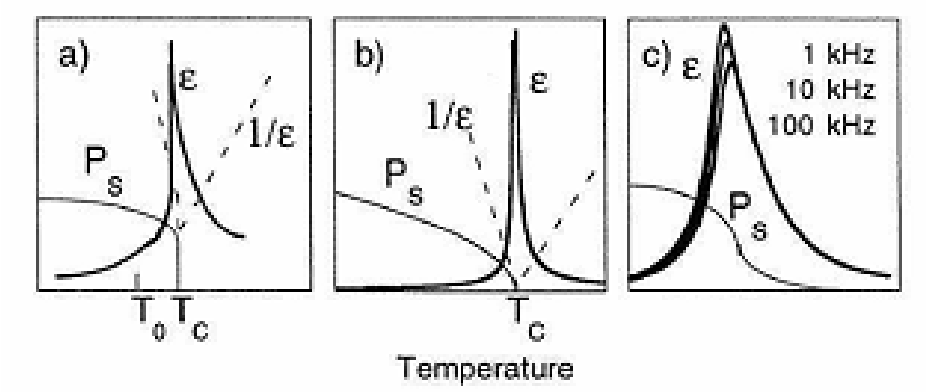

Fig. 1.6. Temperature dependence of the dielectric permittivity (ε) and spontaneous polarization P_s for **(a)** a first-order, **(b)** a second-order ferroelectric and **(c)** a relaxor ferroelectric [25].

temperature is a characteristic feature of ferroelectric material. In fact, both the dielectric anomaly and Curie-Weiss law are predicted in the thermodynamic theory of transition. The dielectric anomaly is not a definite proof of ferroelectricity, which is normally confirmed by hysteresis loop.In some materials, particularly in relaxors, in the absence of any definite phase transition, a third transition, known as diffused phase transition (DPT) occurs. This broad phase transition was first discovered by Smolenskil and Isupov in $BaTiO_3$ – $BaSnO_3$ perovskite solid solutions. Piezoelectric behavior of these materials can be observed even at a temperature above the dielectric maxima [27]. In relaxor ferroelectric materials, phase transition is not sudden but over a certain range of temperature, called Curie range. In the Curie range, these materials exhibit unusual dielectric and ferroelectric properties. In materials with diffused phase transition, dielectric constant peak is observed at different temperatures at different frequencies, in contrast with the normal ferroelectrics. Other properties also show gradual variations throughout the Curie range and no abrupt changes are observed at ferroelectric transition. Broadening of phase transition in ceramics depends on the composition fluctuations and structural disorderness. In systems, where structural order is distributed due to the disturbance in the composition, as in the case of relaxors, phase transition is generally gradual and bandwidth depends on the degree of the disorder. Ferroelectric behavior of these materials within the Curie range can be described by considering the crystal as a collection of small regions, each having normal ferroelectric features with different Curie temperatures [28]. Other features like lorentz parameter etc. may vary from region to region and the macroscopic properties of the crystal depend on the

average behavior over the entire volume. The factors which may affect the ferroelectric behavior of the crystal undergoing diffused phase transition (DPT) are as follows:

(1) Macroscopic inhomogeneties due to errors in fabrication techniques.

(2) Microscopic inhomogeneties due to compositional fluctuations.

(3) Thermal polarization.

(4) Relaxation polarization

(5) Lattice defects

1.5. Poling

Poling is a process during which a high electric field is applied on the ferroelectric ceramic sample to enforce the domains to reorient in the direction of the applied electric field. The poling is possible only in ferroelectric materials and poling steps are shown in *Fig 1.7.* Before poling, the ferroelectric ceramic does not possess any piezoelectric and pyroelectric properties owing to the random orientation of the ferroelectric domains. For domain reorientation, a poling field must be applied on the sample and maintained for certain duration of time. For a given field and poling time, better domain rearrangement is achieved at higher temperature, but lower than T_c. This happens because with the increase in poling temperature, crystalline anisotropy and coercive field, E_c, of the ferroelectric materials decreases. Also, with increasing temperature, space charges, which act against domain motion, decreases in ceramic materials. However, when the poling temperature is too high, problems arise as the electrical conductivity increases and the consequent increase in leakage current would result in sample breakdown during the period of poling. Sample is allowed to cool to room temperature with the field applied and field is removed at room temperature. After poling, a remanant polarization and remanant strain are maintained within the material, and it starts exhibiting piezoelectric and pyroelectric effects [4].

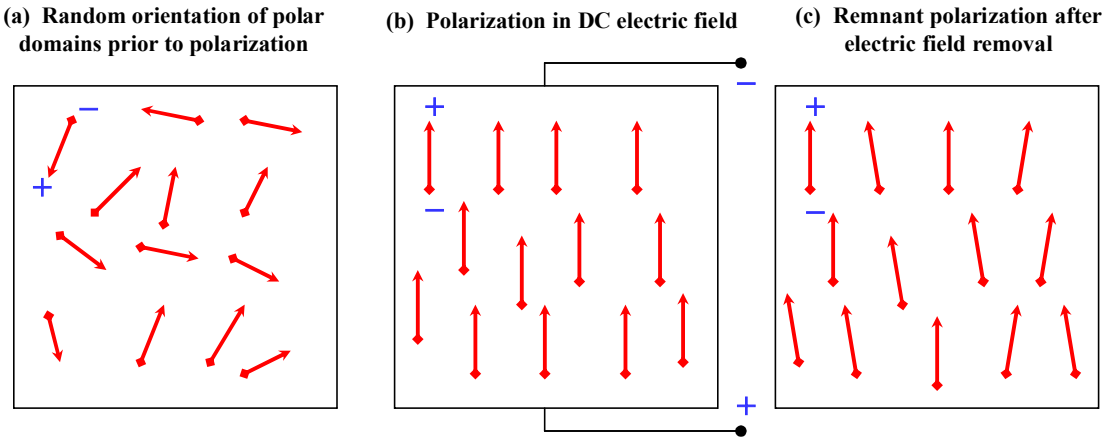

Fig. 1.7. Poling steps in a ferroelectric material.

1.6. Piezoelectricity

The pioneering work on the direct piezoelectric effect in Rochelle salt was presented by Jacques and Pierre Curie in 1880. The word 'piezoelectricity' originates from the Greek word 'piezo', which means 'pressure'. The piezoelectric material develops a potential across its boundaries when subjected to a mechanical stress (or pressure), the effect is called direct piezoelectric effect. This property is exploited to make sensors. Conversely, when an electric field is applied to the material, a mechanical deformation takes place, the effect is known as converse piezoelectric effect and the material can be exploited to make actuator. Thus a piezoelectric material [29] can be used both as sensor and actuator and hence often referred to as smart material. These materials are being used extensively in smart systems, which consist of a sensor, actuator and control system.

These materials are generally physically strong and chemically inert, and they are relatively inexpensive to manufacture. The composition, shape and dimensions of a piezoelectric ceramic element can be tailored to meet the requirements of a specific purpose. For a material to exhibit piezoelectric properties, it must have a permanent dipole and lack a center of symmetry on the atomic scale. The examples of piezoelectric materials include tourmaline, quartz, lead titanate, lead zirconate titanate and barium titanate. Ceramics manufactured from formulations of lead zirconate / lead titanate exhibit greater sensitivity

and higher operating temperatures, relative to ceramics of other compositions, and lead zirconate titanate (PZT) materials currently are the most widely used piezoelectrics.

1.6.1. Mechanism

In a piezoelectric crystal, the positive and negative electrical charges are separated, but symmetrically distributed, so that the crystal overall is electrically neutral.

When some stress is applied, this symmetry is disturbed and the charge asymmetry generates a voltage. Converse piezoelectricity is also revealed by ferroelectrics where application of an electrical field creates mechanical stress (distortion) in the crystal. Because the charges inside the crystal are separated, the applied voltage affects different points within [30] the crystal differently, resulting in the distortion.

1.6.2. Piezoelectric Parameters

The piezoelectric parameters that are of interest when considering the electromechanical effects in piezoelectric materials are the piezoelectric charge coefficients (d_{31}, d_{33}), the piezoelectric voltage coefficients (g_{31}, g_{33}) and the piezoelectric/electromechanical coupling factors (k_{31}, k_{33}, k_p and k_t).

Piezoelectric ceramic is anisotropic and physical constants relate to both the directions of the applied mechanical or electric force and the directions perpendicular to the applied force. Consequently, each constant generally has two subscripts that indicate the directions of the two related quantities, such as stress (force on the ceramic element / surface area of the element) and strain (change in length of element / original length of element) for elasticity. The direction of positive polarization usually is made to coincide with the Z axis of a rectangular system of X, Y, and Z axes. Direction X, Y, or Z is represented by the subscript 1, 2, or 3, respectively, and shear about one of these axes is represented by the subscript 4, 5, or 6, respectively as shown in *Fig. 1.8.* The definitions of the most frequently used constants and equations for determining and interrelating these constants, are summarized here.

The piezoelectric charge constant, *d*, the piezoelectric voltage constant, g, (defined in following sections) and the permittivity, ε, are temperature dependent factors.

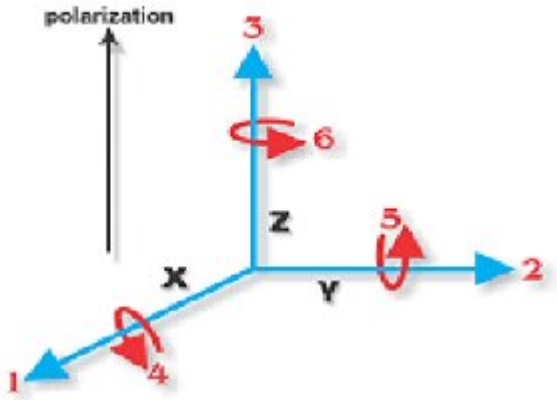

Fig. 1.8. Notation of axis for a poled piezoelectric element.

1.6.2.1. Piezoelectric Charge Coefficient (d)

When a piezoelectric material is subjected to stress, electric charge is generated on the surface. The charge generated per unit force is called piezoelectric charge coefficient and is denoted by '*d*' which is measured in pico-coulomb/Newton (pC/N). High value of d is required for devices such as sonar, ultrasonic cleaner, transducer etc. Piezoelectric charge coefficient [26] is a directional property and is usually specified with subscripts to identify the conditions under which it is determined for e.g., d_{33} and d_{31}. In these piezoelectric charge coefficients, first subscript corresponds to the direction of the applied stress and second corresponds to the direction of the faces of the ceramic on which charges are developed.

1.6.2.2. Hydrostatic Charge Coefficient (d_h)

It corresponds to the effect of development of charge when some pressure is applied on the material. Hydrostatic charge coefficient (d_h) (measured in Coulomb/Newton (C/N) is related to d_{33} and d_{31} piezoelectric charge constants by the relation,

$$d_h = d_{33} + 2d_{31} \qquad \text{.....(1.6)}$$

1.6.2.3. Piezoelectric Voltage Constant (g)

It gives the field produced by a stress in a piezoelectric material. Its usual units are meter volts / Newton (mV/N) and '*g*' constant is related to '*d*' constant by the permittivity as according to relation *1.7*,

$g = d / (\varepsilon' \varepsilon_o)$ .....(1.7)

where g is called the piezoelectric voltage coefficient, ε′ and ε_o are the dielectric constant of the material and permittivity of the free space, respectively. Corresponding to d_{33} and d_{31} piezoelectric constants, there exist g_{33} and g_{31} piezoelectric voltage coefficients. High '*g*' constant is desirable in materials intended to generate voltages in response to a mechanical stress, as in a phonograph pickup.

1.6.2.4. Hydrostatic Voltage Coefficient (g_h)

It gives the field produced by a pressure. It units are meter volts/Newton (mV/N) and it is related to the g_{33} and g_{31} piezoelectric charge coefficients by the relation,

$g_h = g_{33} + 2g_{31}$ .....(1.8)

1.6.2.5. Electromechanical Coupling Factor (k)

Another important parameter of piezoelectric material is the electro-mechanical coupling factor k, which reflects the efficiency of a material. It gives us the measure of the part of the applied electrical energy converted into mechanical energy or vice-versa and it is measured by resonance method [31]. Since conversion of electrical energy into mechanical energy or vice versa is always incomplete, *k* is always less than unity.

$$k^2 = \frac{\text{Mechanical energy converted into electrical energy}}{\text{Input Mechanical energy}}$$ .....(1.9)

The value of k is calculated using the relation:

$k = (1/p((f_a^2 - f_r^2)/f_a^2))^{1/2}$ .....(1.10)

where '*p*' is a numerical factor depending on mode of vibration.

Depending on the mode of energy conversion, there exist various electromechanical coupling factors, for example k_p, k_t and k_{33}. Here, k_p is planar coupling coefficient, related to the energy conversion, when the applied electric field is perpendicular to the generated mechanical vibrations, which are along the plane. Some of the typical values of the k_p are: Quartz: 0.1; $BaTiO_3$: 0.4 and for PZT it lies between 0.5 to 0.7.

For disc shaped ceramics, k_p is typical parameter used for comparing coupling efficiency of the materials. The planar component is used because the stress is two dimensional isotropic. On the other hand radial tension/compression in the plane is perpendicular to poling axis [32]. It is most readily measured by determining the frequency difference between maximum impedence (parallel antiresonance, f_a) and minimum impedence (series resonance, f_r) of an electrode ceramic disc in an electrical circuit [33].

The value of k_p actually signifies the coupling efficiency of electrical and mechanical energies in a thin disc. If the thin disc is polarized in thickness and vibrating in radial expansion and contraction with p equal to 0.79, equation *1.10* becomes

$$k_p = (1.265\ (f_a^2 - f_r^2)/f_a^2))^{1/2} \qquad \text{……..(1.11)}$$

k_t is thickness coupling factor related to the energy conversion, when the applied electric field is in the direction of generated mechanical vibrations and which are along the thickness in the material. Large k_t and small k_p in a piezoelectric material exhibits huge anisotropy behavior. Due to large anisotropy, transverse modes get suppressed resulting in the prevention of pickups due to transverse mode.

1.7. Ferroelectrics for Commercial Applications

Ferroelectric materials have numerous applications. In this section, a brief summary of the major applications is described.

1.7.1. Capacitors

Ferroelectrics have an additional dipolar contribution to their dielectric response as a result of their spontaneous polarization. This dipolar contribution along with the extrinsic domain wall response makes ferroelectrics some of the highest known dielectric constant materials with ε_r values ranging from 5,000 (single crystal $BaTiO_3$ at room temperature) to >50,000 (for some relaxor compositions). However, the strong dependency of dielectric properties on temperature, especially near phase transitions, is needed for many applications. Thus much research is focusing on discovering dopants that will shift T_c, suppress the transition, or create relaxor behavior. Compositionally modified $BaTiO_3$ material is probably

the most successful example and is exploited almost exclusively in the multilayer capacitor industry [4, 34]. PZT also has potential for being exploited in capacitors applications [35].

1.7.2. Tunable Dielectrics

Ferroelectrics also exhibit the property of dielectric tunabilty (change in capacitance/permittivity with applied dc voltage/field). This property makes ferroelectrics attractive for tunable high-frequency solid-state devices. By tuning the dielectric component in an RF circuit, high-frequency signals can be systematically selected, for instance, a miniaturized frequency-tunable filter/antenna [34]. Ferroelectric thin films are especially attractive because of their compatibility with CMOS technology and the low voltages required for tuning. $(Ba,Sr)TiO_3$ has been extensively evaluated because of its high tunability but low dielectric loss in the paraelectric state [37].

1.7.3. Opto-Electronic Devices

The reorientable dipoles of ferroelectric materials create a strong electro-optic response (the refractive index changes with applied electric field). This property can be exploited to fabricate optical wave devices like filters and switches. The prime requirement is that of transparent ferroelectric. Thus, the elimination of porosity and other light scattering centers is crucial. The examples of opto-electronic ferroelectrics include $LiNbO_3$, $(Pb,La)(Zr,Ti)O_3$ (PLZT) and $LiTaO_3$ [36].

1.7.4. Piezoelectric Applications

Ferroelectrics are attractive as piezoelectric materials because of their high piezoelectric coefficients. The quartz has a d_{11} values of ~2 pC/N while PZT has a d_{33} value of >250 pC/N [32]. In addition, the electromechanical coupling coefficient (k^2) for ferroelectrics can be above 0.8 [4], where k^2 describes the ratio of electrical energy converted to mechanical energy or vice versa.

Because ferroelectrics can be poled, they offer the additional advantage of not requiring single crystal or highly-oriented material production; simple ferroelectric ceramics can be made piezoelectric [4, 25]. Consequently, piezoelectric ferroelectrics have been used in gas igniters, ultrasonics, and inkjet printer heads. Thin film ferroelectrics have been especially

appealing for surface acoustic wave filters and actuation/sensing in microelectromechanical (MEMS) systems.

1.7.5. Non-Volatile Memory

Because the polarization state of a ferroelectric can be switched between (at least) two directions, ferroelectric polarization can be used as a form of binary storage. Furthermore, because a ferroelectric maintains a remanent polarization at zero bias, this memory would require no refreshing, it is non-volatile. This application presumes that the polarization is strong enough to be read, easily switchable, and varies little with cycling or time. PZT has been proposed to be a good candidate for memory applications as well.

1.8. Perovskite Structure

The perovskite-type ferroelectrics have been extensively studied due to the simplicity of the perovskite structure, and the relatively common occurrence of ferroelectric behavior in perovskites.

A perfect perovskite crystal with the general formula, ABO_3, is cubic. It consists of corner sharing oxygen octahedra (BO_6) arranged in three dimensions. The larger A cations, monovalent or divalent metal (A: Na^+, K^+, Ca^{2+}, Ba^{2+}, Pb^{2+} etc.) are on the corners of the unit cell. The smaller B cations, tetravalent or pentavalent metal (B: Ti^{4+}, Zr^{4+}, Sn^{4+}, Nb^{5+}, Ta^{5+}, W^{6+} etc.) are at the body center. The oxygen atoms are at the face centers of the cube [3]. The prototype shape of the perovskite which is the cubic one (paraelectric phase) is shown in *Fig. 1.9.(a)*. The packing situation of the perovskite structure may be characterized by a tolerance factor *t* which can be calculated as given below:

$$t=(R_A+R_O)/\sqrt{2}(R_B+R_O) \qquad \ldots\ldots(1.12)$$

where R_A is ionic radii of A site cations, R_B is ionic radii of B site cations and R_O is ionic radii of anion in equation *1.12*. If *t* is equal to 1, the packing is said to be ideal. If *t* is larger than 1, there is too large a space available for B ion, and therefore, this ion can move inside its octahedron. In general, *t* should be $0.9 < t < 1.1$ to form a stable perovskite structure. The

cubic lattice is tetragonally distorted below the curie temperature (*Fig. 1.9(b)-(c)*), which is a displacive ferroelectric phase transition. Some materials also exhibit a rhombohedral ferroelectric phase [3]. It is the off-centered position of the B cation that leads to ferroelectric and antiferroelectric behavior. The B cations have two stable positions relative to the neighboring ions. A potential barrier separates one position from the other. The ion can change positions if enough energy is supplied to the system to allow the ion to surmount the barrier.

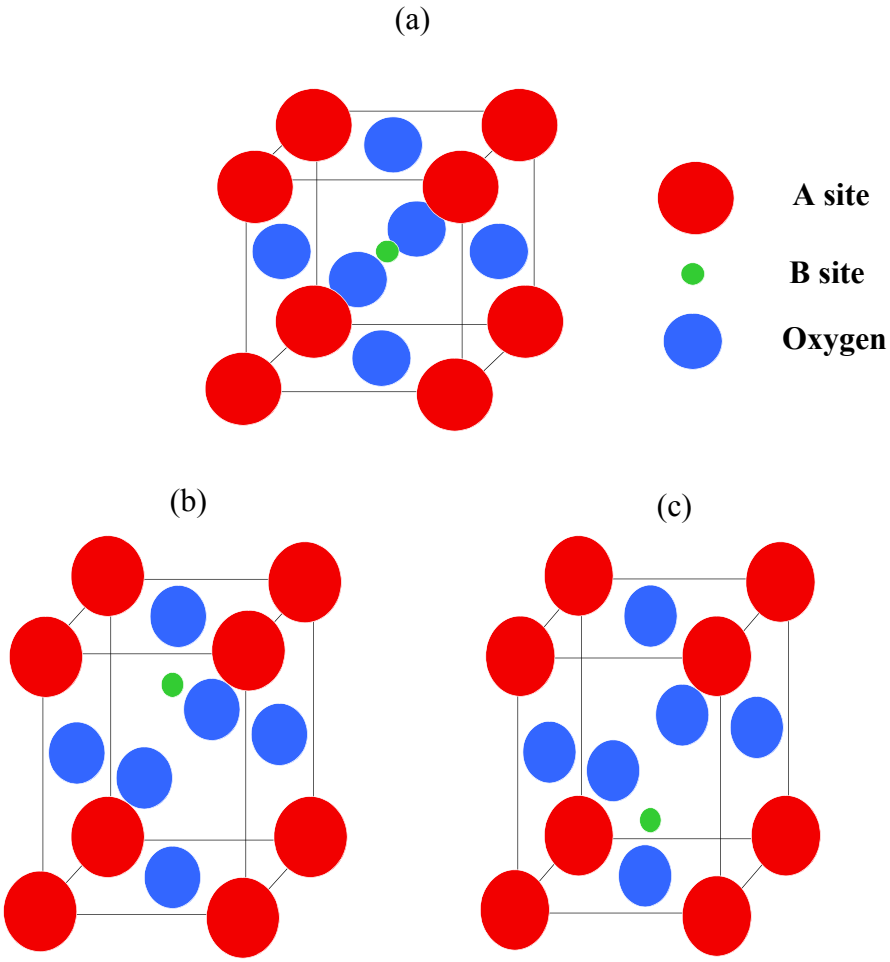

Fig. 1.9. The **(a)** cubic **(b)** tetragonally distorted perovskite crystal cells with up and **(c)** down polarized B atoms.

For a single unit cell of lead zirconate titanate, potential barrier is less than thermal energy at room temperature, so the ion is free to move back and forth. In a crystal, however, the unit cells couple electrically and physically to form domains, as discussed in Section 1.3, for which the energy barrier to switching is much higher than for the single cell [38]. There are several useful ferroelectric oxide materials such as barium titanate ($BaTiO_3$), lead titanate

($PbTiO_3$), lead zirconate titanate ($Pb(Zr,Ti)O_3$) and potassium niobate ($KNbO_3$) which have the perovskite-type structure. In the following sub-section 1.8.1., $Pb(Zr,Ti)O_3$ having perovskite structure is discussed in detail.

1.8.1. Lead Zirconate Titanate

The solid solution lead zirconate titanate, $Pb(Zr_x,Ti_{1-x})O_3$ ($0<x<1$), called PZT, is the most widely utilized ferroelectric ceramic material. This section contains a description of lead zirconate titanate and the effects of dopants on its various properties in varying compositions.

Lead titanate ($PbTiO_3$) is a commonly studied perovskite ferroelectric material which exhibits ferroelectric phase transition [3] and shows good polarization characteristics [39]. Lead zirconate ($PbZrO_3$) is a perovskite which exhibits characteristic antiferroelectric behavior. In an antiferroelectric crystal, neighboring lines of ions displace in opposite directions, creating a zero net polarization that is different from the zero net polarization caused by the random alignment of ions in an unpolarized ferroelectric crystal [40]. When applied field is high, antiferroelectric crystals behave like ferroelectric crystals. The Ti^{4+} ions in $PbTiO_3$ can be partially substituted by Zr^{4+} with a molar ratio x to form a binary system (solid solution) with the following chemical formula $Pb(Zr_xTi_{1-x})O_3$. This solid solution is called lead zirconate titanate (PZT). It also belongs to the perovskite-type ferroelectrics. In this solution, Zr^{4+} and Ti^{4+} occupancy on the B site cation positions is random. PZT compositions possess the advantageous combination of properties such as (1) high electromechanical coupling coefficient; (2) relatively high curie temperature (T_c), which permits operation at temperature up to 200 °C; (3) wide range of dielectric constants; (4) capability to form solid-solutions with many different compositions, thus allowing a wide range of property modifications; (5) can be easily poled and (6) can be sintered at relatively low temperature [5]. PZT is especially attractive for material properties designing. Wide range of physical properties can be obtained by variation of Zr/Ti ratio, particularly in so-called morphotropic phase boundary (MPB) region. The ferroelectric region of the phase diagram consists mainly of two different regions, one the Zr-rich rhombohedral region, (F_R) that contains two phases with space groups R3m and R3c, and the other Ti-rich tetragonal

region (F_T), with space group P4mm. The two regions are separated by a boundary that is nearly independent of temperature, the MPB mentioned above, which lies at a composition close to x=0.48 as illustrated by the phase diagram in *Fig. 1.10.* [42]. Most of the ferroelectric related properties in PZT such as piezoelectric response and remanent polarization approach to a maximum near this MPB. The strong piezoelectric response and ease in poling near the MPB is a result of the domain structure. At the MPB, both the tetragonal and rhombohedral distortions are thermodynamically stable. Within the MPB region, the 6 domain states of the tetragonal coexist with the 8 domain states of the rhombohedral phase. This results in 14 possible directions for the spontaneous polarization in the unit cell as all 180°, 90°, 109° and 71° domain walls are active. Thus, the extraordinary ability of PZT at the MPB to re-orient its polarization allows it to retain a large remanent polarization. Moreover, the activity of 3 non-180° domain walls creates a large extrinsic contribution to its piezoelectric response [25].

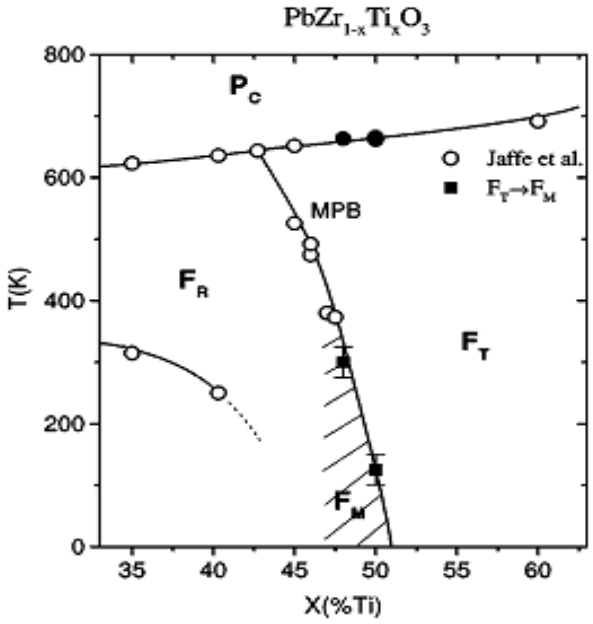

Fig. 1.10. Phase diagram of the $PbZrO_3$ / $PbTiO_3$ solid solution system (modified) [42]. The data of Jaffe et al. [4] are plotted as open circles. The F_T-F_M and P_C-F_T transition temperatures for x=0.48 and x=0.50 are plotted as solid symbols [42].

The PZT phase diagram of Jaffe et al. [4] which covers only temperatures above 300 K has been accepted as the basic characterization of the PZT solid solution. But recently, another feature of the morphotropic phase boundary has been revealed by the discovery of a

ferroelectric monoclinic phase (F_M) in the $Pb(Zr_{1-x}Ti_x)O_3$ ceramic system. From a synchrotron x-ray powder diffraction study of a composition with x=0.48, a tetragonal-to-monoclinic phase transition was discovered at 300 K. The space group is C_m, and the temperature dependence of the monoclinic angle gives immediately the evolution of the order parameter for the tetragonal-monoclinic (F_T-F_M) transition [42].

In order to modify properties of PZT for specific application, dopant or modifier are used to optimize and improve their basic properties for specific applications [4, 43]. These modifiers create various types of defects in the crystal structure which results in significant changes in domain structures and electromechanical properties. These defects may result in increased coercive field, E_c or an internal biasing of the hysteresis loop if they are randomly distributed or the defect dipoles have the same orientation respectively. There are generally three types of modifiers.

(i). Isovalent additives are the ones in which the substituting ion has same valency and has approximately the same size as of the replaced ion such as Sr^{2+}/Ba^{2+} replacing Pb^{2+} or Sn^{4+} replacing (Zr^{4+},Ti^{4+}). These substituents usually lead to inhibited domain orientation and poorly developed P-E hysteresis loops, lower dielectric loss, low compliance, and higher ageing rates. Ba modified PZT exhibit deteriorated ferroelectric, dielectric and piezoelectric properties with increase in Ba^{2+} content in place of Pb^{2+} ion [44]. These modifiers are used to change curie temperature for some applications. For example, the transition temperature of Sr-modified PZT ceramics decreases about 9.5^oC per each atomic percent of Sr concentration [45].

(ii). The donors are compensated either by A site vacancies or by electrons and can reduce the p-type conductivity of the PZT by as much as 3 orders of magnitude such as La^{3+}/Sm^{3+} replacing Pb^{2+} or, Nb^{5+} replacing (Zr^{4+},Ti^{4+}). These additives/substituents in combination with corresponding vacancies enhance domain orientation with respect to undoped material. Ceramics produced with these additives are characterized by square hysteresis loops, high dielectric constant and dielectric loss, improved piezoelectric properties, reduced ageing, high mechanical compliance and easy depoling. These type of ceramics are called 'Soft PZT's' and dopants are called softeners [4, 46].

Material compositions like PMN-PT, $Pb(Mg_{1/3},Nb_{2/3})O_3$ exhibit relaxor ferroelectric behavior. Curie temperature is dependent on frequency which characterizes ferroelectric

relaxors. Relaxors are characterized by a very slim P-E hysteresis loop, small E_c, no remanent polarization, higher dielectric constants than soft ferroelectrics, and null piezoelectric constants. If high concentrations of softeners (La^{3+}) are added in PZT, for instance PLZT 10/65/35, then it also exhibits relaxor behavior [47].

Table 1.1.

Comparison of effect of doping on various properties of soft, hard and relaxor PZT ferroelectrics.

S.No.	Property	Soft Ferroelectrics	Hard Ferroelectrics	Relaxor Ferroelectrics
1	Dielectric constant	Increases	Decreases	Increases more
2	Dielectric loss factor	Increases	Decreases	-
3	Hysteresis loss	Increases	Increases more	Very small hysteresis loss
4	Elastic compliance	Increases	Decreases	-
5	Piezoelectric planar coefficients	Increases	Decreases	Null Piezoelectric planar coefficients
6	Electrical resistivity	Increases	-	-
7	Mechanical loss factor	Increases	-	-
8	Coercive field (E_c)	Decreases	Increases	Increases more
9	The Curie point (T_c)	Decreases	Increases	Increases more (Frequency dependence of T_c)
10	Remanent polarization (P_r)	Increases	Decreases	No Remanent polarization
11	Remanent strain	decreases	Increases	No Remanent strain

(iii). The acceptors are compensated by oxygen vacancies and usually have only limited solubility in the lattice such as Na^+/K^+ replacing Pb^{2+} or Fe^{3+}/Mn^{2+} replacing (Zr^{4+}, Ti^{4+}). These additives lead to opposite effects to those of donors. Ceramics with acceptor additives are characterized by poorly developed hysteresis loops as domain reorientation is limited, lower dielectric constant and dielectric losses, low piezoelectric properties, higher ageing rate, low compliances and difficult to depole. These ceramics are referred as 'Hard PZT's' while the dopants are termed as hardeners [4]. *Table 1.1.* depicts the comparison between soft, hard and relaxor ferroelectric PZTs showing the opposite trend in various properties.

1.9. Background of the Proposal

In lead based perovskite compounds, such as PMN-PT, PNN-PZT, PZT and PLZT very useful properties have been observed for commercial device application. Among these, PZT is a promising material for its use in piezoelectric transducers, ferroelectric memories, electro-optic and pyroelectric devices. For memory applications, hysteresis behaviour is exploited. A huge temperature dependence of spontaneous polarization near phase transition temperature (T_c) is observed for these materials. Material with high T_c and piezoelectric coefficient (d_{33}) is required for actuator applications. Suitably modified PZTs show excellent electro-optic properties and these materials are the key components in displays and optical communication systems.

PZT is also called "smart material" as it can be used for sensors and actuators both. However, these compositions have an obvious disadvantage of volatility and toxicity of 'lead'. Modified lead titanate zirconate powders have also attracted interest, owing to their good ferroelectric and pyroelectric properties. In general, with the amount of dopant content, the compositional modification (doping) by single dopant leads to unstable electrical properties with drastic variations for the PZT ceramics. Soft and hard PZT ceramics are commercially available and widely employed in various applications. The complex doping of two or more elements is expected to combine the properties of donor doped and/or acceptor doped PZT, which could exhibit better stability or improved piezoelectric and dielectric properties than those of the single element doped PZT.

C. Prakash and O. P. Thakur [48] investigated effect of Sm modification on structural and dielectric properties of PLZT ceramics fabricated by double sintering route. With increasing Samarium concentration (x) in $Pb_{0.925-x}Sm_xLa_{0.075}(Zr_{0.20}Ti_{0.80})_{0.981}O_3$, density decreases. The dielectric constant was found to increase while curie temperature and loss decreases significantly with increasing Sm content. Pyroelectric coefficient was observed to be maximum 3.8 x 10^{-4} for x=0.015. R. Ranjan et. al. [49] studied $Pb_{1-x}Sm_x(Zr_{0.55}Ti_{0.45})_{1-x/4}O_3$ (PSZT) (x = 0.00, 0.03, 0.06 and 0.09) ceramics synthesized by mixed oxide method. Dielectric analysis reveals that these tetragonal compounds have transition temperature well above the room temperature. The diffusivity of compounds exhibited the values between 1 and 2 indicating the greater disorder in the system. The temperature dependence of ac

conductivity indicated that the conduction process is due to singly ionized (in ferroelectric region) and doubly ionized (in paraelectric region) oxygen vacancies. The electrical studies done by S.R. Shannigrahi et al. on modified PZT (PRZT 8/60/40, R= Nd, Sm, Eu, Gd, Dy, Er, La, Yb) with various dopants have revealed that these materials can be considered as good dielectric materials as they possess high dielectric constant and low dielectric loss [50]. Tetragonal PRZT compounds lead to a stable ferroelectric state over a wide range and the phase transition in these materials is diffuse-type and of second order. The results of piezoelectric measurements show that these compounds are of soft type and suitable for phonographic pick-up and similar devices.

The polycrystalline samples [51] of $Pb_{1-x}Sm_x(Zr_{0.60}Ti_{0.40})_{1-x/4}O_3$ (PSZT) where x=0.00, 0.03, 0.06 and 0.09 were studied by R. Ranjan et al. by high-temperature solid-state reaction technique. The impedance analysis of single phase tetragonal crystal system indicates the presence of bulk resistive contributions in the materials which is found to decrease on increasing temperature. The nature of variation of resistances with temperature suggests a typical negative temperature coefficient of resistance (NTCR) type behavior of the materials.

J. E. Garcia et. al. [52] experimentally studied dielectric and direct piezoelectric responses in doped and undoped PZT (Zr/Ti: 60/40, 53/47, 40/60). The correlation between the dielectric constant and dielectric losses is discussed in terms of the Rayleigh law. Only materials in rhombohedral phase or in morphotropic phase boundary doped with donor impurities fit adequately with the Rayleigh model. Donor impurities considerably increase the mobility of domain walls and also the dielectric and piezoelectric non-linear response as rise in the dielectric constant and losses in relation to the pure material is observed while the hardener impurities produce a decrement of them. Single phase tetragonal polycrystalline compounds $Pb_{0.92}(La_{0.1}Fe_{0.9})_{0.08}(Zr_{0.60}Ti_{0.40})_{0.98}O_3$ (PLFZT) were fabricated by S. Dutta et al. [53] by traditional solid state route. The Cole–Cole plots indicate that the dielectric phenomenon of PLFZT is due to conductive grain boundaries. The temperature variation of real permittivity gives evidence of the ferroelectric phase transition as well as of the relaxation behavior. The dielectric processes in the materials have been shown to be due to the existence of relaxation and resonance polarization and thermally activated flips of polar regions.

Gerson [54] showed that electro-mechanical properties of PZT ceramics could be tailored by adding small quantities of tri or pentavalent ions (e.g. La, Nd, Ta or Nb) at the Pb sites. Among various dopants at the A sites of PZT unit cell, La^{3+} ion is the most suitable for many piezoelectric devices [55–58]. It is reported that Pb^{2+} ions could be substituted by the La^{3+} because of its comparable ionic size [59]. It has been reported that substitution of Pb^{2+} by La^{3+} ion creates vacancies in the A site of perovskite ABO_3 structured PZT ceramics and improves the optical quality of PLZT [60, 61]. With the substitution of La vacancies are believed to break the long-range interaction between ferroelectrically active octahedra containing B site cations [62]. Above a critical La concentration, the decoupling is sufficiently strong such that the macroscopic transformation into a long-range ferroelectric state is destroyed and a state characterized by nanodomains is established. Hence, the macroscopic properties change from normal to relaxor ferroelectric types [63]. The macroscopic properties of relaxors are characterized by a frequency dependent broadening of the dielectric response, and by slim-loop hysteresis behavior near the dielectric maxima [64]. In the relaxor state, it is believed that correlation between polar nanodomains control the macroscopic response characteristics and the freezing of polarization fluctuations into a state with glass-like characteristics [65].

Compositionally, PLZT ceramics exhibit various structures according to La amount and Zr/Ti ratios i.e. tetragonal or rhombohedral or pseudocubic relaxor ferroelectrics or cubic paraelectrics. The rhombohedral crystal structures of PLZT 9/65/35 are found to have DPT (diffuse phase transition) characteristics. The dielectric properties are found to be quite sensitive to the sintering temperature. The dielectric constant increases appreciably with the increase of sintering temperature [66]. Tetragonal PLZT bulk ceramics with composition 9/56/44 possess sufficient optical transparency for optoelectrical device applications [67].

X. Dai et al. [68] systematically studied rhombohedral PLZT 65/35 and 80/20 compositions which demonstrated ferroelectric nature and diffuse phase transition. The evolution of a polar nanodomain state from a normal micron-sized domain state with increasing La content onto the A site of the perovskite (ABO_3) was observed which resulted in interruption of long-range polar order in PZT. The emergence of this polar cluster state was characterized by the onset of strong frequency dispersion in the dielectric response,

indicative of relaxor behavior. The La content that drives the structure into the relaxor state was found to be related to the lattice distortion of the undoped base composition.

Xiang et al. [69] reported reduction of the tetragonality in La modified PZT 52/48 ceramics. Lanthanum substitution has a strong effect on the level of diffuseness of the phase transition. The dielectric peak temperatures shift to lower temperature with increasing lanthanum content. The dielectric properties of 7.6 mol% lanthanum-modified PZT possess a relaxor behavior. Polycrystalline complex compounds of PLZT (x/40/60) with formula $Pb_{1-x}La_x(Zr_{0.40}Ti_{0.60})_{1-x/4}O_3$+10% PbO prepared from the nano-size individual oxides powders by hot-pressed process showed that the grain size increases from 2 to 7 μm when La content increased from 7 to 13 mol.%. The dielectric constant increases with La content increasing and the ferroelectric properties are sensitive to the variation of La content [70]. M. Ichikia et al. proposed electrostatic-optical motor as a new application device that uses photovoltaic lead lanthanum zirconate titanate (PLZT 3/52/48) as an energy transducer from optical energy to electrical energy. It was shown that a poling field over 20 kV/cm is necessary to obtain the electrostatic force of PLZT. The obtained photo and dark conductivities were 6.3×10^{-12} m $\Omega^{-1}W^{-1}$ and 8.8×10^{-10} Ω^{-1}m respectively [71]. The $(Pb,La)(Zr,Ti)O_3$ ceramic with 10% La concentration, being in the near vicinity of morphotropic phase boundary (MPB), has been reported to be good quadratic modulator material [72].

PLZT (14/50/50) film showed the maximum charge density, which is good for DRAM capacitors [73]. L. B. Kong et al. fabricated PLZT 7/60/40 ceramics from their oxide mixture via a direct sintering process in which different levels of excess PbO (0, 10 and 20 mol%) were also used. Their study revealed that this simple one-step process will be favorable for cost reduction and increased productivity of not only ferroelectric but also for other ceramic materials [74]. PLZT 7/60/40 composition is also one of the most important candidates for piezoelectric applications due to its extremely high piezoelectric coefficients (d_{33}=710 pC/N, k_p=0.72) [72, 75-76]. F. Cordero et al. [77] measured an elastic and dielectric susceptibility in two different PLZT compositions relaxor (PLZT9/65/35) and partially ferroelectric (PLZTN 7/60/40) with 0.02 oxygen vacancies. In relaxor PLZT memory, inelastic compliance and dielectric susceptibility are depressed by an increase of O vacancies, while in the ferroelectric, there is no memory unless aging is protracted for long

times. This is considered as evidence that in the relaxor case memory is intrinsic while in the non relaxor case it is due to slow migration of defects.

D. Kuscer et al. [78] studied orthorhombic lanthanum modified lead zirconate titanate (PLZT) with a lanthanum content of 6 and 10 mol% in PZT (90/10) as a function of A- and B-compensation model. The densification of B site compensated PLZT occurs at lower temperatures and leads to higher density when compared to A site compensated PLZT. The dielectric response characteristics of the A- and B-compensated PLZT are comparable, indicating that a small amount of PbO liquid phase does not deteriorate the dielectric constant of PLZT. The lattice parameters of both compositions of the A- and B-compensated ceramics do not vary significantly. H. J. Kleebe et al. [79] emphasized the fact that the in $PbZr_{0.6}Ti_{0.4}O_3$ material solubility limit of Fe^{3+} is approximately 1.0 mol *%*. EDS analysis revealed an enrichment in iron and a depletion in lead in grains of 3 mol% Fe^{3+} doped PZT. Selected area diffraction (SAD) in conjunction with EDS analysis allowed the unequivocal identification of the crystalline secondary phase magnetoplumbite ($PbFe_{12}O_{19}$) in PZT with 3 mol% Fe. This composition behaves as a composite material as iron-doping is above the solubility limit in ferroelectric PZT (60/40) and this may be regarded as a promising candidate for a multiferroic material.

Compositionally modified PZT (53/47) doped with $La^{+3}$and Nb^{+5}, and both the softeners, i.e., La^{+3} and/or Nb^{+5}, and hardener, Fe^{+3} ceramics were prepared B. W. Lee et al. [80]. As Fe ion content increased in the La and/or Nb doped PZT, Q_m increased while k_p and ε_r values decreased. The improved piezoelectric properties, i.e., enhanced Q_m with remaining higher k_p were obtained in the PZT compositions doped with La^{+3} and Fe^{+3}. For 1.0 mol% La and 2.0 mol% Fe doped PZT composition, relatively high Q_m and k_p values of 580 and 0.53, respectively, were obtained. A strong influence of dopants on grain size is observed by M.D. Durruthy-Rodriguez et al. [81] as concentration of La, Nb and La+Nb grows in PZT (54/46). The substitution at A site and the simultaneous substitutions in the A and B site lead to mixture of tetragonal and rhombohedral phases, while substitution in the B place, the structure is tetragonal at least in 95%. Substitutions on the B site contribute more significantly to the Curie temperature drop, with a minimum for PZTN 0.8%.

Lot of work has been done on different kinds of modifications of Mn at A/B sites of PZT both in forms of thin films and bulk. Though some work has already been reported on

the substitution of Mn at the Zr site of PZT [82–86]. The polycrystalline samples of $Pb(Zr_{0.65-x}Mn_xTi_{0.35})O_3$ (x= 0, 0.05, 0.10, 0.15) (PZMT) were prepared by B. Tiwari and R. N. P. Choudhary [87] by conventional solid-state reaction method. Structural analysis of compounds confirmed single-phase rhombohedral structure for Mn substituted samples. Microstructural analysis of the surface of the compounds by scanning electron microscopy (SEM) exhibits that there is a significant change in grain size on introduction of Mn at the Zr-site. SEM micrographs reveal that except for the slight increase in grain size at 0.10% of Mn doping grain size shows a decreasing trend with increase in Mn concentration. The reason for the decrease of both the crystallite and the grain sizes can be attributed to segregation of Mn at grain boundaries. The existence of low frequency dispersion indicates that the charge carriers may be either ionic or electronic in nature. Mn doping increases ε_r, T_c and $tan\delta$. The ac conductivity also showed an improvement in modified PZT with increase in Mn concentration at all frequencies. Modulus analysis by nondestructive complex impedance spectroscopy (CIS) technique indicated the presence of a single phase, non- Debye type of conductivity relaxation and possibility of hopping mechanism for electrical transport processes in some of the Mn substituted samples [88].

The ferroelectric, dielectric and piezoelectric properties of Ce doped PZT (60/40) compositions have been reported by B. Sahoo et al. The XRD analysis shows the presence of rhombohedral phase up to 2 mol% ceria while tetragonal phase is found at higher amount of Ce. The ferroelectric, dielectric and piezoelectric properties increase with the addition of ceria with a maximum at 2 mol% and then decrease. The higher piezo properties associated with low ceria concentration are attributed to rhombohedral phase [89]. The effect of Pr substitution at the Pb site on the structural and electrical properties of the $(Pb_{1-z}Pr_z)(Zr_{0.60}Ti_{0.40})_{1-z/4}O_3$ (z= 0.07, 0.08, 0.10) compositions is reported by S.R. Shannigrahi et al.. The compositions possess tetragonal structure, exhibit ferroelectric DPT. The transition temperature, P_r and E_c decreases with increase of Pr^{3+} ions. These compositions have potential for device applications around the room temperature range [90]. V.A. Chaudhary et al. reported that lattice parameters, unit cell volume, theoretical density and porosity all vary with Zr content in $PbZr_xTi_{1-x}O_3$ where x=0, 0.2, 0.4, 0.6, 0.8, 1.0. The activation energy was found to decrease with increase in Zr content [91]. The temperature dependence of the crystalline structure and the lattice parameters of $Pb_{1-x}La_xZr_{0.40}Ti_{0.60}O_3$ ferroelectric ceramic

system with $0.00 \leq x \leq 0.21$ was investigated by A. Mesquita et al. [92]. The samples with $x \leq 0.11$ show a cubic-to-tetragonal phase transition while for x=0.12 sample, a spontaneous phase transition from a relaxor ferroelectric state (cubic phase) to a ferroelectric state (tetragonal phase) is observed upon cooling below the T_{max} indicating increase in tetragonality.

It has been ascertained from the exhaustive literature survey that the compositional variation in the chemical formula resulting from the substitution of rare earth elements, other dopants and the ratio of Zr/Ti is the major tool for controlling the properties of these materials over a wide range. Dielectric and piezoelectric properties are of prime importance and are in general dependent on structural properties besides its chemical composition. As already discussed, the highest electromechanical properties of PZT ceramics occur near the MPB. However, for better reproducibility of material properties, it is desirable to obtain ceramics with composition slightly distant from the MPB region so that the properties are less dependent on fluctuation of the Zr/Ti ratio, and therefore, would vary less from one composition to other.

1.10. Proposed Objectives of the Present Work

The compositionally modified lead zirconate titanate (doped-PZT) ceramics with their improved electrical properties are widely utilized in the dielectric and piezoelectric applications. The properties can also be tailored over wider range by changing the dopants concentrations. La and Sm can be exploited as A site substituents because ionic radii (in 12 coordinates) of La^{3+} (1.50 Å) and Sm^{3+} (1.38 Å) is smaller than Pb^{2+} (1.63 Å) [93]. The most significant recent application involves incorporating ferroelectrics into silicon devices. The high dielectric constant materials are being developed for increased charge storage in a smaller area in memory chips. The ability of ferroelectrics to exist in two different polarization states in the absence of field is being used for non-volatile ferroelectric memories. It is revealed form literature survey that La and Sm addition in PZT improves the dielectric and ferroelectric properties hence PZT can be used for charge storage and non-volatile ferroelectric memory devices. The high dielectric constant values of substituted PZT are used in ever smaller multi-layer ceramic capacitors. La substitution has been reported to

improve piezoelectric properties of PZT making it a potential candidate for actuator application. In La-substituted PZT (for high enough La concentration) the substitution of La^{3+} for Pb^{2+} at the A sites produces randomly distributed Pb^{2+} vacancies (one vacancy for every two La^{3+} ions) which lead to a relaxor state. Relaxors are especially utilized for this purpose not only because of their very high dielectric constants but because of occurrence of those high values at near room temperature and show gradual temperature dependence.

The introduction of Mn at B site is done as ionic radii of Mn^{4+} (0.67 Å) (in 6 coordinates) is smaller than that of Zr^{4+} (0.86 Å)/Ti^{4+} (0.74 Å) [93]. It has been reported to obtain the lower dielectric loss, higher electromechanical coupling factor (k_p) and higher quality factor (Q_m). It is clear from the literature survey that complex doping is a useful tool to tailor material properties. The substitution amount of Fe and Nb is restricted to 1 mol %. The solubility limit of Fe in PZT (60/40) is 1 mol% [79]. Fe acts as grain growth inhibitor and 1 mol% of its substitution in addition to other substituents in modified PZT would not lead to drastic variation in material properties. A small amount of Nb in place of Zr/Ti increases bulk resistivity and reduces aging effects [46]. A large amount of work has been carried out on the modified PZT with its variable Zr/Ti ratio but no systematic study has yet been reported on the influence of the combined effect of hard (acceptor, Fe and Mn) and soft dopants (donor, Sm, La and Nb) complex substitution on structural, dielectric, ferroelectric and piezoelectric properties in PZT (60/40). The objective of the subject investigation is to report the systematic comparative study on the crystal structures, microstructures, electric (dielectric, polarization), and piezoelectric properties for better understanding the nature of phase transition in modified PZT 60/40 ceramics. The objectives of the present thesis are as follows:

(i). To synthesize modified Lead zirconate titanate (PZT) compositions and the modifications were carried out by substituents viz. La, Sm, Mn etc.

(ii). To prepare the samples in the form of pellets of synthesized materials by solid state route and to optimize process parameters in order to get good quality dense ceramics.

(iii). To systematically characterize the materials for structural, dielectric and ferroelectric properties. The measurements were carried out at different temperatures.

(iv). To understand the composition-structure-property relationship in synthesized materials.

It is well known that doping is an effective way to further improve the material performance, and keeping in view that the substitution rate and substitution site do play an important role to alter the properties a series of compositions with suitable substituents have been selected for a detailed investigation. The following ceramic compositional series have been prepared by the solid state route.

1. $Pb_{1-x}Sm_x(Zr_{0.60}Ti_{0.40})_{0.98}Fe_{0.01}Nb_{0.01}O_3$ (where x = 0, 0.0025, 0.0050, 0.0075, 0.01, 0.02, 0.04, 0.06, 0.08) (PSZFNT-Series A)
2. $Pb_{1-x}La_x(Zr_{0.60}Ti_{0.40})_{0.98}Fe_{0.01}Nb_{0.01}O_3$ (where x = 0, 0.0025, 0.0050, 0.0075, 0.01, 0.02, 0.04, 0.06, 0.08) (PLZFNT -Series B)
3. $Pb(Zr_{0.60}Ti_{0.40})_{0.98-x}Mn_xFe_{0.01}Nb_{0.01}O_3$ (where x = 0, 0.005, 0.010, 0.015, 0.02) (PZFMNT-Series C)

The structural properties were studied using XRD and SEM, and the dielectric properties over a wide range of temperature at different frequencies have been studied. Ferroelectric and piezoelectric properties were also studied.

References

[1]. R. C. Buchanan, *Ceramic Materials for Electronics*, Marcel Dekker Inc.; New York (1986).

[2]. D. W. Richerson, *Modern Ceramic Engineering*, Marcel Dekker; New York (1992).

[3]. M. E. Lines and A. M. Glass, *Principles and applications of ferroelectrics and related materials,* Oxford university press; New York (2001).

[4]. B. Jaffe, W. R. Cook and H. Jaffe, *Piezoelectric Ceramics*, Academic Press; New York (1971).

[5]. G. H. Haertling, J. Am. Ceram. Soc. **82** (1999) 797.

[6]. P. R. Coursey and K. G. Brand, Nature **157** (1946) 297.

[7]. S. Miyake and R. Ueda, J. Phys. Soc. Jpn. **1** (1946) 32.

[8]. B. M. Vul and I. M. Goldman, Doklady Akademii Nauk SSSR. **46** (1945) 154.

[9]. E. Wainer, Trans. Electrochem. Soc. **89** (1946) 331.

[10]. A. Hippel, R. G. Breckenridge, F. G. Chesley and L. Tisza, Ind. Engg. Chem. **38** (1946) 1097.

[11]. B. M. Vul and I. M. Goldman, Doklady Akademii Nauk SSSR, Seriya A. **49** (1945) 177.

[12]. W. F. Forrester and R. M. Hinde, Nature **156** (1945) 177.

[13]. H. P. Rooksby, Nature **155** (1945) 484.

[14]. B. Jaffe, R. S. Roth and S. Marzullo, J. Appl. Phys. **25** (1954) 809.

[15]. F. John and G. Shirane, *Ferroelctric crystals,* Pergamon; New York (1962).

[16]. B. T. Batthais and A. V. Hippel, Phy. Rev. **73** (1998) 1378.

[17]. B. Wul and I. M. Goldman, C. R. Acad. Sci. U. R. S. S. **46** (1945) 177.

[18]. J. C. Burfoot and G. W. Taylor, *Polar Dielectrics and Their Applications*, Macmillan Press Ltd; London (1979).

[19]. H. Blattner, W. Kanzig, W. J. Merz and H. Sutter, Phys. Acta. **21** (1948) 207.

[20]. S. Stemmer, S. K. Streiffer, F. Ernst and M. Ruhle, Phil. Mag. A **71** (1995) 713.

[21]. D. Damjanovic, *Science of Hysteresis*, Vol.III, Ch.4 (2005) 337.

[22]. I. Bunget and M. Popescu, *Physics of Solid Dielectrics*, Elsevier; New York (1984).

[23]. L. L. Hench and J. K. West, *Principles of Electronic Ceramics*, John Wiley & Sons;

New York (1989).

[24]. G. A. Smolenski, *Ferroelectric and related materials,* Gordan and Breach Science Publishers; London (1993).

[25]. D. Damjanovic, Rep. Prog. Phys. **61**(1998) 1267.

[26]. M. S. Vijaya and G. Rangarajan, *Materials Science,* Tata Mcgraw-Hill (2006).

[27]. J. K. Juneja, *"Studies on modified Lead Titanate Based electronic ceramics*", (Ph.D. Thesis), Chaudhary Charan Singh University, Meerut (2001).

[28]. L. E. Cross, Ferroelectrics **76** (1987) 241.

[29]. L. E. Cross and R. E. Newnham, Am. Ceram. Soc. **3** (1987) 289.

[30]. J. Fousek, Ferroelectrics **113** (1991) 3.

[31]. P. R. Chowdhary and S. B. Deshpande, Ind. J. Pure. Appl. Phys. **17** (1979) 571.

[32]. H. Jaffe, Proc. IRE **61** (1961) 1161.

[33]. T. Tevachalaungkul, "*Effects of Tin (IV) modification on Lead Zirconate Titanate Piezoelectric Ceramics",* (M.Sc. Thesis in Applied Analytical and Inorganic Chemistry) Faculty of raduate Studies, Mahidol University (1997).

[34]. A. J. Moulson and J. M. Herbert, *Electroceramics: Materials, Properties,Applications*, Chapman and Hall; New York (1997).

[35]. M. M. Zhang, Z. Jia and T. L. Ren, Solid State Electron. **53** (2009) 473.

[36]. J. Nath, D. Ghosh, J. P. Maria, A. I. Kingon, W. Fathelbab, P. D. Franzon and M. B. Steer, *IEEE Transactions of Microwave Theory and Technology*. **53** (2005).

[37]. A. K. Tagantsev, V. O. Sherman, K. F. Astafiev, J. Venkatesh and N. Setter, J. Electroceram. **11** (2003) 5.

[38]. J. T. Evans and J. A. Bullington, *IEEE 7th International Symposium on Applications of Ferroelectrics*, New York (1990) 692.

[39]. Q. Zhang, R. W. Whatmore, Z. Huang, M. E. Vickers, J. Phys. IV France **8** (1998) 79.

[40]. C. Kittel, *Introduction to Solid State Physics*, John Wiley and Sons (7th ed.); Hoboken, New Jersey (1996).

[41]. E. Sawaguchi, J. Phys. Soc. Jpn. **8** (1953) 615.

[42]. B. Noheda, D. E. Cox, G. Shirane, J. A. Gonzalo, L. E. Cross and S. E. Park, Appl. Phys. Lett. **74** (1999) 2059.

[43]. H. Jaffe and D. A. Berlincourt, Proc. IEEE. **53** (1965) 1372.

[44]. R. Koduri and M. Lopez, J. Phys. D: Appl. Phys. **39** (2006) 4466.

[45]. T. Ikeda, J. Phys. Soc. Japan **14** (1959) 1286.

[46]. K. P. Rema, A. S. Divya and V. Kumar, J. Phys. D: Appl. Phys. **42** (2009) 075420

[47]. D. Viehland, J. F. Li and Q. Tan, Philo. Magazine B **76** (1997) 59.

[48]. C. Prakash and O. P. Thakur, Mater. Lett. **57** (2003) 2310.

[49]. R. Ranjan, R. Kumar, B. Behera and R. N. P. Choudhary, Mater. Chem. Phys. **115** (2009) 473.

[50]. S. R. Shannigrahi, F. E. H. Tay, K. Yao and R. N. P. Choudhary, J. Euro. Ceram. Soc. **24** (2004) 163.

[51]. R. Ranjan, R. Kumar, B. Behera and R. N. P. Choudhary, Physica B **404** (2009) 3709.

[52]. J. E. Garcia, R. P´erez, A. Albareda and J. A. Eiras, J. Euro. Ceram. Soc. **27** (2007) 4029.

[53]. S. Dutta, R. N. P. Choudhary and P. K. Sinha, Ceram. Int. **33** (2007) 13.

[54]. R. Gerson, J. Appl. Phys. **31** (1960) 188.

[55]. G. H. Haertling, Ferroelectrics **75** (1987) 25.

[56]. S. Takahashi, Ferroelectrics **41** (1982) 143.

[57]. K. H. Hardtl and D. Hennings, J. Am. Ceram. Soc. **55** (1972) 230.

[58]. L. Ramji, S. C. Sharma and D. Rajiv, Ferroelectrics **100** (1989) 43.

[59]. G. H. Haertling and C. E. Land, J. Am. Ceram. Soc. **54** (1971) 1.

[60]. A. Oshima, K. Tshiosaki and S. Koizumi, Jpn. J. Appl. Phys. **33** (1994) 4940.

[61]. K. Oshima and K. Tsuzuki, Jpn. J. Appl. Phys. **33** (1994) 5389.

[62]. N. W. Thomas, J. Phys. Chem. Solids **51** (1990) 1419.

[63]. C. Randall, D. Barber, R. Whatmore and P. Grove, J. Mater. Sci. **21** (1987) 4456.

[64]. L. E. Cross, Ferroelectrics **76** (1987) 249.

[65]. D. Viehland, S. J. Jang, L. E. Cross and M. Wuttig, Phys. Rev. B **43** (1992) 8316.

[66]. H. R. Rukmini, R. N. P. Choudhary and D. L. Prabhakar, Mater. Lett. **44** (2000) 96.

[67]. B. S. Chiou, J. N. Kuo and H. T. Dai, J. Elec. Mater. **19** (1990) 393.

[68]. X. Dai, Z. Xu, J. F. Li and D. Viehland, J. Mater. Res. **11** (1996) 618.

[69]. P. H. Xiang, N. Zhong, X. L. Dong, R. H. Liang, H. Yang and C. D. Feng, Mater. Lett. **58** (2004) 2675.

[70]. Y. Zhang, A. L. Ding, P. S. Qiu, X. Y. He, X. S. Zheng, H. R. Zeng and Q. R. Yin,

Mater. Sci. Engg. B **99** (2003) 360.

[71]. M. Ichikia, Y. Morikawa, Y. Mabunec and T. Nakada, J. Euro. Ceram. Soc. **24** (2004) 1709.

[72]. G. H. Haertling and C. E. Land, Ferroelectrics **3** (1972) 269.

[73]. S. B. Mah, N. W. Jang, J. H. Park, D. S. Paik and C. Y. Park, Mater. Res. Bull. **35** (2000) 1113.

[74]. L. B. Kong, J. Ma, R. F. Zhang and T. S. Zhang, J. Alloys Compds **39** (2002) 167.

[75]. G. S. Snow, J. Am. Ceram. Soc. **56** (1973) 479.

[76]. D. Viehland, X. Dai, J.F. Li and Z. Xu, J. Appl. Phys. **84** (1998) 458.

[77]. F. Cordero, F. Cracium, A. Franco and C. Galassi, Ferroelectrics **35** (2007) 78.

[78]. D. Kuscer, J. Korzekwa, M. Kosec and R. Skulski, J. Euro.Ceram. Soc. **27** (2007) 4499.

[79]. H. J. Kleebe, S. Lauterbach, L. Silvestroni, H. Kungl, M. J. Hoffmann, E. Erdem and R. A. Eichel, App. Phys. Lett. **94** (2009) 142901.

[80]. B. W. Lee and E. J. Lee, J. Electroceram. **17** (2006) 597.

[81]. M. D. Durruthy-Rodriguez, L.D. Perez-Fernandez, A. Pelaiz-Barranco and F. Calderon- Pinar, Appl. Phys. A **95** (2009) 423.

[82]. A. Ignatiev, Y. Q. Xu, N. J. Wu and D. Liu, Mater. Sci. Engg. B **56** (1998) 191.

[83]. H. Li, Z. Yang, X. Zong and Y. Chang, Mater. Sci. Engg. B **130** (2006) 288.

[84]. E. Boucher, B. Guiffard, L. Lebrun and D. Guyomar, Ceram. Int. **32** (2006) 479.

[85]. C. P. Shaw, S. Gupta, S. B. Stringfellow, A. Navarro, J. R. Alcock and R.W. Whatmore, J. Euro. Ceram. Soc. **22** (2002) 2123.

[86]. Q. Zhang and R. R. Whatmore, J. Euro. Ceram. Soc. **24** (2004) 277.

[87]. B. Tiwari and R. N. P. Choudhary, Solid State Sci. **11** (2009) 219.

[88]. B. Tiwari and R. N. P. Choudhary, J. Phys. Chem. Solids **69** (2008) 2852.

[89]. B. Sahoo and P. K. Panda, J. Mater. Sci. **42** (2007) 9684.

[90]. S. R. Shannigrahi, R. N. P. Choudhary and H. N. Acharaya, J. Mater. Sci. Lett. **18** (1999) 345.

[91]. V. A. Chaudhary and G. K. Bichile, Physica B **405** (2010) 534.

[92]. A. Mesquita, V. R. Mastelaro and A. Michalowicz, Phase Transitions **83** (2010) 251.

[93]. M. W. Barsoum, *Fundamentals of Ceramics*, McGraw Hill; New York (1997).

CHAPTER II

Material Synthesis & Characterization Techniques

In this chapter, the ceramic technique employed for the preparation of ceramic bulk samples is discussed. All compositions in bulk presented in this thesis were synthesized by conventional ceramic technique. The characterization techniques employed for physical, structural, ferroelectric, dielectric and piezoelectric properties are presented. The optimum temperature of sintering is also discussed as sintering temperature is an important parameter that decides the material properties.

2.1. Introduction

The PZT ceramics and technology of their processing is well developed and has been described in many books [1-3], review papers [4-5], and separate articles dedicated to various aspects of PZT processing [6-15]. There are a number of techniques that are normally employed to synthesize ceramic materials. Solid state route is one of them. It is conventional, cheapest and simplest way to fabricate ceramic material compositions of required shapes and sizes. A solid-state reaction is a direct reaction between starting reagents (usually powders) at high temperature. High temperature provides the necessary energy for the reaction to occur. Solid-state reaction is usually slow because during the reaction, a large amount of bonds break, and the ions migrate through a solid. The limiting factor in solid state reaction is usually diffusion. So the rate-controlling step in a solid-state reaction is the diffusion of the cations through the product layer. Solid-state reaction occurs much more quickly with increasing temperature and reaction does not normally occur until the reaction-temperature reaches at least 2/3 of the melting point of one of the reactants.

In this methodology of preparation, the metal oxides/carbonates of analytical grade (AR grade) are taken as starting materials. These oxide materials are weighed in desired stoichiometric ratio with due consideration for impurity and moisture contents and ball milled (dry or wet, depending upon milling techniques) to get fine particle size (typically between 1 to 10 μm) [16]. An attempt to reduce the size of the particles further may affect the homogeneity and purity of the material. Distilled water is usually used as wetting medium as it is available with adequate purity at low cost and is non-inflammable. Next step is the solid state reaction between the constituents of starting materials at suitable temperature. This process is called firing or calcination. During calcination, control over stoichiometry is essential so volatile constituents have to be compensated. Calcination causes the constituents to interact by inter diffusion of their ions and resulting in homogeneous compounds. Hence, calcination is considered as part of the mixing process. Calcination also controls the shrinkage during sintering. After calcination, the powders are ball milled again for better homogeneity. The powder is then compacted to give desired shape, known as green body. In lead based ceramics, density of the materials greatly affects the materials properties [17]. It depends on the technique used for shaping of the material, as some green body

formation techniques do not require addition of binder, which is detrimental to the densification of the material. Hence, a general discussion on the shaping of the material is also presented. The final stage of preparation of ceramics by solid state route ends with sintering which provides densification (>95%) depending upon the optimization processing parameters, pressing technique and programmed sintering. After sintering, the compacted and sintered ceramics can be cut to desired shapes, lapped, polished and electroded before electrical characterization.

2.2. Material Synthesis: Solid State Route

Perovskite ferroelectrics form an important class of electroceramic materials and are widely used in a number of electronic applications. Properties of these ceramics are controlled predominantly by compositions. But at the same time these properties are affected by the grain size, porosity which are influenced by method of fabrication. Usually polycrystalline materials are prepared by this solid state route and hence this method is termed as conventional route also. Amongst the non conventional methods; hydrothermal synthesis, spray drying techniques, wet chemical method are commonly used for preparation of ceramic materials. This section comprises the details of the solid state method used for the fabrication of bulk samples of modified lead zirconate titanate system. A flowchart describing the main steps of the solid state route involved in PZT processing is shown in *Fig. 2.1*.

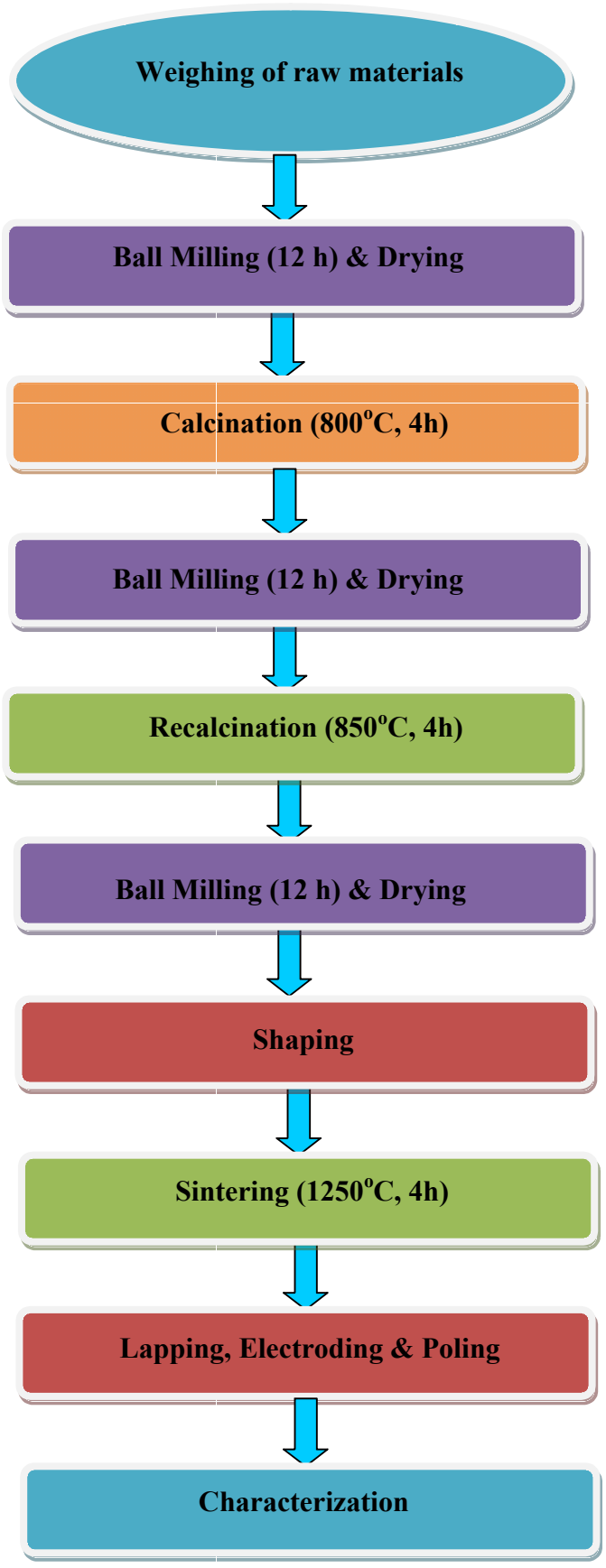

Fig. 2.1.

A Flow Chart depicting the conventional Solid State Route for bulk modified PZT samples

2.2.1. Ball Milling and Drying

Modified lead zirconate titanate with different concentrations of La, Sm and Mn was prepared by conventional solid state route using high purity metal oxides (99.9 %) in stoichiometric proportion. Excess PbO (2 wt%) powder was taken to counteract the volatilization of PbO during sintering. The process of ball milling is described as reduction of particle size by means of mechanical force. The oxides were subjected to ball milling in distilled water using zirconia balls as grinding media in polyethylene bottles for 12 h. Ball milling (see *Fig. 2.2.*) was done so as to reduce particle size and homogeneous mixing of powders. The wet slurry was then subjected to drying in oven at 120^{o}C. The oven was fitted with an air circulation arrangement and exhaust for quick drying of the slurry.

The compositional series fabricated by solid state route are as follows:

(i). $Pb_{1-x}Sm_x(Zr_{0.60}Ti_{0.40})_{0.98}Fe_{0.01}Nb_{0.01}O_3$ (where x = 0, 0.0025, 0.0050, 0.0075, 0.01, 0.02, 0.04, 0.06, 0.08) (PSZFNT-Series A)

(ii). $Pb_{1-x}La_x(Zr_{0.60}Ti_{0.40})_{0.98}Fe_{0.01}Nb_{0.01}O_3$ (where x = 0, 0.0025, 0.0050, 0.0075, 0.01, 0.02, 0.04, 0.06, 0.08) (PLZFNT-Series B)

(iii). $Pb(Zr_{0.60}Ti_{0.40})_{0.98-x}Fe_{0.01}Nb_{0.01}Mn_xO_3$ (where x = 0, 0.005, 0.010, 0.015, 0.02) (PZFMNT-Series C)

Fig.2.2. Conventional ball mill.

2.2.2. Calcination

Calcination is a pre-heat treatment step before final sintering, during which either the partial or complete phase of the compound is formed. It also helps in removing the unwanted gases and products during the decomposition of the constituent compounds e.g. carbonates get converted to oxide and CO_2 goes out. Calcination also helps in homogenizing the materials and reducing the shrinkage during the subsequent sintering process of the finally shaped samples. In general, four physical processes are involved in the calcination of the raw materials: (i) Linear expansion of the particles (< 400^{o}C) (ii) Solid phase reaction (400-750^{o}C) (iii) Contraction of product (750-850^{o}C) and (iv) Grain growth (> 850^{o}C). Synthesis of the phase of a compound takes place by solid-phase reaction, which involves the chemical reaction through atomic diffusion among grains at temperature below the melting points of the raw materials [18]. Usually, the calcination temperature is chosen high enough to cause reaction, but low enough to facilitate subsequent grinding. In materials, having volatile constituents, the calcination temperature must be kept low enough to avoid loss of the volatile components. The samples were calcined in closed alumina crucible at 800^{o}C and recalcined at 850^{o}C for 4 h in a programmable furnace (see *Fig. 2.3.*) with heating and cooling rate of 5^{o}C/min. The calcined powder was ground in agate pestle mortar and ball milled again for 12 h and then slurry was put into oven for drying at 120^{o}C.

Fig. 2.3. Programmable furnace for calcination and sintering.

2.2.3. Shaping

The ball milled powder obtained after calcination is subjected to shaping. A polymeric binder is added into the powder, for giving sufficient strength to green samples so that handling between shaping and sintering may not be difficult. One of the most important requirements of the binder is that it should be possible to remove the binder from the pressed shapes without any disruptive effect. The dried powder mixtures were mixed with small amount of diluted (3% in water) polyvinyl alcohol (PVA) binder and uniaxially pressed in form of circular discs of 15 mm diameter and 1 mm thickness. There are various shaping methods which include Uniaxial Pressing, Isostatic Pressing, Calendering, Extrusion, Jiggering, Injection Moulding, Silk Screening, Slip Casting, Band Casting. Among these different shaping techniques, in the present study uniaxial pressing technique has been used.

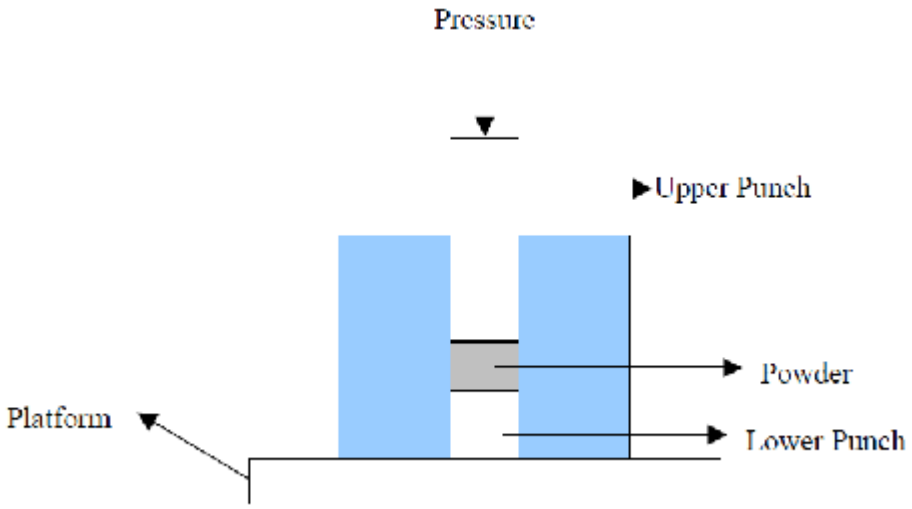

Fig. 2.4. Uniaxial pressing

Uniaxial pressing is used to make compacts of small sizes with discs of the calcined powder. It is carried out in a die having movable top. A cavity is formed at the bottom in lower portion. This cavity is filled with free flowing granulated powder and then it is struck with the top of the die. The process is shown in *Fig. 2.4*. In the present work, hydraulic press (manufactured by Hind Hydraulics *Fig. 2.5.*) was used for pressing and with the help of the top-punch pressure of 200 kg/cm^2 (10 tonn) is applied for 1-2 min. A lot of care at various levels of mixing is needed while using this pressing technique, as samples prepared by this

technique show the mechanical cracks and layering after sintering. Highly polished die and punch surfaces help to reduce wall friction and tools are made of hardened steels to minimize wear and tear and maintain surface finish.

Fig. 2.5. Hydraulic press for uniaxial pressing

2.2.4. Sintering

The aim of sintering is to yield compacted dense polycrystalline materials from green samples. The sintering is basically a heat treatment given to material for densification process in which, at an appreciable temperature, the atomic motion is more violent and the area between grains in contact increases due to the thermal expansion of the grains and finally only one interface between two grains remains. This corresponds to a state with much lower surface energy. In this state, the atoms on the grain surfaces are affected by neighbouring atoms in all directions, which results in densified ceramics [18]. At the beginning of the sintering process, the lattice distortion and internal strain are reduced by atomic diffusion but as temperature increases further, a recrystallization process takes place through atomic diffusion. During recrystallization, new crystal nuclei form and grow at grain boundaries and in other regions inside the grain with higher free energies. Meanwhile, some grains grow by swallowing up other smaller grains. In the recrystallization stage, grain growth is usually realized through the motion of grain boundaries. In general, higher the sintering temperature, larger the grains would grow, as the grain growth is caused by atomic diffusion, which increases with the increase in

sintering temperature. However, the density of a ceramic is affected by the sintering temperature and holding time in a more complex fashion. If the sintering temperature is too high or the sintering time is too long, the density of the lead based ceramics will be reduced resulting from PbO evaporation at high temperatures. Since, the grain growth is caused by atomic diffusion, a higher sintering temperature and a larger hold time would result in larger grains. The oxide ceramics should be sintered in an oxidizing atmosphere or in air. Further, in lead based ferroelectric ceramics, evaporation of PbO takes place above 800^{o}C and creates Pb vacancies which affect the material properties considerably [19]. The green bodies were sintered in air medium at 1250^{o}C for 4 h in closed alumina crucibles. The pellets were heated at 500^{o}C for 2 h to remove binder. A lead rich atmosphere was maintained to minimize lead loss during sintering. Here, in the present case, $PbZrO_3$ powder was kept along with the material to be sintered for maintaining lead rich atmosphere along with an excess amount of lead during weighing of raw materials. The sintering profile is depicted in *Fig. 2.6.*

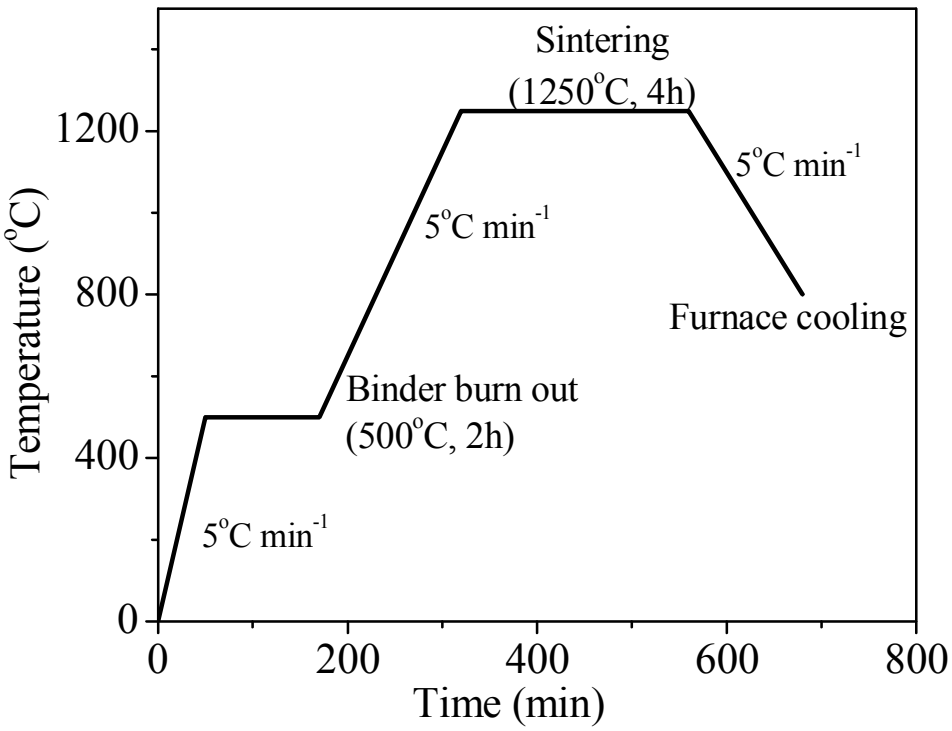

Fig. 2.6. Time-Temperature sintering profile for modified PZT.

2.3. Characterization Techniques

This section will discuss the various characterization techniques used in fabrication of the modified PZT ceramics which include X-ray crystallographic analysis for phase identification, SEM analysis for microstructural analysis, densification and porosity, characterization techniques employed for electrical and piezoelectric measurements.

2.3.1. Phase Identification

The X-ray diffraction technique was used to analyse crystalline structures, phases and lattice parameters, in the material. X-rays are electromagnetic radiation with typical photon energies in the range of 100 eV-100 keV. For diffraction applications, only short wavelength x-rays (hard x-rays) in the range of a few angstroms to 0.1 Å (1 keV-120 keV) are used. The wavelength of x-rays is comparable to the size of atoms; they are ideally suited for probing the structural arrangement of atoms and molecules in a wide range of materials. The energetic x-rays can penetrate deep into the materials and provide information about the bulk structure [20-21].

The basic principle is that, for a fixed wavelength (λ), the constructive interference occurs for a fixed set of an inter planer spacing (d) and at an incidence angle (θ) (*Fig. 2.7)*. According to Bragg's condition of diffraction:

$$2d\,Sin\theta = n\lambda \qquad \ldots\ldots(2.1)$$

For "reflection" to occur from a set of parallel planes of atoms in a structure, these "reflections" must be in phase so that they constructively reinforce each other and generate a measurable signal. The geometry required for constructive interference can be seen in the *Fig. 2.7.*

If the path difference (ABC) for the diffracted rays 1 and 2 is exactly one wavelength then they will reinforce each other by constructive interference. Under the same conditions the path difference A'B'C' for rays 1 and 3 will be two wavelengths they will also interfere constructively.

For cubic system, *d* is given by

$$1/d^2=(h^2/a^2+k^2/b^2+l^2/c^2) \quad \text{.....(2.2)}$$

where *h*, k, *l* are Miller indices and *a* (a=b=c for cubic) is side of unit cell.

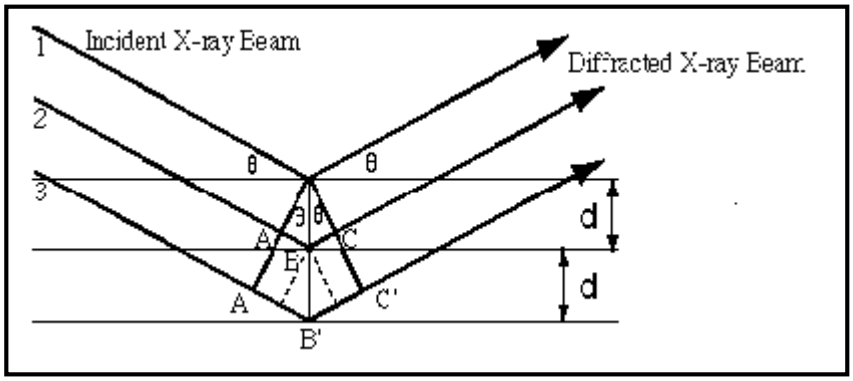

Fig. 2.7. Bragg's law for reflection

Combining the above two equations we get a relation, which predict the diffraction angle, θ. For any set of planes, for a given 'λ' if the following condition is satisfied, we can calculate the h, k and l values for different Sinθ and determine the unit cell parameter.

$$\text{Sin}^2\theta = (\lambda^2/4a^2)(h^2/a^2+k^2/b^2+l^2/c^2) \quad \text{.....(2.3)}$$

Similarly, the relation for a tetragonal and rhombohedral system is

$$1/d^2 = [(h^2+k^2)\, a^2 + l^2/c^2] \quad \text{..... (2.4)}$$

$$1/d^2 = [(h^2+k^2+l^2)\, \sin^2\theta + 2(hk+kl+lh)(\cos^2\theta - \cos\theta)] / a^2(1+2\cos^3\theta - 3\cos^2\theta) \quad \text{..... (2.5)}$$

It is seen that diffraction directions are determined by the shape and size of the unit cell. The intensities of diffracted beams are determined by the positions of the atoms within the unit cell and it follows that we must measure intensities if we are to obtain any information about the atomic positions. It is also found that for many crystals, there are particular atomic arrangements, which reduce the intensities of some diffracted beams to zero. In such cases, there is simply no diffracted beam at the angle predicated by the above equations [22].

While indexing for cubic structure, it has to be kept in mind that for simple cubic and simple tetragonal all (h k l) values are permissible, yet reflections corresponding to $(h^2+k^2+l^2)$ values equal to 7, 15, 23…. are all absent. The reflection peaks for bcc satisfy the condition h+k+l = 2n. where, n is natural number. For fcc structure, the reflection peaks are found to have (h k l) values either all even or all odd.

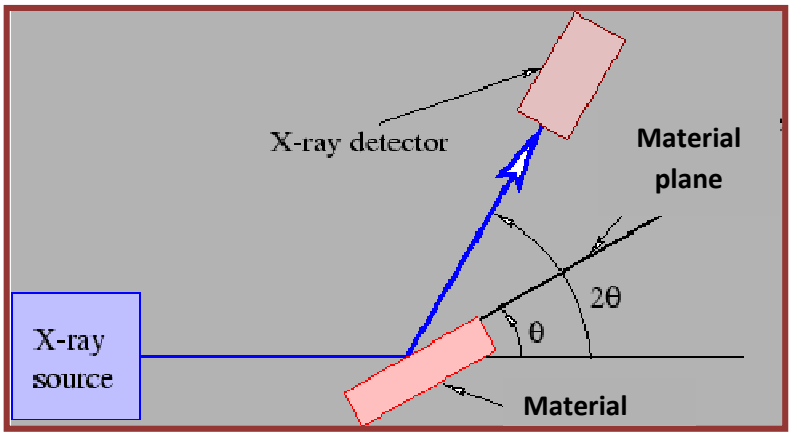

Fig. 2.8. The schematic diagram for Bragg's diffraction

The X-ray diffraction patterns of modified PZT compositions in the present thesis were recorded using D8 Advance X-ray diffractometer (Bruker AXS) at room temperature with CuK_α (λ=1.54 Å) radiation. The diffraction angle, 2θ, was varied from 20^o to 70^o. All the lattice parameters (a, b, c, α) were calculated using the standard formula (2.4) and (2.5) and powderX software with an error of 0.05 in 2θ value.

2.3.2. Microstructure Analysis

The scanning electron microscope was used to determine the average crystallite size and the surface morphology of the bulk and thin films. It gives information about the grain evolution and grain size in the bulk and thin films. It also gives the information about the inter-granular and the intra-granular pores and the distribution of grains in the bulk samples. SEM measurements are based on the principle of irradiating the specimen with a finely focussed electron beam. Secondary electrons, backscattered electrons, auger electrons, characteristic x-rays and several other radiations are released from the specimen. Generally,

the secondary electrons are collected to form the image in the SEM mode. The microstructure of freshly broken sintered modified PZT specimens was studied by scanning electron microscope (JEOL JSM 6510LV, Japan). The broken pieces were placed on brass stubs and coated with Au using ion sputter. The average grain size of the samples was determined by linear intercept method.

2.3.3. Density

The bulk density (d_{ex}) was measured by the method based on the Archimedes principle and is given by the relation as follows:

$$d_{ex} = (W_a / W_a - W_w) \times d_w \quad \text{……..(2.6)}$$

where d_{ex} (g/cc) is the density of the sample. Here, W_a and W_w are the weights of the sample in air and in water, respectively. d_w is the density of water which is taken 1.0 g/cc in the present case.

Theoretical density, d_{th} (g/cc) was computed from the lattice parameters using the relation,

$$d_{th} = (Z \cdot M)/(N \cdot V) \quad \text{…….. (2.7)}$$

where Z is the number of molecules in a unit cell and is equal to 1 for the present system, M is the molecular weight, N is the Avogadro's number and V is the unit cell volume.

Relative density (%) was calculated using the formula

$$d_{rel}\,(\%) = (d_{ex}/d_{th}) \times 100\ \% \quad \text{…….. (2.8)}$$

and Porosity (P) was estimated using the relation

$$P\,(\%) = [1-(d_{ex}/d_{th})] \times 100\ \% \quad \text{…….. (2.9)}$$

In most of the electrical applications sintered ceramics are required to have minimum porosity i.e. maximum density. For application point of view properties reach their optimum values at the highest density, while porosity in excess of 25-30% allows the absorption or ingress of moisture leading to many serious problems [16]. However, there are cases where porosity is quite desirable: for example, in humidity and gas sensors and where thermal shock resistance is of overriding importance.

2.3.4. Electroding and Poling

The selection of suitable electrode for the test materials is very important. After sintering, lapping and polishing, the ceramic material is converted in the form of parallel plate capacitor for further electrical characterization. Thus, to study the electrical properties of the bulk ceramic, the electrical contacts were made by depositing silver electrodes on both sides of the pellet using silver epoxy. The coated pellets were then put in furnace in the temperature range 400-500^{o}C for 1 h for firing the silver paste.

Fig. 2.9. Poling setup

The modified PZT samples were subjected to a high DC field to bring about the rearrangement of spontaneous polarization of the domain structure thereby producing a resultant polarization. For obtaining good properties, a field higher than coercive field (E_c) is applied at higher temperature during poling. The poling was done at 150^{o} C in silicon oil bath by applying field strength of ~20 kV/cm for 1 h. The piezoelectric properties for the bulk samples were studied on electrically poled parallel flat discs. The poling unit is shown *Fig. 2.9.*

2.3.5. Hysteresis Measurement

The ferroelectric nature of the bulk samples was analyzed using an automatic PE loop tracer system (Agilent Technologies Ltd.). The P-E loop tracer (shown in *Fig. 2.10.*) is based on Sawyer-Tower circuit and is operated at discrete frequencies ranging 20-1000 Hz. Hysteresis loop of the ferroelectric samples can be measured at various voltage ranges from -

3000 V to +3000 V and with temperature variations from 30°C to 200°C. Apart from hysteresis, the instrument also allows us to measure fatigue, retention of bulk ferroelectric samples.

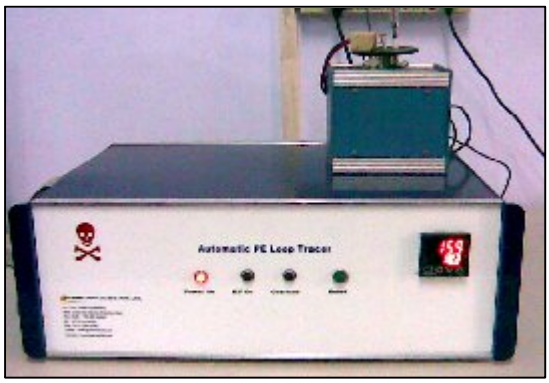

Fig. 2.10. P-E hysteresis loop tracer

2.3.6. Dielectric Measurements

The dielectric properties of the modified PZT bulk samples were measured as a function of temperature (30°C to 500°C) at discrete frequencies of 100 Hz, 1 kHz, 10 kHz, and 100 kHz using Agilent 4263B LCR meter (Agilent Tech. Ltd) as shown in *Fig. 2.11*. The LCR meter is interfaced with instrument controller and hot stage through IEEE–488 and temperature controller through serial port for automatic data acquisition. The acquired data can be saved in worksheet form for further analysis. The instrument is equipped with an in-built dc source to supply voltage -40 V to 40 V. The software allows visualization of an online trace of the measured parameters. The dielectric constant measures the amount of charge that an electroded disc of material can store, relative to the charge that stored by electrodes separated by air or vacuum at the same voltage. In other words, dielectric constant can be defined as,

$\varepsilon_r = \varepsilon/\varepsilon_o = C\ d/\ \varepsilon_o\ A$ ..... (2.10)

where, ε= permittivity of dielectric material, A= area of the electrodes, ε_o = permittivity of free space = 8.85 x 10^{-12} F/m and d = thickness of the samples.

Dissipation factor (*tan* δ) is a measure of the dielectric loss in a material and is defined as the ratio of the imaginary part ε'' to the real part ε' of the dielectric constant. In the present work, samples were placed in metal-ferroelectric-metal (MFM) configuration (silver

as a top and bottom electrode). For present study, room temperature measurement of ε and loss tangent ($tan\ \delta$) of samples was done as a function of ac frequency (20Hz to 1MHz) using Agilent 4284A LCR meter.

Fig. 2.11. LCR meter for dielectric measurements.

2.3.7. Piezoelectric Coefficient Measurement

2.3.7.1. Piezoelectric Charge Coefficient (d_{33})

The piezoelectric charge coefficient (d_{33}) of electrically poled parallel flat discs was measured using Concord d meter (Model-2 from Concord Electroceramic Industries *Fig. 2.12.*). This is based on the Quazi-static method based on Berlincourt principle. The d meter consists of electronic driver, force head and d_{33} read out. The force head has an electromagnetic driver which vibrates the internal calibration piezo element as well as the piezo test specimen which is mechanically in series. It is so designed that it facilitates measurement of d_{33} coefficient for a variety of piezoelectric materials of varying sizes and shapes. The piezoelectric sample under test is clamped within the jaws of the force head unit for testing. The oscillator and electromagnetic driver provide ac voltage to the electromagnetic driver in the force head and the charge developed by the sample is measured and displayed digitally in d_{33} read out. The measurable d_{33} range by d meter is 50-1000 pC/N with accuracy up to ±5.0%.

The piezoelectric charge coefficient (d_{33}) is defined as charge per unit force both in the direction of polarization of a piezoelectric material i.e.

$$d_{33}=(\partial D_3) / (\partial T_3)_E \qquad \text{.....(2.11)}$$

where D is the dielectric displacement vector and T is the applied stress vector.

(The 3-axis is by convention the axis of polarization of piezoelectric ceramics materials).

Principle of operation:

d_{33} = Q/F= CV/F .....(2.12)

where Q (=CV) is charge developed per unit electrode area, C is capacitance, V is voltage and F is force in Newton (N)

Fig. 2.12. Piezo d meter

The instrument should always be calibrated with the standard value at a particular temperature. The value of d_{33} is displayed along with polarity. The -ve sign indicates that negative charge is generated at upper electrode as the specimen is compressed. The +ve sign indicates the upper electrode is connected to the +ve terminal of the poling source. A force of 0.1 N at a frequency of 80 Hz is applied on the electroded surfaces of poled piezoelectric ceramic samples. Force is applied by a mechanical probe, which also supports the sample and provides electrical connections to the two surfaces of the samples. The piezoelectric voltage generated is fed to an electronic driver, which after processing displays d_{33} on a microprocessor controlled digital monitor in pC/N. Stress is applied only on a small area and piezoelectric charge is generated only on the area under stress i.e. d_{33} is a point property.

2.3.7.2. Electromechanical Coupling Coefficient (k_p)

Electromechanical coupling coefficient, k_p, was determined by the resonance-anti-resonance method using impedance-frequency data from an impedance analyzer (Agilent Technologies, 4294A).

2.4. $Pb(Zr,Ti,Fe,Nb)O_3$ System: Processing Parameters and Optimization of Sintering Temperature

Our first objective was to select a modified PZT composition that exhibits good piezoelectric as well ferroelectric properties. PZFNT in which Fe and Nb content was restricted upto 1 mol% as according to literature survey, was selected as a promising candidate for further studies. As per the literature available for the piezoelectric/ferroelectric properties, composition of PZFNT with Zr/Ti: 60/40 is selected. However, optimization of sintering temperature was done for the starting composition i.e. PZFNT (60/40) and this composition was further considered as the starting point for further part of research. In lead-based ferroelectric systems, heat treatment temperature significantly influences the system properties which include the perovskite phase evolution, microstructure and density of the material [18, 23-24]. Special precautions are often used in sintering of electronic ceramics particularly involving PZT. Heating rates and hold times at maximum temperature are critical for microstructural development and grain size control in PZT based systems. Sintering cycles may include intermediate temperature annealing or controlled cooling to relieve residual strains or avoid deleterious phase transformations. Atmosphere control may be important to prevent loss of volatile components or avoid reduction reactions. In continuous production, sequential burnout (organics) and sintering may take place in the same furnace, requiring complex temperature cycles even for relatively simple devices. Hence in order to select optimum temperature for sintering, PZFNT composition was sintered at different temperatures. A systematic study has been performed on Samarium (Sm^{3+}), Lanthanum (La^{3+}) and Manganese (Mn^{4+}) substituted modified PZT (PZFNT) compositions. A comparative study of structural, microstructural, ferroelectric, dielectric and piezoelectric properties of PZFNT and PSZFNT, PLZFNT and PZFMNT with all sites compensated at A and B sites has been presented in next chapters.

The starting oxides for all the compositions were AR grade PbO, TiO_2, ZrO_2, La_2O_3, Sm_2O_3, Fe_2O_3, Nb_2O_5 and MnO_2 powders. For the compensation of lead loss an excess of 2% lead (PbO) was added in the initial PZFNT composition itself $Pb_{1-x}(Zr_{0.60}Ti_{0.40})_{0.98}Fe_{0.01}Nb_{0.01}O_3$ (x = 0). In order to optimize the sintering temperature, the

green samples were sintered at four different temperatures. The powder mixture was ball milled for 12 h in distilled water using zirconia balls and dried in oven. The dried powder was calcined at 800^{o}C for 4 h in a conventional furnace. The calcined powder ball milled and recalcined at 850^{o}C for 4 h. Recalcined powder was ball milled and then dried powders were mixed with small amount of dilute polyvinyl alcohol (PVA) binder and uniaxially pressed in form of circular discs of 15 mm diameter and 1mm thickness at a pressure of 200 kg/cm^2. The discs were sintered at different temperatures in range of 1150-1300^{o}C for 4 h in closed alumina crucible in lead rich atmosphere to minimize lead loss during sintering. The steps involved in synthesis of bulk samples are shown in *Fig. 2.1*. The temperature-time sintering profile is shown in *Fig. 2.6*. Phase identification of sintered pellets was done by using D8 Advance X-ray diffractometer (Bruker AXS) in a range of bragg angles ($20^{o} \leq 2\theta \leq 70^{o}$) with step size of 0.02^{o}. The sintered pellets were lapped and electroded using silver epoxy. Hysteresis loops were recorded using automatic PE loop tracer. The room temperature dielectric properties were also measured over a frequency range 20-10^6 Hz using an Agilent 4284A LCR meter at 30^{o}C using an automated system. The poling was done at 150^{o} C in silicon oil bath by applying field strength of ~20 kV/cm for 1 h. The piezo-coefficient, d_{33}, is measured on electrically poled parallel flat discs using Concord d meter (Model-2 Concord Electroceramic Industries, India).

Fig 2.13. depicts the bulk density of the PZFNT sample as a function of the sintering temperature. As the sintering temperature increases the bulk density of samples increases at first, reaches maximum value at sintering temperature 1250^{o}C. This is due to grain growth with rise in temperature with close packing of grains together. The sintered density decreased slightly with higher sintering temperature of 1300^{o}C that may be due to the loss of lead. The linear shrinkage (diameter) increases up to 1250^{o}C but decreases afterwards. X-ray diffraction patterns of PZFNT samples sintered at different temperatures are shown in *Fig. 2.14.* The diffraction peaks correspond to tetragonal phase of perovskite-type structure. The peak positions and intensities matches with JCPDS file no. (33-0784). There is no trace of pyrochlore phase in XRD patterns of any of the samples sintered at different temperatures. As the sintering temperature is increasing the peaks are shifting towards lower angle side indicating the increase in lattice parameters.

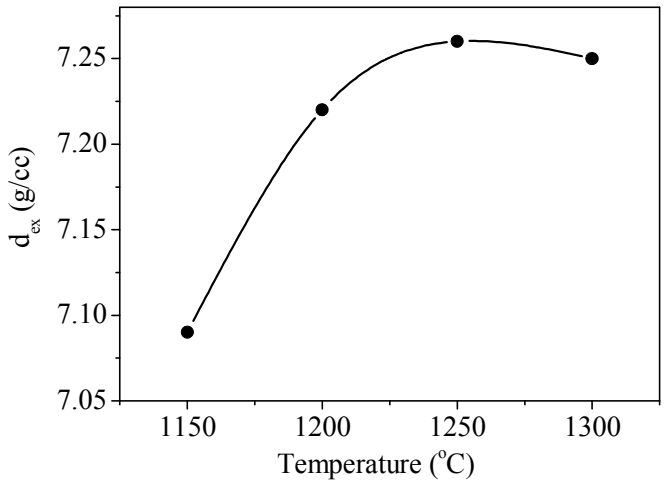

Fig. 2.13. Bulk densities of PZFNT sample as a function of sintering temperatures.

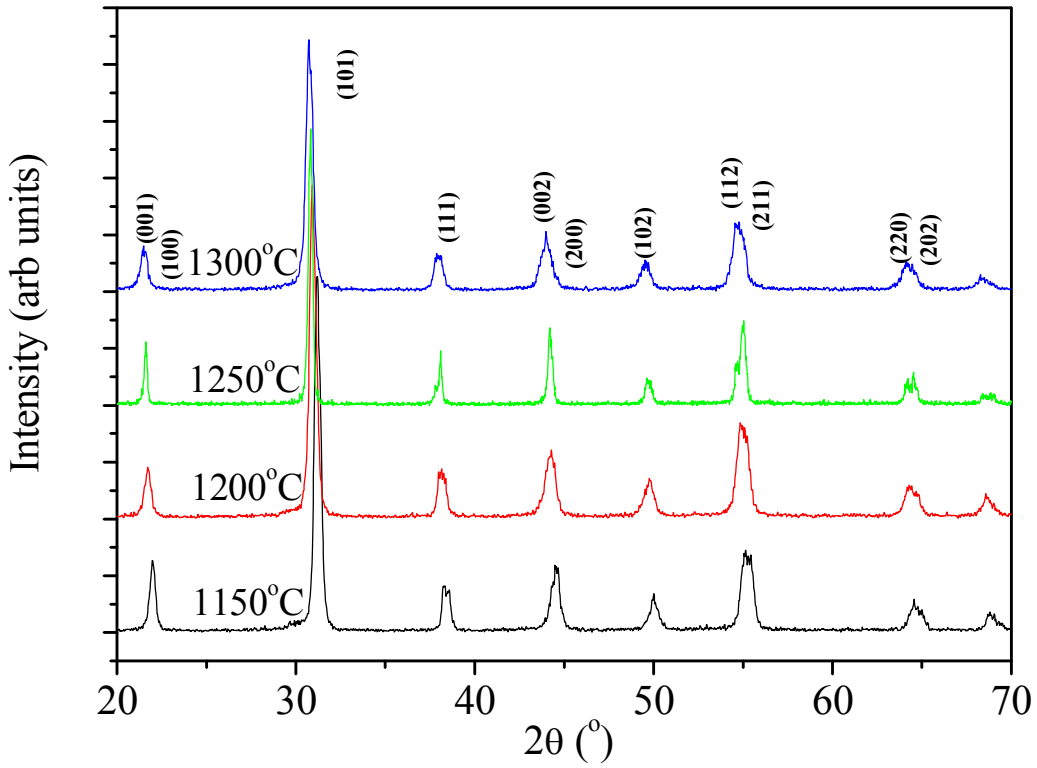

Fig 2.14. XRD patterens of PZFNT samles at different sintering temperatures.

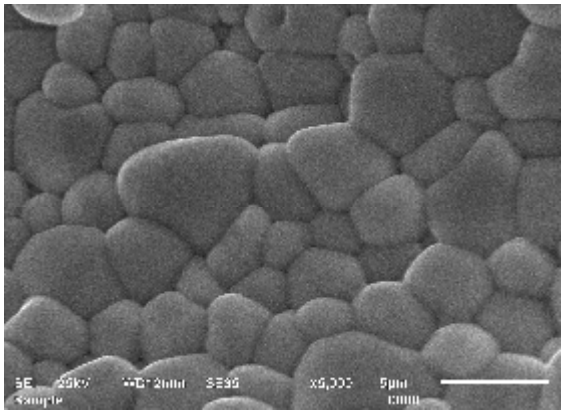

1150^{o}C

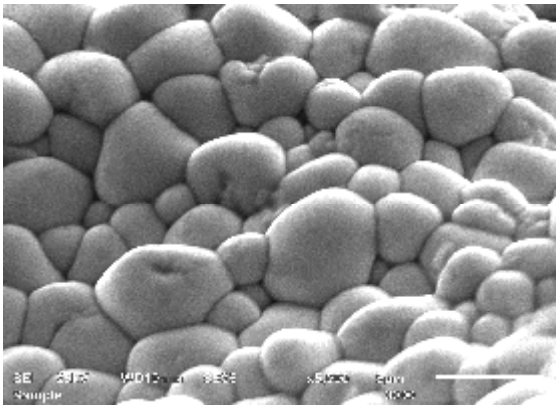

1200^{o}C

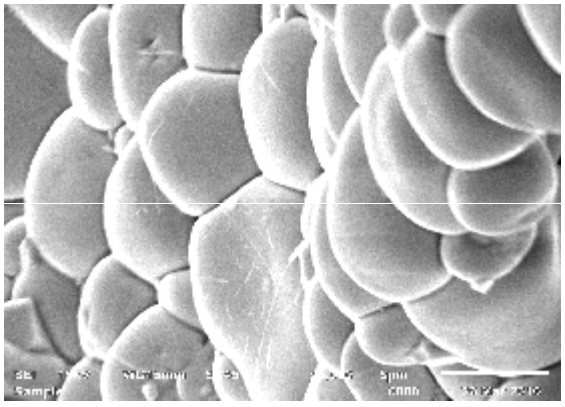

1250^{o}C

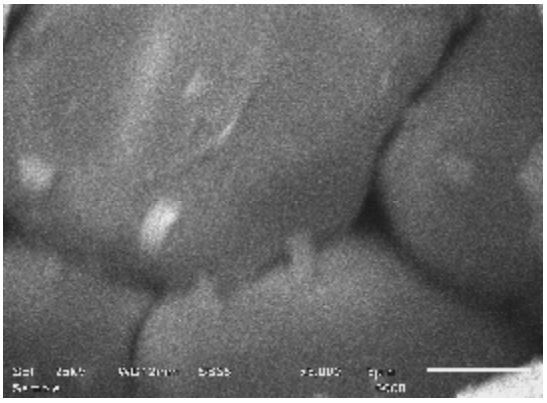

1300^{o}C

Fig. 2.15. SEM micrographs of PZFNT ceramics sintered at different temperatures.

Table 2.1.
Variation of grain size, ferroelectric, room temperature dielectric and piezoelectric parameters with sintering temperature.

Sintering Temperature (^oC)	Linear Shrinkage (%)	Grain size (μm)	Rem. Pol. P_r ($\mu C/cm^2$)	Coer. Field E_c (kV/cm)	Dielectric constant, ε_{RT}	Dielectric loss, $tan\delta_{RT}$	d_{33} (pC/N)
1150	9.63	2.8	10.6	6.3	428	0.019	122
1200	10.02	3.3	12.2	6.0	438	0.012	138
1250	10.29	4.1	13.0	6.9	498	0.010	143
1300	10.09	10.0	9.9	6.6	407	0.015	140

The scanning electron micrographs of PZFNT samples sintered at different temperatures are shown in *Figs. 2.15.* The average grain size was calculated using the linear intercept method and was found in the range of ~3 to 10 μm. It can be depicted from the micrographs that with the increase in sintering temperature, porosity in the samples decreases and grain size increases. During sintering, the grains coalesce so as to reduce total surface energy of the system [25]. Therefore as grain size increases, porosity decreases with the increase in sintering temperature.

Figs. 2.16 (a-e). depict the P-E hysteresis behaviour of modified PZFNT samples. It shows that as sintering temperature increases from 1150 to 1250^{o}C, remanant polarization (P_r) increases form ~11 μC/cm^2 to 13 μC/cm^2 while decreases to 10 μC/cm^2 at 1300^{o}C. The same trend is observed in variation of piezoelectric coefficient, d_{33}. This can be correlated to increase in density and increase in grain size. The enhancement in dielectric constant can be due to increase in grain size. The grain boundaries and domain walls restricts the domain reorientation and domain wall motion. There is no particular trend in variation of coercive field, E_c with sintering temperature. As the grain size increases, the volume fraction of grain boundaries is reduced that leads to easier alignment of domains with field which in turn increases P_r. The grain size variation in addition to ferroelectric, dielectric and piezoelectric parameters are listed in *Table 2.1.*The increase in sintering temperature leads to increase in room temperature dielectric constant. *Fig. 2.17.* shows the dielectric constant and loss variation for PZFNT sample as a function of frequency. The ε_{RT} decreases with increases in frequency. The higher value of ε at lower frequencies can be attributed to simultaneous presence of all types of polarizations (i.e. interfacial, ionic, dipolar, electronic, space charge

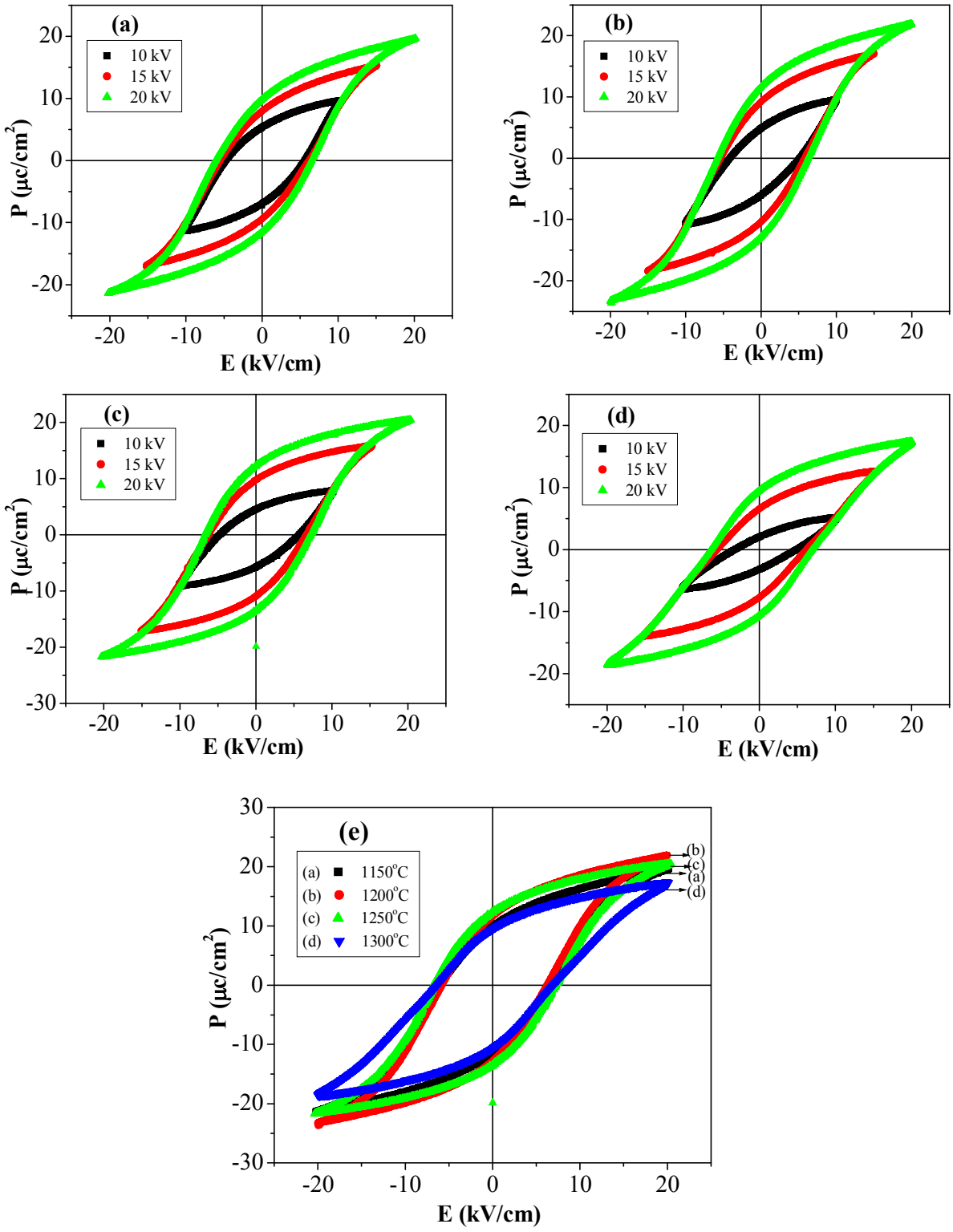

Fig. 2.16. P-E hysteresis curves of modified PZT samples at (a) 1150°C (b) 1200°C (c) 1250°C (d) 1300°C (e) Comparison of PE loop at different sintering temperatures.

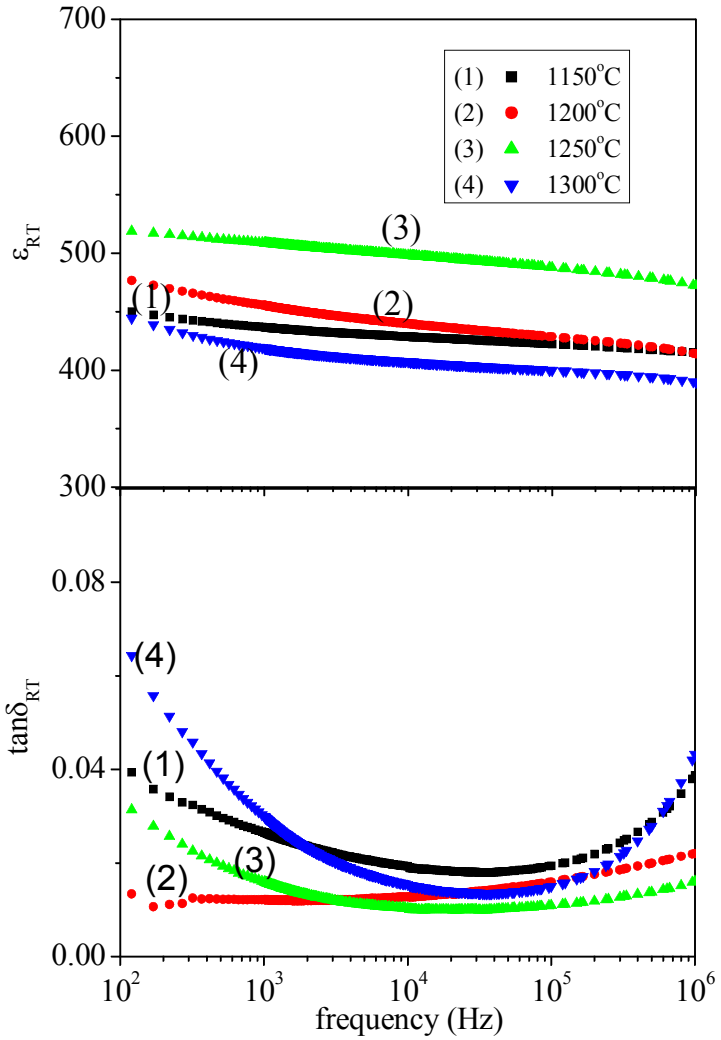

Fig. 2.17. Room temperature variation of dielectric constant and loss with frequency at different sintering temperatures.

etc.) in the compounds. At lower frequencies, the contribution to dielectric constant from the space charge polarization is maximum, which reduces slowly with the increase of frequency. The space charge arises from the charge accumulation at grain boundaries and at the electrode interface which is mainly due to vacancies of lead and oxygen. With the increase of frequency, these dipoles due to space charge do not respond at higher frequencies resulting in decrease in the dielectric constant. At higher frequencies, the main contribution to ε comes from the electronic polarization as other types of polarizations become ineffective. Unlike dielectric constant, $tan\delta_{RT}$ first decreases and then continuous increase with increase in

frequency. This nature of variation of ε_{RT} and $tan\delta_{RT}$ with frequency was observed for other modified PZT compositions as well [26-27]. This increase in $\tan\delta_{RT}$ at higher frequencies is due to the presence of hardener Fe^{3+} ions at B site in lattice and extrinsic loss phenomenon [28-29].

It can be concluded from the results that sintering temperature plays a vital role on structural, ferroelectric, dielectric and piezoelectric properties. The bulk density, remanant polarization (P_r), room temperature dielectric constant (ε_{RT}) and piezoelectric coefficient (d_{33}) were observed to be highest for composition sintered at 1250^{o}C. The room temperature dielectric loss ($tan\delta_{RT}$) is the minimum for the sample sintered at 1250^{o}C. As sintering temperature is increased to 1300^{o}C, the lead loss deteriorates the investigated properties. Hence, optimum temperature for sintering for PZFNT composition at which dielectric, ferroelectric and piezoelectric properties are optimized is 1250^{o}C.

References

[1]. B. Jaffe, W. R. Cook and H. Jaffe, *Piezoelectric Ceramics*, Academic Press; New York (1971).

[2]. B. Noheda, Solid State Mat. Sci. **6** (2002).

[3]. W. D. Kingery, *Ceramic Fabrication Processes,* John Wiley Sons Inc.; New York (1956).

[4]. G. H. Haertling, J. Am. Ceram. Soc. **82** (1999) 797.

[5]. M. Kahn, D. Burks, I. Burn and W. Schulze, *Electronic Ceramics: Properties, Devices, and Applications*, Ed. by L.M. Levinson; New York (1988).

[6]. S. S. Chandratreya, R. M. Fulrath and J. Pask, J. Am. Ceram. Soc. **64** (1981) 422.

[7]. K.H. Hardtl and H. Rau, Solid State Commun. **5** (1969) 41.

[8]. R.L. Holman and M. Fulrath, J. Appl. Phys. **44** (1973) 5227.

[9]. A. I. Kingon and J. B. Clark, J. Am. Ceram. Soc. **66** (1983) 253.

[10]. L. B. Kong, J. Ma, R. F. Zhang and T. S. Zhang, J. Alloys Compds. **339** (2002) 167.

[11]. Z. He and J. Ma, J. Phys. Chem. Solids **64** (2003) 177.

[12]. M. Hammer and M.J. Hoffmann, J. Am. Ceram. Soc. **81** (1998) 3277.

[13]. Y. Yoshikawa and K. Tsuzuki, J. Am. Ceram. Soc. **75** (1992) 2520.

[14]. P. G. Lucuta, F. Constantinescu and D. Barb, J. Am. Ceram. Soc. **68** (1985) 533.

[15]. J. Ryu, J. J. Choi and H. E. Kim, J. Am. Ceram. Soc. **84** (2001) 902.

[16]. A. J. Moulson and J. M. Herbert, *Electroceramics:Materials, Properties and Applications*, Chapman and Hall; New York (1997).

[17]. M. H. Lente, A. L. Zanin, S. B. Assis, I. A. Santos, J. A. Eirask and D. Garcia, J. Euro. Ceram. Soc. **24** (2004) 1529.

[18]. Y. Xu, *Ferroelectric Materials and Their Applications*, Elsevier Science Pub. Co.; New York, USA (1991).

[19]. A. H. Webster, T. B. Weston and N. E. H. Bright, J. Am. Ceram. Soc. Bull. **50** (1967) 490.

[20]. S. K. Chatterjee, *X-ray Diffraction: Its Theory and Applications,* Prentice Hall of India Private Limited; New Delhi (1999).

[21]. B. D. Cullity, *Elements of X-ray Diffraction*, Addison-Wesley Publication Company Inc.,

Reading, Massachusetts, Menlo Park; California (1978).

[22]. A. R. Verma and N. Srivastava, *Crystallography for Solid State Physics*, Wiley Eastern Limited; New Delhi (1982).

[23]. S. L. Swartz and T. R. Shrout, Mater. Res. Bull. **17** (1982) 1245.

[24]. K. Katayama, M. Abe, T. Akiba and H. Yanagida, J. Euro. Ceram. Soc. **5** (1989) 183.

[25]. S. Kang, J. H. Lee, J. J. Kim, H. Y. Lee and S. H. Cho, J. Euro. Ceram. Soc. **24** (2004) 1031.

[26]. M. Zivkovic, D. Stojanovic, C. R. Foschini, V. Paunovic and D. Mancic, Science of Sintering **35** (2003) 133.

[27]. S. B. Narang and D. Kaur, Ferroelectric Letters **36** (2009) 20.

[28]. L. I. Maissel and R. Glang, *Handbook of Thin Film Technology*, McGraw-Hill; New York (1970).

[29]. R. Rai, S. Mishra and N. K. Singh, J. Alloys Compds. **487** (2009) 494.

CHAPTER III

Structural & Microstructural Properties of Substituted $Pb(Zr,Ti,Fe,Nb)O_3$ System

Lanthanum, samarium and manganese substituted modified PZT ceramics were prepared by conventional solid state route. Lanthanum and samarium are well known softeners while manganese is a hardener and impact of their substitution on A and B site on structural and microstructural properties of modified PZFNT compositions are discussed in this chapter and the results are compared with undoped modified PZT composition.

3.1. Introduction

This chapter illustrates the combined structural and surface morphological studies on substituted modified PZT ceramics. The physical properties of bulk ferroelectric ceramics decide the course of electrical and piezoelectric properties. X ray diffraction analysis (XRD) provides the structural changes when substitution of the cations is done in modified PZT. The properties of ferroelectrics are related to their ceramic microstructure which includes the grain size, grain shape, grain-grain orientation and grain boundaries, as well as to the crystal structure, domain configuration, and electronic and defect structures. The effect of La, Sm and Mn substituents on microstructural development is presented in this chapter. Density measurements of bulk samples have also been discussed.

3.2. Structural Properties of Substituted PZFNT Compositions

The substituted PZFNT compositional series for structural analysis are as follows:

(i). $Pb_{1-x}Sm_x(Zr_{0.60}Ti_{0.40})_{0.98}Fe_{0.01}Nb_{0.01}O_3$ (where x = 0, 0.0025, 0.0050, 0.0075, 0.01, 0.02, 0.04, 0.06, 0.08) (PSZFNT-Series A)

(ii). $Pb_{1-x}La_x(Zr_{0.60}Ti_{0.40})_{0.98}Fe_{0.01}Nb_{0.01}O_3$ (where x = 0, 0.0025, 0.0050, 0.0075, 0.01, 0.02, 0.04, 0.06, 0.08) (PLZFNT-Series B)

(iii). $Pb(Zr_{0.60}Ti_{0.40})_{0.98-x}Fe_{0.01}Nb_{0.01}Mn_xO_3$ (where x = 0, 0.005, 0.010, 0.015, 0.02) (PZFMNT-Series C)

3.2.1. Structural Analysis of Sm-Substituted PZFNT Ceramics

X-ray diffraction patterns of the PSZFNT ($Pb_{1-x}Sm_x(Zr_{0.60}Ti_{0.40})_{0.98}Fe_{0.01}Nb_{0.01}O_3$ (where x=0-0.08)) specimens at room temperature are shown in *Fig. 3.1*. The basic PZFNT composition exhibits tetragonal structure (JCPDS file no. 33-0784) of PZT. The analysis shows that all the Sm substituted samples are in pure perovskite phase except for 2 mol% Sm-substituted composition as it reflects additional peaks of $PbTi_3O_7$ (JCPDS file No. 21-0949) for a 2θ value around 29° which is due to the presence of poor pyrochlore phase in the PSZFNT structure [1-2]. It has been reported that in the formation of perovskite phase,

pyrochlore phase formation is an essential step [3]. This type of compound is considered as oxygen deficient compound with a metastable transient phase [4]. It is found that XRD pattern of PZFNT is pyrochlore free, whereas for Samarium concentration i.e. for x=0.02 in PSZFNT, pyrochlore/metastable transient phase was seen whose percentage was evaluated as 4% using the relation [5]

[Ipyro/(Ipyro+Iperov)]x100 ……(3.1)

which is negligibly small and hence the materials can be considered as single-phase [6-7]. The appearance of this extra phase may be attributed to Pb deficiency in the PSZFNT ceramics.

The ionic radii of Sm^{3+} (1.38 Å) is smaller than that of Pb^{2+} (1.63 Å) hence with Sm substitution, the original peak position of the ingredient is shifting towards higher angle side indicating the decrease in lattice parameter. It can be seen from *Fig. 3.2.* that 'a' decreases faster while 'c' increases at slower rate resulting in increased tetragonality. The trend in lattice parameters and lattice volume is shown in *Table 3.1.*

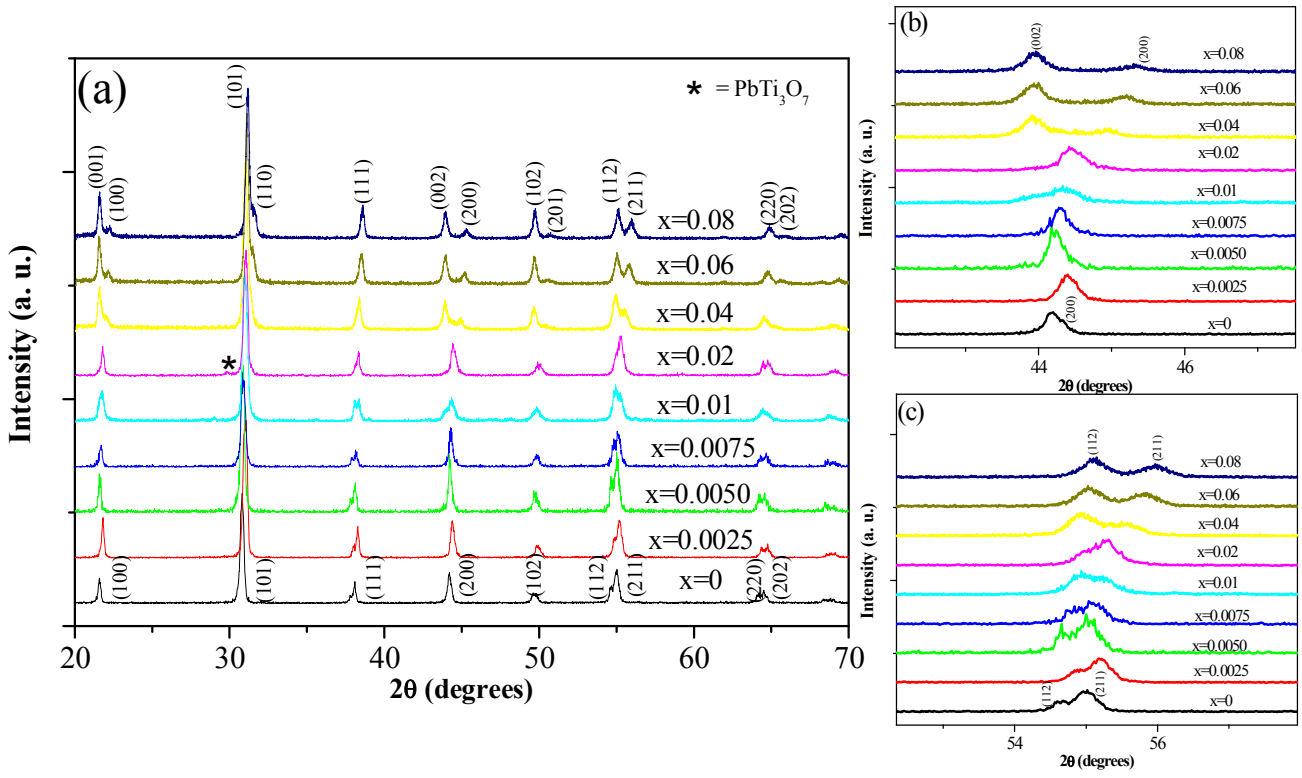

Fig.3.1. (a) X-ray diffraction patterns of the Series A (PSZFNT) samples with different amount of Sm substitution (b) shifts in (002), (200) and (c) (112), (211) peaks in 2θ ranges of (42-48^o) and (52-58^o).

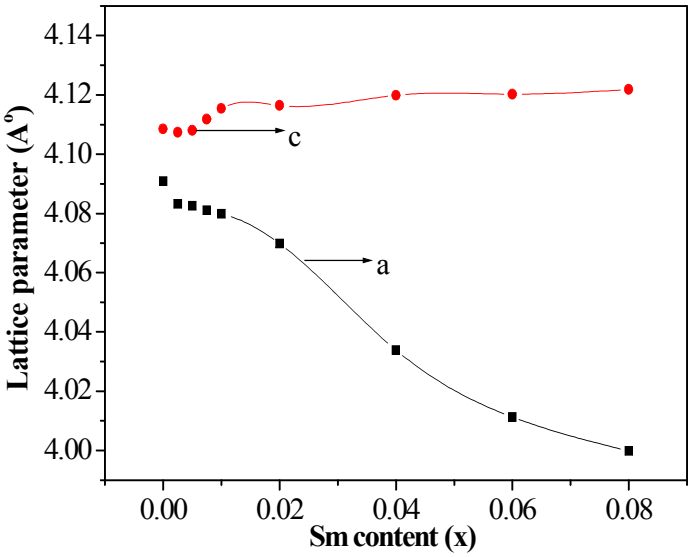

Fig.3.2. Variation in lattice parameters (a, c) with Sm content (x = 0-0.08).

Table 3.1.

Lattice parameters of Series A (PSZFNT) samples

x	Structure	a (Å)	c (Å)	c/a	Lattice Volume (Å^3)
0	Tetragonal	4.0908	4.1085	1.0047	68.75
0.0025	Tetragonal	4.0832	4.1073	1.0059	68.47
0.0050	Tetragonal	4.0825	4.1080	1.0062	68.46
0.0075	Tetragonal	4.0810	4.1118	1.0075	68.48
0.01	Tetragonal	4.0798	4.1154	1.0087	68.49
0.02	Tetragonal	4.0698	4.1164	1.0114	66.22
0.04	Tetragonal	4.0338	4.1198	1.0213	67.04
0.06	Tetragonal	4.0112	4.1202	1.0271	66.29
0.08	Tetragonal	3.9998	4.1218	1.0305	65.94

Increase in Sm concentration increases the c/a ratio which result in strong tetragonal phase with peak splittings at (002) and (200) and (112) and (211) respectively (see *Fig. 3.1(b)-(c)*), which confirms the homogeneous diffusivity of Sm in PZFNT lattice. For x≥0.04, tetragonal phase with its characteristics peak splitting at 2θ in the range of 43–46^o has clearly been observed. The lattice volume decreases from 68.75 Å^3 to 65.79 Å^3 with increase in Sm amount from 0 to 8 mol%.

3.2.2. Structural Analysis of La-Substituted PZFNT Ceramics

The XRD patterns (refer *Fig. 3.3.*) of La substituted compositions ($Pb_{1-x}La_x(Zr_{0.60}Ti_{0.40})_{0.98}Fe_{0.01}Nb_{0.01}O_3$ (where x=0-0.08)) show single phase perovskite structure. The compositions from x=0 to x=0.06 exhibited tetragonal structure (JCPDS file no. 33-0784). The peaks are shifting towards higher angle side with higher La concentrations (x = 0-0.08). This trend in peak shifting may be attributed to decrease in lattice parameters which can be depicted by variation in 'a' and 'c' as shown in *Fig. 3.4.* and *Table 3.2*. Since ionic radii of La^{3+} (1.50 Å) is smaller than Pb^{2+} (1.63 Å) hence La ion replaces Pb site. It can be seen that the tetragonality increases with increase in La content up to x=0.04 but decreases for x≥0.06 indicating the onset of a phase transformation from tetragonal to cubic (JCPDS file no. 46-0336). A magnified picture of the fine changes in the (002), (200) peaks and (112), (211) peaks are shown in the *Fig. 3.3(b)-(c)*. It can be depicted from *Table 3.2*. that lattice volume decreases from 68.75 $Å^3$ to 66.79 $Å^3$ with increase in La amount from 0 to 8 mol%.

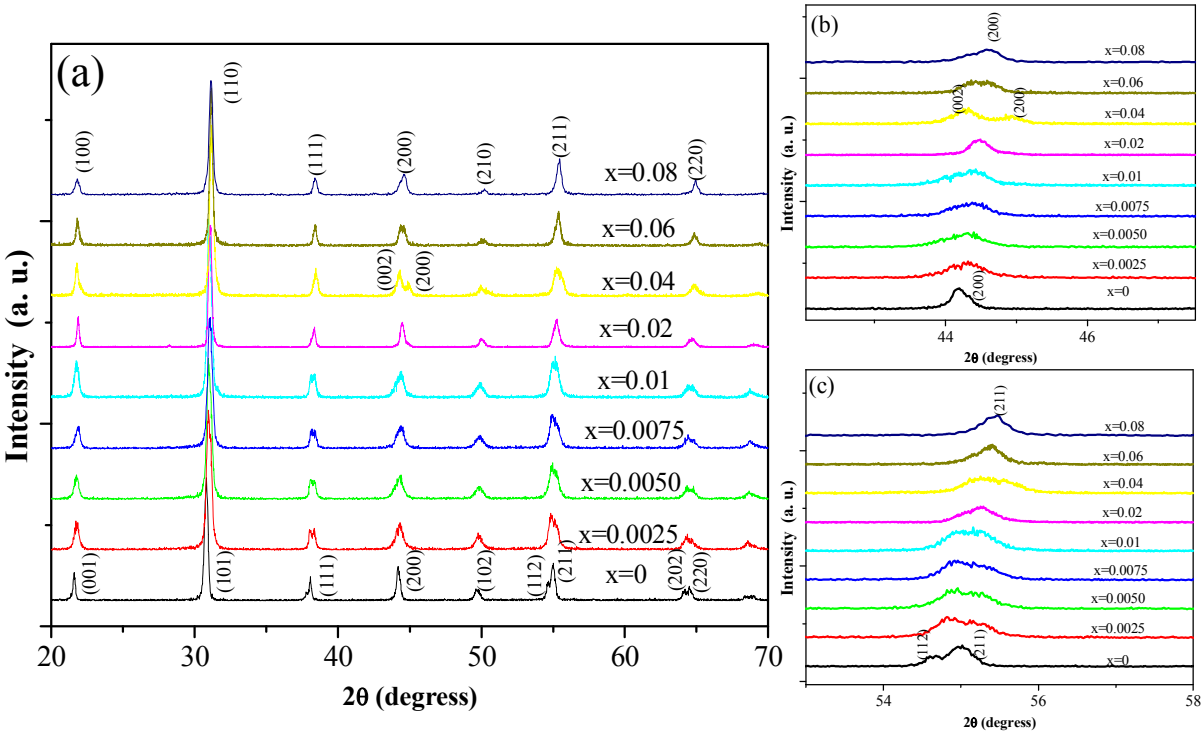

Fig.3.3. (a) X-ray diffraction patterns of the Series B (PLZFNT) samples with different amount of La substitution (b) shifts in (002), (200) and (c) (112), (211) peaks in 2θ ranges of (42-48°) and (52-58°).

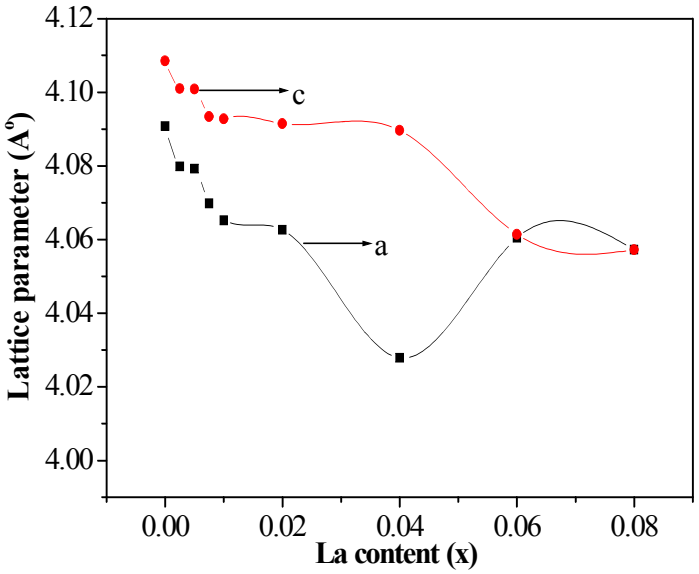

Fig.3.4. Variation in lattice parameters (a, c) with amount of La (x = 0-0.08).

Table 3.2.

Lattice parameters of Series B (PLZFNT) samples.

x	Structure	a (Å)	c (Å)	c/a	Lattice Volume (Å^3)
0	Tetragonal	4.0908	4.1085	1.0047	68.75
0.0025	Tetragonal	4.0798	4.1010	1.0052	68.26
0.0050	Tetragonal	4.0792	4.1008	1.0053	68.24
0.0075	Tetragonal	4.0698	4.0934	1.0058	67.80
0.01	Tetragonal	4.0652	4.0928	1.0067	67.63
0.02	Tetragonal	4.0626	4.0915	1.0071	67.52
0.04	Tetragonal	4.0278	4.0896	1.0153	66.35
0.06	Tetragonal	4.0604	4.0614	1.0002	66.95
0.08	Cubic	4.0572	4.0572	1.0000	66.79

3.2.3. Structural Analysis of Mn-Substituted PZFNT Ceramics

The changes in the lattice parameters and the crystal structure of Series C with Mn substitution in PZFNT are summarized in *Table 3.3*. All XRD patterns of the Mn-substituted PZFNT specimen show rhombohedral structure (JCPDS file no. 73-2022 of PZT) (refer *Fig.*

3.5). There is an extra peak of Mn_2O_3 at ~30.2^o for x=0.015 and 0.02 which corresponds to the JCPDS file no. (02-0902). On the other hand, it can be seen that the diffraction peaks shift to the higher angle with increasing amount of MnO_2 addition which indicates the decrease of lattice constant with increase in MnO_2. Kulscar [8] reported that Cr and Mn exist in more than one valence state in the PZT system. There are other researchers who have also observed reduction of additives added to PZT solid solution [9–11]. At low partial pressures of O_2 and PbO vapor, Mn^{4+} is reduced to Mn^{2+} and Mn^{3+} and is preferred at A sites [12]. The experiments show that the Mn^{4+} is not observed in the Mn-doped PZT ceramics by electron spin resonance (ESR) [13]. As Mn^{3+} has an ionic radius of (0.78 Å) which is closer to the ionic radii of Zr^{4+}/Ti^{4+} (0.86 Å / 0.74 Å) hence it substitutes B site (x≤0.015) and acts as acceptor ion creating oxygen vacancies, resulting in decrease in lattice parameters.

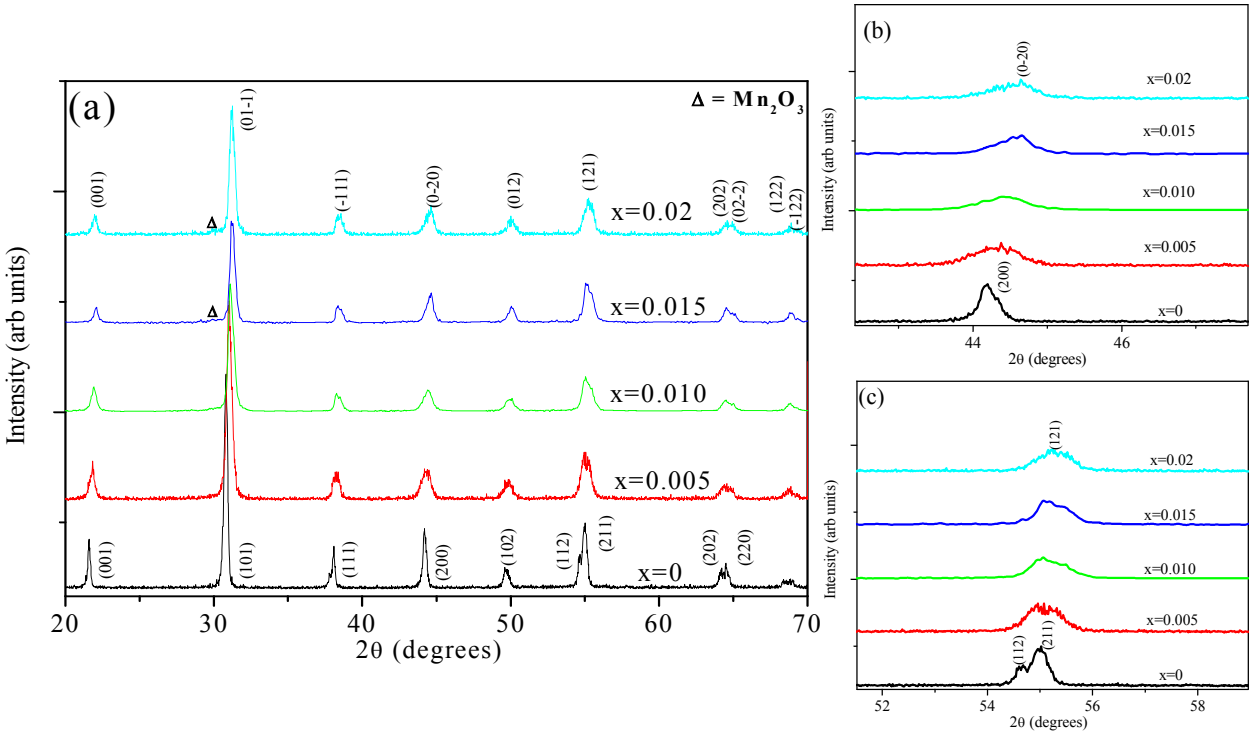

Fig.3.5. (a) X-ray diffraction patterns of the Series C (PZFMNT) samples with different amount of Mn substitution (b) shifts in (200) and (c) (112), (211) peaks in 2θ ranges of (42-48^o) and (52-58^o).

Table 3.3.

Lattice parameters of Series C (PZFMNT) samples.

x	Structure	a (Å)	c (Å)	α (°)	Lattice Volume (Å^3)
0	Tetragonal	4.0908	4.1085	90.00	68.75
0.005	Rhombohedral	4.0762	4.0762	89.90	67.73
0.010	Rhombohedral	4.0751	4.0751	89.80	67.67
0.015	Rhombohedral	4.0642	4.0642	89.70	67.13
0.02	Rhombohedral	4.0652	4.0652	89.68	67.18

For higher concentrations of MnO_2 (x>0.015) existence of Mn^{2+} along with Mn^{3+} in PZFNT cannot be ruled out. Mn^{2+} has ionic radii of 0.97 Å which is closer to the ionic radii of Pb^{2+} (1.63 Å) in comparison to Zr^{4+}/Ti^{4+} (0.86 Å/ 0.74 Å), thus we believe that Mn^{2+} is going onto the A site and drives out PbO from the system. Also, it is an established fact that introduction of oxygen vacancies lead to shrinking of the unit cell [14]. It thus seems that when Mn^{2+} goes to A sites then it leads to reduction in oxygen vacancies which in turn increases the unit cell volume and lattice parameters.

3.3. Density Measurements of Substituted PZFNT Compositions

In the present study, the experimental density has been measured by Archimedes principle as discussed in chapter 2. The experimental density, theoretical density and relative density of all samples of *Series A, B* and *C* is tabulated in *Table 3.4.* From this table it can be observed that for Series A experimental density increases from 7.26 g/cc for x=0 to 7.43 g/cc for x = 0.02 and then decreases whereas for Series B, density increases up to x=0.01 where it is 7.69 g/cc and then decreases. The relative density increases to ~92% upto 1 mol% and decreases to ~89% in Sm-substituted compositions while it increases to ~94% with increase in La upto 1 mol% and decreases to ~71% for higher La concentrations in La-substituted series.

The number of Pb vacancies in PZT is closely related to the types and valence of dopants. The donor dopnats in PZT create Pb vacancies at A-site which are compensated by electrons [15]. The substitution of Sm^{3+} and La^{3+} will create more Pb^{2+} vacancies in PZT lattice in order to maintain electroneutrality. More and more Pb ions become surplus in the PZFNT lattice. This metallic lead is oxidized into PbO and this volatile PbO helps in filling the pores by providing a liquid phase along grain boundaries in which material transport is facilitated resulting in better densification with increasing Sm and La content. Therefore, the relative density of the substituted PZT ceramics increases with addition of La and Sm from x=0 to 0.01. The decrease in relative density for x>0.01 may be attributed to the decrease in diffusivity of Pb vacancies, which results from the cation gradients within the PZT grains and/or the dopant segregation at grain boundaries. Similar results have been reported as other donor dopants were employed [16].

Table 3.4.

Variation of experimental (d_{ex}), theoretical (d_{th}) and relative density (d_{rel}) with substituent amount in PZFNT.

Series A				Series B				Series C			
x	**d_{ex} (g/cc)**	**d_{th} (g/cc)**	**d_{rel} (%)**	**x**	**d_{ex} (g/cc)**	**d_{th} (g/cc)**	**d_{rel} (%)**	**x**	**d_{ex} (g/cc)**	**d_{th} (g/cc)**	**d_{rel} (%)**
0	7.26	8.047	90.22	0	7.26	8.047	90.22	0	7.26	8.047	90.22
0.0025	7.32	8.063	90.78	0.0025	7.14	8.113	88.01	0.005	7.50	8.154	91.98
0.0050	7.39	8.079	91.46	0.0050	7.31	8.125	89.97	0.010	7.51	8.158	92.05
0.0075	7.40	8.071	91.68	0.0075	7.49	8.184	91.52	0.015	7.06	8.222	85.87
0.01	7.41	8.064	91.76	0.01	7.69	8.215	93.61	0.02	7.10	8.214	86.56
0.02	7.43	8.326	89.24	0.02	7.55	8.262	91.38	-	-	-	-
0.04	7.36	8.197	89.79	0.04	7.32	8.478	86.34	-	-	-	-
0.06	7.37	8.261	89.21	0.06	6.84	8.471	80.75	-	-	-	-
0.08	7.33	8.276	88.57	0.08	6.04	8.560	70.56	-	-	-	-

The addition of MnO_2 also has significant influence on the experimental density as well as on relative density. For the samples of Series C, experimental density is found to be 7.51 g/cc, maximum for x = 0.01, and then decreases with further increase in Mn substitution. It can clearly be observed that the ceramics have high relative density ~92% in the MnO_2 substitution range of 0-1.0 mol%, as shown in *Table 3.4*..The substitution of Mn^{3+} in place of Zr^{4+}/Ti^{4+} leads to unbalance of valence states which finally led to the creation of oxygen vacancies. The oxygen vacancies are beneficial for the transfer of mass and energy between the reactants and facilitate the densification of ceramics at low sintering temperature. It is also observed in that for MnO_2 > 1.0 mol%, there is significant drop in relative density which falls to ~86%. A higher porosity is observed which means that the specimens are not sintered effectively. It is expected that Mn ions are homogeneously dissolved in PZFNT ceramics when the MnO_2 addition is below 1.0 mol%, but further addition of MnO_2 will inhibit grain growth due to accumulation of Mn ions at the grain boundaries [13]. This may be due to the fact that beyond this concentration, Mn is either going onto A sites as Mn^{2+} or to the grain boundaries. The X-ray results also support the above conclusion. When Mn^{2+} goes to A sites then Pb volatilization takes place. Due to lead loss for higher Mn content experimental density as well as relative density decreases.

3.4. Microstructural Analysis of Substituted PZFNT Compositions

Microstructure directly influences material properties of lead zirconate titanate. A study of microstructure is necessary in view to control the chemical homogeneity, composition, atomic arrangement, grain morphology and size. The grain size in lead zirconate titanate is greatly influenced by type and amount of additives and is one of the important factors providing useful information for further investigation of other electrical properties such as dielectric, piezoelectric and ferroelectric properties. Average grain size is measured by linear intercept method and is given in *Table 3.5*. The systematic understanding of the effects of La, Sm and Mn addition on microstructure of PZT ceramics is presented. The microstructures of the freshly fractured surfaces of sintered samples of all the compositions are shown in *Figs. (3.6)-(3.8)*. With increase in substituent content, microstructural change is clearly observed in terms of different grain size and distribution of

porosity. It can be seen from the micrographs that the samples show uniform grain growth and grain compaction with well-defined grain boundaries with the increase in substitution of Sm and La in PZFNT ceramics. The grain size increases with increase in La and Sm for small value of substitution ($0 \leq x \leq 0.0050$) and decreases for high value of substitution ($0.0075 \leq x \leq 0.08$). The possible reason for a large grain size for the 0.5 mol% Sm and La substituted sample is the complete solubility of Sm and La in PZFNT lattice. The grain size decreases in series C from 4.1 μm to 1.4 μm with Mn addition in PZFNT composition as x increases from 0 to 0.015. This reduction in grain size is due to the inhibition of grain growth by the oxygen vacancies as a result of Mn addition. There is not much change in average grain size when x increases from 0.015 to 0.02. This is due to the fact that Mn ions are homogeneously dissolved in PZFNT ceramics when the MnO_2 addition is below 1 mol% but further addition of MnO_2 will inhibit grain growth due to accumulation of Mn ions at the grain boundaries resulting in enhanced porosity. This is also evident from the density measurements which also follow the same trend.

Table 3.5.

Variation of grain size with substitution (x) in PZFNT compositions.

Series A		Series B		Series C	
x	**Average grain size (μm)**	**x**	**Average grain size (μm)**	**x**	**Average grain size (μm)**
0	4.1	0	4.1	0	4.1
0.0025	4.2	0.0025	6.0	0.005	2.3
0.0050	7.5	0.0050	7.5	0.010	3.0
0.0075	3.3	0.0075	3.7	0.015	1.4
0.01	5.5	0.01	3.6	0.02	1.6
0.02	3.6	0.02	1.0	-	-
0.04	2.5	0.04	2.0	-	-
0.06	1.9	0.06	1.6	-	-
0.08	1.3	0.08	2.6	-	-

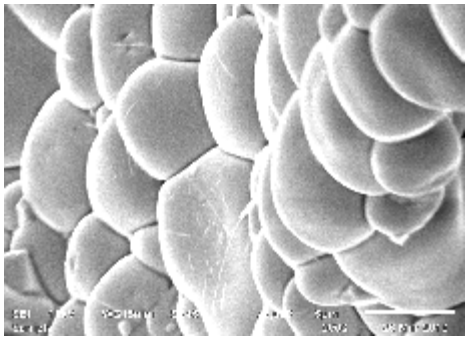

x=0

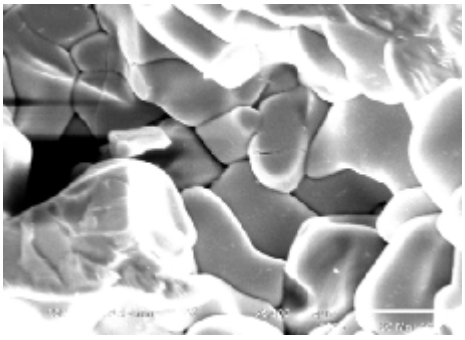

x=0.0025

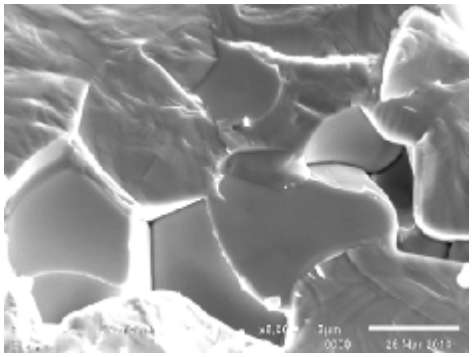

x=0.0050

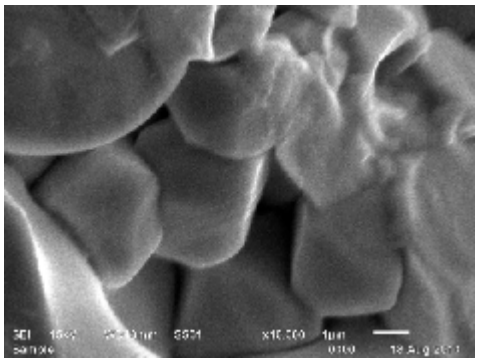

x=0.0075

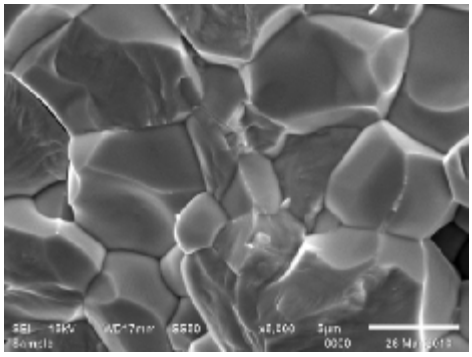

x=0.01

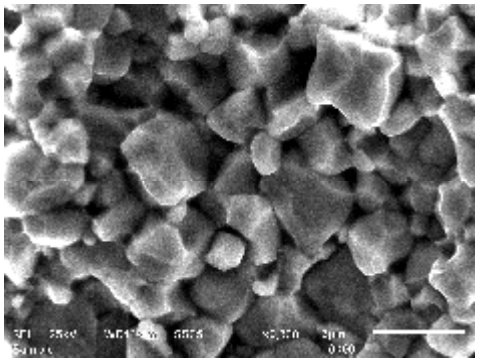

x=0.02

Fig.3.6. Scanning electron micrographs of fractured surface of Series A samples for x=0-0.08 (continued).

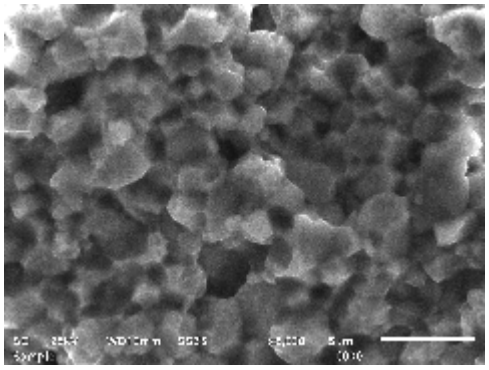

x=0.04

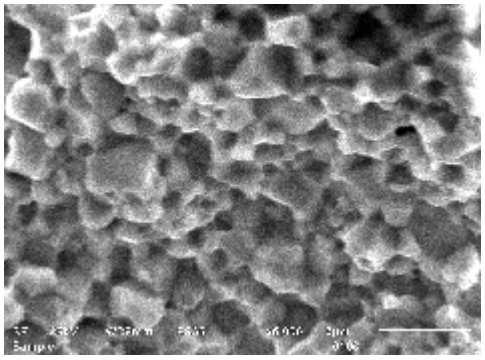

x=0.06

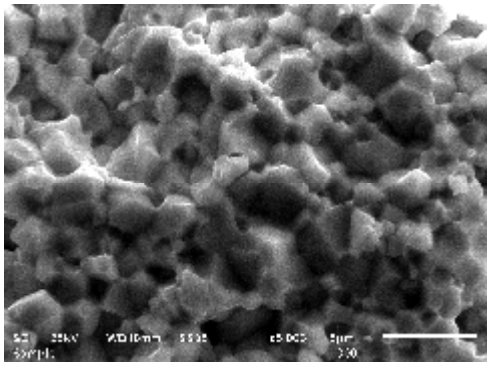

x=0.08

Fig.3.6. Scanning electron micrographs of fractured surface of Series A samples for x=0-0.08.

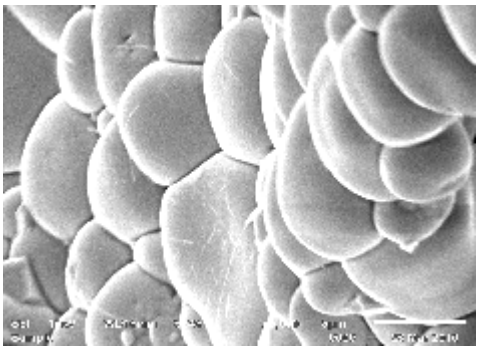

x=0

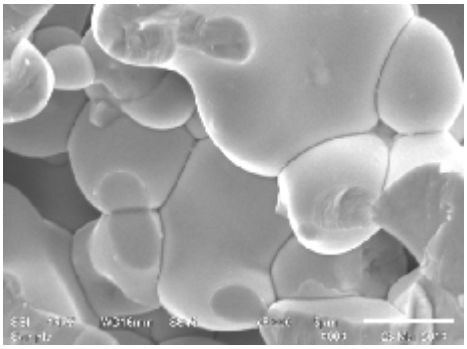

x=0.0025

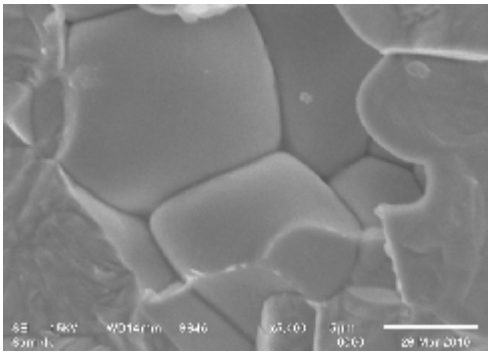

x=0.0050

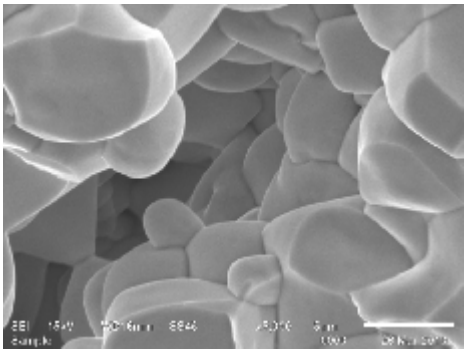

x=0.0075

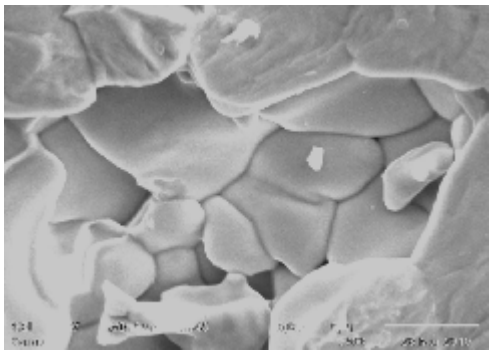

x=0.01

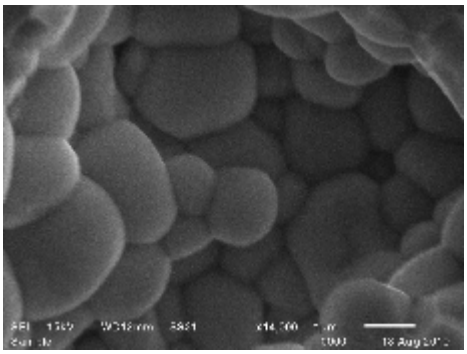

x=0.02

Fig.3.7. Scanning electron micrographs of fractured surfaces of Series B samples for x=0-0.08 (continued).

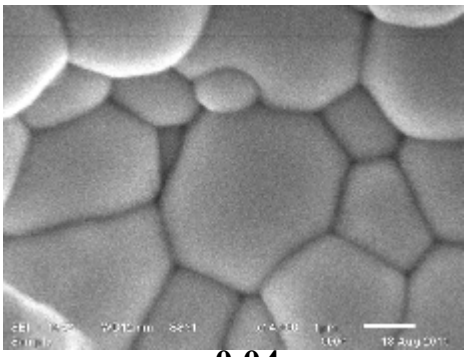

x=0.04

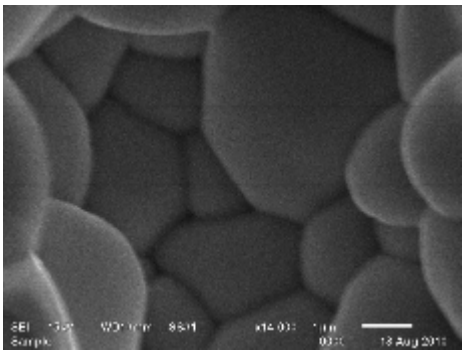

x=0.06

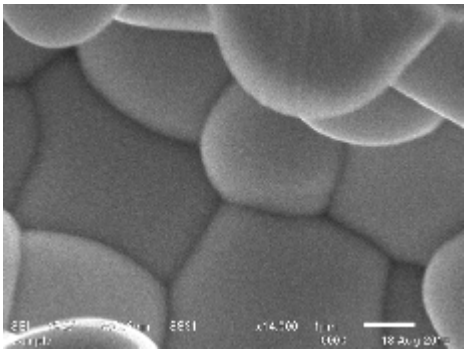

x=0.08

Fig.3.7. Scanning electron micrographs of fractured surfaces of Series B samples for x=0-0.08.

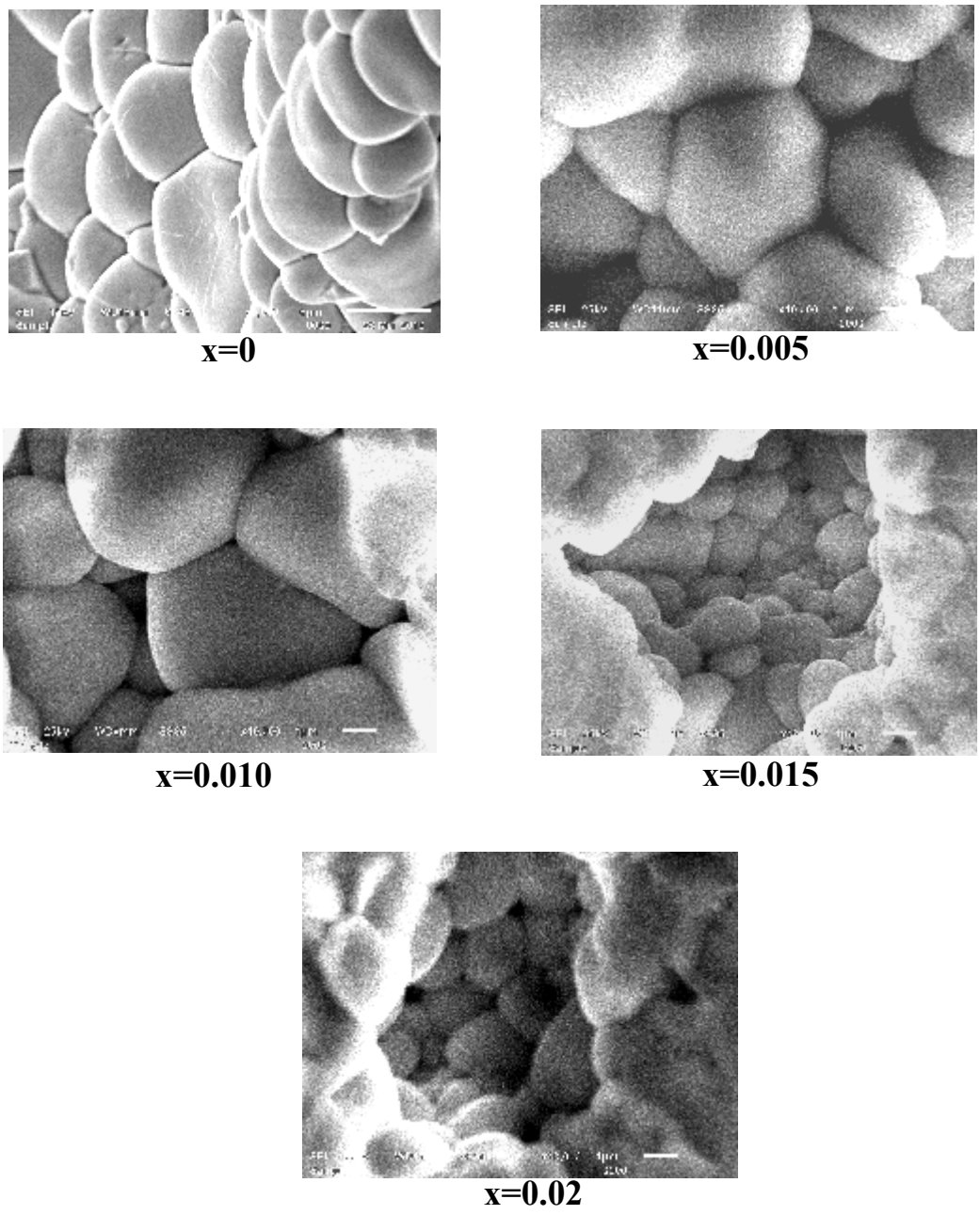

Fig.3.8. Scanning electron micrographs of fractured surface of Mn-substituted PZFMNT samples.

References

[1]. J. Lian, L. Wang, J. Chen, K. Sun, R. C. Ewing, J. M. Farmer and L. A. Boatner, Acta Mater. **51** (2003) 1493.

[2]. S. R. Shannigrahi, R. N. P. Choudhary and H. N. Acharaya, Mater. Lett. **39** (1999) 318.

[3]. A. H. Carim, B. A. Tuttle, D. H. Doughty and S. L. Martinez, J. Am. Ceram. Soc. **74** (1991) 1455.

[4]. K. G. Brooks, I. M. Reaney, R. Klissurska, Y. Haung, L. Bursill and N. Setter, J. Mater. Res. **9** (1994) 2540.

[5]. S. L. Swartz and T. R. Shrout, Mater. Res. Bull. **17** (1982) 1245.

[6]. A. Govindan, H. D. Sharma, A. K. Tripathi, P. K. C. Pillai and T. C. Goel, Ferroelectrics **134** (1992) 217.

[7]. S. R. Shannigrahi, R. N. P. Choudhary and H. N. Acharya, Mater. Sci. Engg. B **60** (1999) 31.

[8]. F. Kulcsar, J. Am. Ceram. Soc. **42** (1959) 343.

[9]. P. R. Chowdary and S. B. Deshpandey, J. Mater. Sci. **22** (1987) 2209.

[10]. T. Izaki, H. Henda and A. Watnabe, Jpn. J. Appl. Phys. **31** (1992) 3045.

[11]. T. Kamiya, T. Suzuki, T. Tsurumi and M. Daimo, ibid. **31** (1992) 3058.

[12]. D. Hennings and H. Pompulun, J. Am. Ceram. Soc. **57** (1974) 527.

[13]. L. X. He and C. E. Li, J. Mater. Sci. **35** (2000) 2477.

[14]. A. J. Moulson and J. M. Herbert, *Electroceramics:Materials, Properties and Applications*, Chapman and Hall; New York (1997).

[15]. R. F. Zhang, H. P. Zhang, J. Ma and Y. Z. Chen and T. S. Zhang, Sol. St. Ion. **166** (2004) 219.

[16]. M. D. Durruthy-Rodríguez, L. D. Pérez-Fernández, A. Peláiz-Barranco and F. Calderón-Pinar, Appl. Phys. A **95** (2009) 423.

CHAPTER IV

Dielectric, Ferroelectric & Piezoelectric Properties of Substituted $Pb(Zr,Ti,Fe,Nb)O_3$ System

Influence of Samarium, lanthanum and manganese substitution on dielectric, ferroelectric and piezoelectric properties of modified PZT is presented and the results are compared with those of undoped modified PZT. Effects of La and Sm substitution at the A site while Mn substitution at B site are found to be quite promising as their addition result in significant improvement in properties.

4.1. Introduction

PZT is the most extensively studied perovskite material due to its wide range of piezoelectric, pyroelectric and ferroelectric device applications [1-7]. The characteristics of the lead zirconate titanate systems can be modified by a number of single or complex doping by multiple A and B site ions which include acceptors, donors and isovalent dopants. Lot of work has been done on modification of PZT with dopants at A or B site in ABO_3 type perovskite structure [8-9]. Several studies on PZT with various dopants viz. Nd, Sm, Eu, Gd, Dy, Er, La, Yb etc. have been done and these materials are prescribed as good dielectric materials due to their high dielectric constant and low dielectric loss [10]. The materials which possess high and broad maxima of permittivity are often utilized for device fabrication [11-13]. The doping of La in PZT system near MPB results in promising piezoelectric, dielectric, pyroelectric and optical properties [14-19]. The La_2O_3 addition in PZT increases the room temperature dielectric constant, mechanical quality factor and squareness of hysteresis loop but reduces curie temperature [20].

PZT ceramics, with variable Zr/Ti ratios and variable dopant concentrations, have been reported to exhibit a variety of ferroic phases such as ferroelectric (FE), anti-ferroelectric (AFE) and para-electric (PE) phases [21-26]. Tetragonal PLZT bulk ceramics with composition 9/56/44 prepared by hot pressing, possesses sufficient optical transparency for optoelectrical device applications [27]. Rhombohedral PLZT 65/35 and 80/20 compositions demonstrate ferroelectric nature and diffuse phase transition [28-29]. PLZT compounds exhibit broadening of dielectric peaks or diffuse phase transitions with relaxation behavior in the transition temperature [30-32]. Both tetragonal and rhombohedral PZT show a diffuse phase transition (DPT) in the dielectric behavior [33–39]. N.W. Thomas reported the relaxor behavior of La substituted PZT as La addition disrupts the long-range polar order of ferroelectric PZT by weakening the ferroelectric interactions [40]. Until now many theoretical and experimental papers have been dedicated to compositions of PLZT x/65/35 or PLZT x/40/60 [41–44]. The PLZT 7/60/40 is one of the most important candidates for piezoelectric applications due to its extremely high piezoelectric coefficients (d_{33}=710 pC/N, k_p=0.72), as reported in the literature [45–47]. MnO_2 is one of the most interesting and useful

additives because Mn ions have multivalence states of Mn^{2+}, Mn^{3+} and Mn^{4+}. In the PZT piezoelectric ceramics, MnO_2 additive is usually recognized as acceptor or "hard" doping element. Mn ions prefer to substitute Ti^{4+} in the B site rather than Pb^{2+} in the A site because the radius of Mn is closer to that of Ti^{4+} [48-49]. PZT modified by Mn is of particular interest since the introduction of manganese (separately or together with other dopants) leads to the formation of hard ferroelectric piezoceramics which are used to fabricate various power devices (hydrophone systems, piezoelectric motors, piezoelectric transformers, and others) [50-54]. Manganese has a variable valency, significant electronegativity and high polarizability and forms predominantly covalent bonds with oxygen. In PZT doped with manganese figure of merit (F_D) improves with MnO_2 addition and hence it is one of the promising materials for infrared detectors as [55]. Zhang et al. examined ferroelectric and pyroelectric properties in sol-gel prepared Mn-doped PZT thin films and concluded that Mn-doped PZT thin films can be considered excellent candidates for both memory devices and pyroelectric applications [56]. Structural and dielectric properties of Mn-modified PZT 65/35 compositions have been reported by B. Tiwari et al. [57]. MnO_2 addition in PZT increases the mechanical quality factor under strong field and low-frequency [58]. Increasing MnO_2 concentration resulted in decrease in tetragonality of PZT which is closely related to decrease in curie temperature [59]. Guiffard et al. [8] have reported conductivity mechanisms of doubly doped (Mn with Nb/F) PZT ($Pb_{0.89}(Ba,Sr)_{0.11}(Zr_{0.52}Ti_{0.48})O_3$). Klimov et al. [60] studied the structural and piezoelectric properties of $(Pb_{0.96}Sr_{0.04})(Zr_{0.5275}Ti_{0.4675}Mn_{0.005})O_3$ system. Hall and Cherdhirunkorn [61] studied the effects of sintering on phase and microstructures of $Pb(Zr_{0.52}Ti_{0.48})_{1-x}Mn_xO_{3-y}F_y$ complex system. Park et al. [62] investigated piezoelectric properties of Nb and Nb/Mn co-doped $Pb(Zr_{0.53}Ti_{0.47})O_3$ ceramics. R. Koduri et al. reported that 1.5 mol% Mn-substituted modified PZT (53/47) composition exhibits d_{33}=486 pC/N and k_p=0.57 which make them suitable for sensor and actuator applications [63].

With the growing interest in developing new materials for device applications, a large number of ferroelectric oxides have been studied in a wide range of compositions and stable structures, in the form of single crystal, thin film and ceramics. The $Pb(Zr,Ti)O_3$ based solid solution systems have been investigated by the addition of various additives and with other

ABO_3-type perovskite for improving sinterability, dielectric, electrical and piezoelectric properties. There are many researchers who have tried to improve the properties of PZT near the morphotropic phase boundary (MPB) using various techniques [20]. In this chapter influence of different Sm, La and Mn contents on dielectric, ferroelectric and piezoelectric properties of the PZFNT (x/60/40), in composition distant from MPB, is presented.

The La, Sm and Mn substituted PZFNT compositional series for subject investigation are as follows:

i) $Pb_{1-x}Sm_x(Zr_{0.60}Ti_{0.40})_{0.98}Fe_{0.01}Nb_{0.01}O_3$ (where x = 0, 0.0025, 0.0050, 0.0075, 0.01, 0.02, 0.04, 0.06, 0.08) (PSZFNT-Series A)

ii) $Pb_{1-x}La_x(Zr_{0.60}Ti_{0.40})_{0.98}Fe_{0.01}Nb_{0.01}O_3$ (where x = 0, 0.0025, 0.0050, 0.0075, 0.01, 0.02, 0.04, 0.06, 0.08) (PLZFNT -Series B)

iii) $Pb(Zr_{0.60}Ti_{0.40})_{0.98-x}Mn_xFe_{0.01}Nb_{0.01}O_3$ (where x = 0, 0.005, 0.010, 0.015, 0.02) (PZFMNT-Series C)

4.2. Dielectric Properties of Substituted Modified PZFNT

In the present study, all substituted PZFNT samples exhibit the dielectric constant (ε) and loss ($tan\delta$) dependence on temperature at different frequencies ranging from 10^2-10^5 Hz. The dielectric spectra are characterized by dielectric peaks that correspond to the expected ferroelectric-to-paraelectric transitions. As temperature increases, dielectric constant (ε) firstly increases slowly and then rapidly upto maximum value (ε_{max}) at a specific temperature called curie point or curie temperature (T_c) which is characterized by ferroelectric-paraelectric phase transition. When temperature is increased further ε decreases. This is a characteristic feature of ferroelectric materials. In this thesis, we have referred the transition temperature (T_c) as "curie temperature" and it is the temperature (T_m) at which dielectric constant achieves maximum value. In this section, room temperature variation of dielectric properties with frequencies of bulk PZFNT system followed by temperature dependence of dielectric constant and loss has been discussed.

4.2.1. Room Temperature Variation of ε and tanδ with Frequency

The room temperature variation of the dielectric constant (ε_{RT}) and loss ($tan\delta_{RT}$) of Sm and La substituted PZFNT as function of frequency (10^2-10^6 Hz) is depicted in *Figs.4.1.(a-d)-4.2.(a-d)*. It is found that as frequency increases, dielectric constant decreases, which is a typical characteristic of dielectric/ferroelectric material. The higher value of ε_{RT} at lower frequencies can be attributed to simultaneous presence of all types of polarizations (i.e. interfacial, ionic, dipolar, electronic, space charge etc.) in the compounds. As frequency is increased, those with large relaxation times cease to respond and hence the decrease in dielectric constant. At lower frequencies, the contribution to dielectric constant from the space charge polarization is maximum, which decreases slowly with the increase of frequency. The space charge arises from the charge accumulation at grain boundaries and at the electrode interface, mainly due to vacancies of lead and oxygen. With the increase of frequency, these dipoles due to space charge having large relaxation times do not respond at higher frequencies resulting in decrease in the dielectric constant. At higher frequencies, the main contribution to ε comes from the electronic polarization as other types of polarizations become ineffective. The value of ε_{RT} increases from 440 to 1170 as x increases from 0 to 0.01 due to increase in density up to 1 mol% Sm content and afterwards decrease in dielectric constant is observed due to pyrochlore phase formation (as shown in the XRD patteren for x=0.02) and reduction in grain size for x≥0.01. In series B, as La amount increases from 0 to 6 mol%, the dielectric constant increases from ~440 to ~5500 and it decreases as La content increases further.

The loss tangent ($tan\delta$) greatly influences the usefulness of a dielectric in electronic applications. In practice, it is found that lower dissipation factor is associated with materials of lower dielectric constant while higher dielectric constant materials by virtue of high polarization mechanisms, display higher dissipation factor. Low relaxation time is associated with instantaneous polarization processes and large relaxation time with delayed polarization processes. The loss contribution is maximized at a frequency where the applied field has the same period of the relaxation process. But unlike dielectric constant, $tan\delta_{RT}$ shows continuous increase with increase in frequency. This nature of variation of ε_{RT} and $tan\delta_{RT}$ with frequency was observed for other modified compositions as well [64-65]. This increase

in $tan\delta_{RT}$ with frequency is due to the presence of hardener Fe^{3+} ions at B site in lattice which is attributed to some extrinsic loss phenomena [66-67].

In *Fig. 4.3 (a-d).* ε_{RT} and $tan\delta_{RT}$ both decrease slowly on increasing frequency which accounts for the normal behavior of dielectric/ferroelectric material. The dielectric constant increases from 440 to 700 while loss decreases from 0.018 to 0.007 as amount of MnO_2 increases from 0 to 0.05 mol%. This trend in dielectric constant and loss can be explained in terms of enhanced densification. This substitution causes oxygen vacancies in the perovskite lattice and therefore, causes internal space charge inside the grains which hinders domain-wall movements. The reduction of domain-wall mobility produces the hard effects that include lower dielectric constant and loss, lower piezoelectric coefficient, lower remnant polarization and higher coercive field [68]. On the other hand, some researchers have found that Mn doping can cause "soft" and "hard" effects simultaneously in PZT when Mn doping ratio is low [69-70]. The dielectric loss increases with increase in MnO_2 ≥1 mol% indicating the appearance of conducting boundary layers as amount of Mn ions increases in PZFNT. The similar trend is observed in other systems as well [71-72]. Hence, it is concluded that these multivalence Mn ions simultaneously substitute the A and B site cations to produce the soft and hard effects at the same time. The dielectric dispersion is large for higher concentrations of Mn ions in PZFNT which is attributed to space charge accumulation.

4.2.2. Variation of ε and tanδ with Temperature

In the present study, dielectric properties of Sm, La and Mn substituted samples are measured as a function of temperature at discrete frequencies in the range 10^2-10^5 Hz. The typical variation in the dielectric constant and loss with temperature for the three different substituted PZFNT formulations represented by *Series A, B* and *C* are shown in *Figs. 4.4, 4.5* and *4.6* respectively. In series A, there is a significant increase in dielectric constant at T_m, ε_{max}, from ~11096 to ~17867 with increase in x from 0 to 0.0075 which is due to the increase in dipole moment of the lattice and afterwards ε decreases up to 0.08 as shown in *Figs. 4.4.* The position of dielectric maxima does not change with frequency. This indicates characteristics of normal ferroelectrics [73]. It is also clear that an increase in frequency

causes a decrease in the maximum value of the dielectric constant, whereas only a small shift in curie temperature could be observed. Due to varying amounts of Sm substitution, the crystal structures of different compositions do not maintain the same lattice parameters resulting in different curie temperatures, at which crystal changes its symmetry along with the unit cell parameters. The value of T_m decreases with increases in samarium concentration. The decrease in transition temperature is mainly due to decrease in rattling space in the PZFNT lattice which normally occurs due to shrinkage in lattice volume and substitution of lesser ionic size substituents. As Sm^{3+} is having lesser ionic size than Pb^{2+} this causes shrinkage in PZFNT lattice. Overall this variation in T_m can be correlated to decrease in grain size with increase in Sm content. In series B, the increment in the ε_{max} value from ~11096 to ~40841 as x increases from 0 to 0.005 in the PLZFNT compound implies that the substitution of La^{3+} ion increases the dipole moment of the lattice up to x=0.005 and decreases afterwards. It has also been observed that the dielectric peak shifts towards the low-temperature side and the maximum dielectric constant decreases with increasing La^{3+} content for x ≥0.005. As there is increase in La concentration, a systematic decrease in transition temperature T_m takes place from 355^{o}C to 79^{o}C. T_m is decreasing with La substitution because the grain size is decreasing with rare earth ions addition. For the composition with x=0.08, dielectric peak could not be observed in measurement range of temperature as facility is not available for measurement below room temperature. It is interesting to note that at room temperature samples having La content x ≥ 0.06 remain in paraelectric cubic phase and are well supported by the XRD results. However, the value of T_m shifts to higher temperatures with increasing frequency for x=0.06. Also, the maximum in the dielectric constant and dielectric loss do not coincide at the same temperature *(Fig. 4.5.)*. In this relaxor type composition, exhibiting diffuse phase transition, the remanent polarization, P_r, gradually decreases to zero on increasing the temperature towards T_m as can be seen in *Fig. 4.18*. The dielectric peak is found to be narrower with increasing La^{3+} content up to x=0.01 and width of peak increases with increase in La content for x≥0.02. The dielectric spectrum is a broadened curve rather than a sharp peak (as in normal ferroelectrics) around T_m, which is one of the most important characteristics of a disordered perovskite structure with a diffuse phase transition. This behavior in La substituted samples is due to the difference in the ionic radii of La with Pb and Zr/Ti. Since ionic radii of La is 1.50 Å respectively

midway between those of Zr (0.86 Å) /Ti (0.74 Å) and Pb (1.63Å) hence La may substitute equally at both A and B site. La^{3+} ion have different valency than that of Pb^{2+} and Zr^{4+}/Ti^{4+} ions, substitution by La ion produces a charge imbalance and charge compensation requires that electron, electron holes, or vacancies may be produced. This attributes to substitutional fluctuations and structural disorder in the arrangement of cations at the A site which is occupied here by the Pb^{2+} with La^{3+} additives, those are compensated by lattice size vacancies, and/or at the B site occupied by Zr^{4+}, Ti^{4+}, Fe^{3+} and/or Nb^{5+} with lattice site vacancies, leading to microscopic heterogeneities in the composition and thus a distribution of different local Curie points. A statistical treatment based on a postulated Gaussian distribution of local Curie temperatures which is associated with compositional fluctuations has been given by Rolov and Tela [74].

The dielectric parameters of Mn-doped compositions of Series C are shown in *Table 4.3*. As in normal ferroelectrics, the dielectric constant of Mn-substituted PZFNT samples increases gradually with increase in temperature to T_m and on further increasing the temperature ε decreases (*Fig. 4.6*). The value of ε_{max} for 2 mol% Mn-substituted samples is ~26959 is more than the basic modified PZT (ε_{max}~ 11096). This is due to the reason that Mn^{3+} replaces Zr/Ti at B site of ABO_3 structure as its ionic radius (0.78 Å) is less than Zr (0.86 Å)/Ti (0.74 Å) which give rise to local deformation of the perovskite unit cells. The structural change from tetragonal to rhombohedral structure after MnO_2 introduction results in easier orientation of dipoles which in turn increases ε. In addition, the increase in dielectric constant is related to increase in density as well. As concentration of MnO_2 is increased further, dielectric constant decreases and loss increases which can be correlated to decrease in grain size. Hence "hardening effect" of MnO_2 dominates which in turn decreases ε and enhances *tanδ*. It is interesting to notice that curie temperature decreases with increase in amount of MnO_2 from 0 to 1 mol% and increases afterwards emphasizing that solubility limit of MnO_2 in PZFNT lattice is only 1 mol% and it accumulates at the grain boundaries for Mn amount of 1 mol%. T_m is decreasing upto 1 mol% with Mn addition in Series C but slight increase is observed for $x \geq 0.015$. This variation is in accordance to grain size variation with Mn substitution in basic PZFNT matrix. The segregation of Mn at grain boundaries for Mn content more than 1 mol% is responsible for increase in T_m. The trend of curie temperature with cations substitution tabulated in *Table 4.4*.

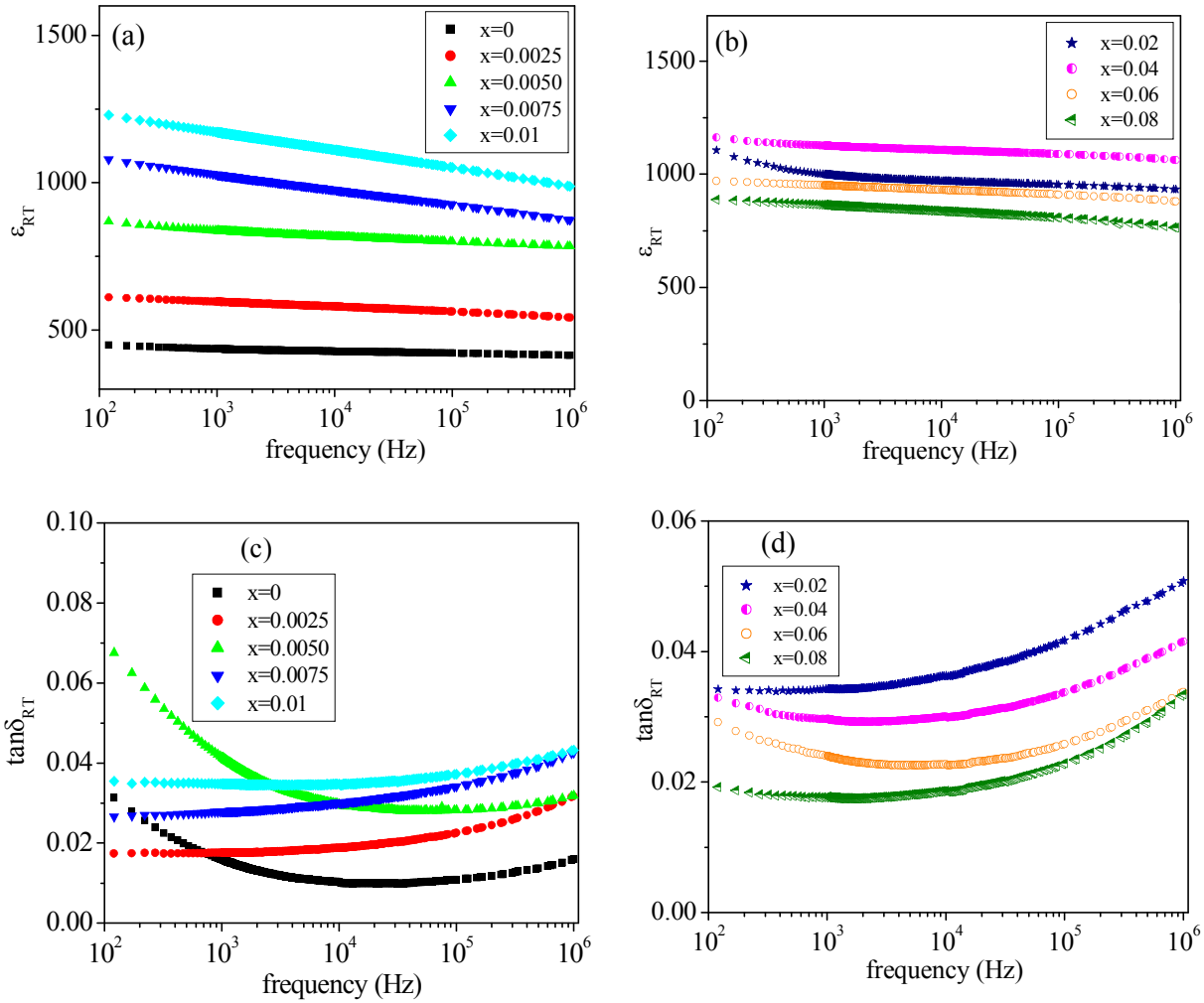

Fig. 4.1. Variation of (a) and (b) dielectric constant (ε_{RT}), (c) and (d) loss tangent ($tan\delta_{RT}$) of Series A as a function of frequency at room temperature.

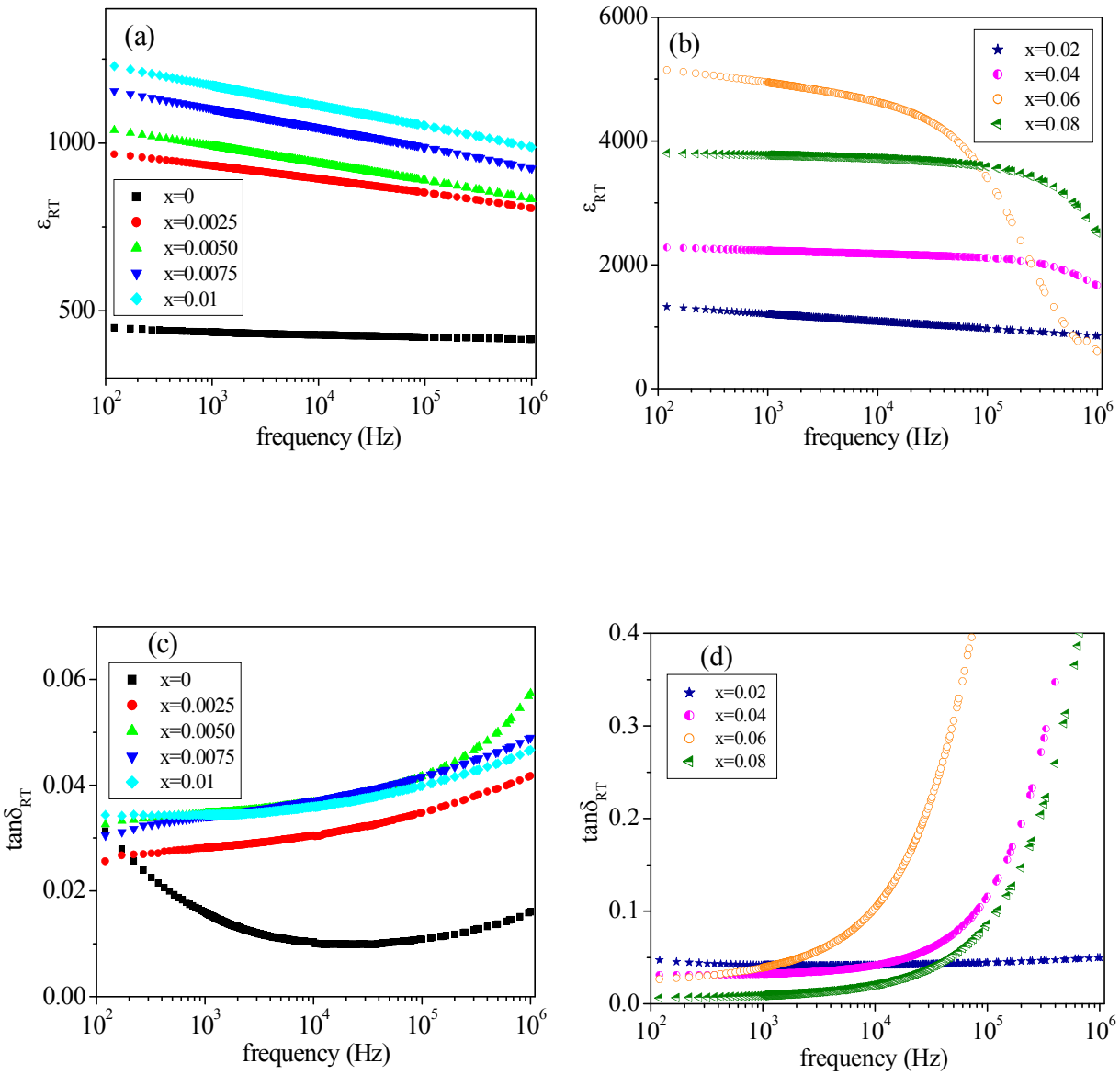

Fig. 4.2. Variation of (a) and (b) dielectric constant (ε_{RT}), (c) and (d) loss tangent ($tan\delta_{RT}$) of Series B as a function of frequency at room temperature.

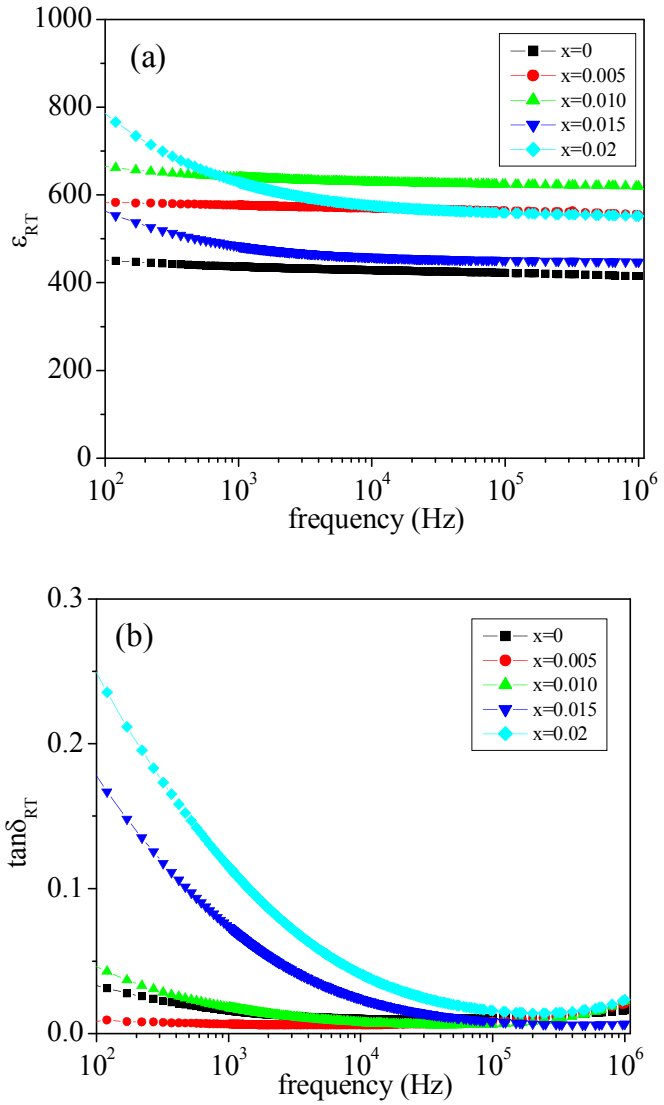

Fig. 4.3. Room temperature variation of (a) dielectric constant (ε_{RT}) (b) loss tangent ($\tan\delta_{RT}$) of Series C as a function of frequency.

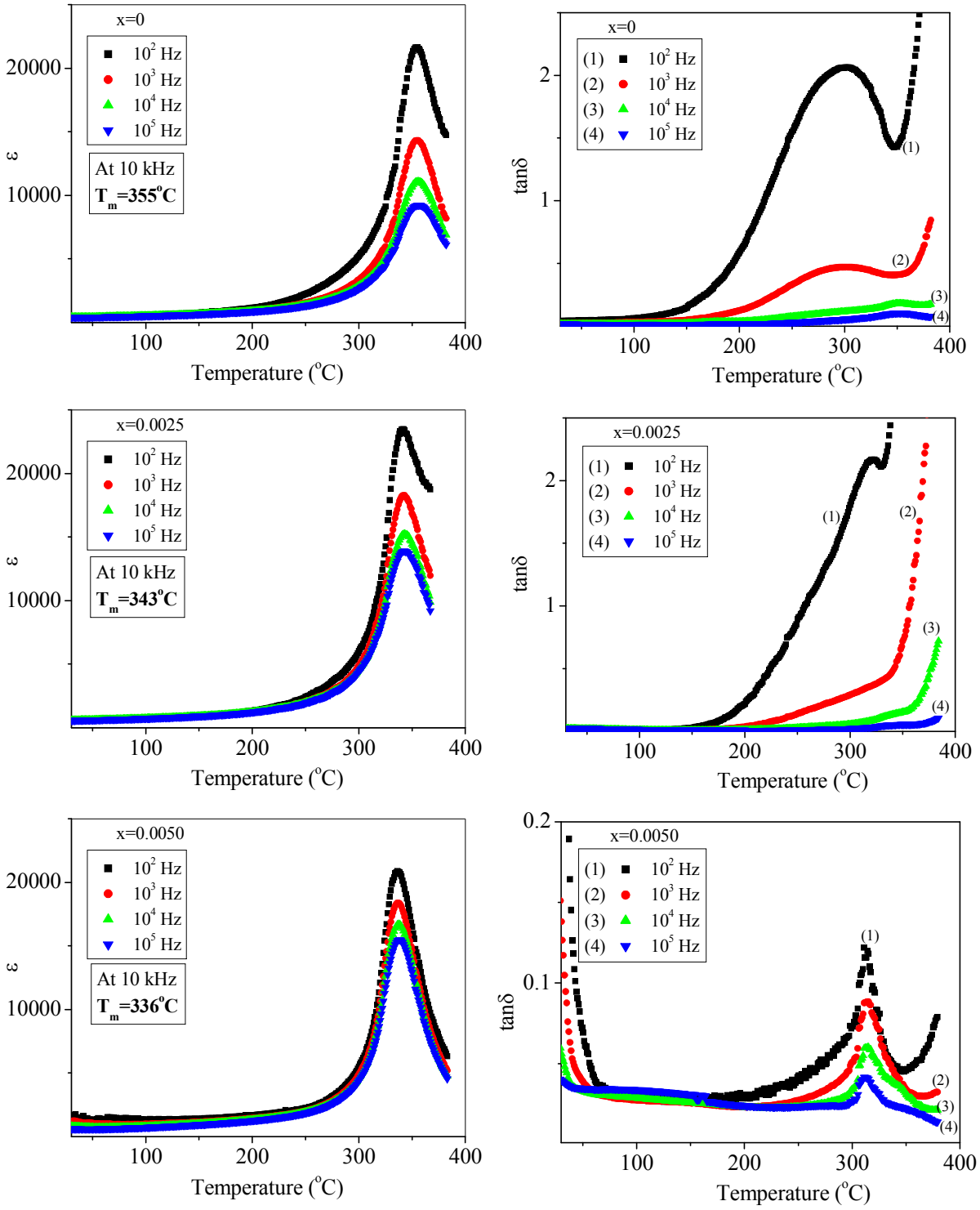

Fig. 4.4. Variation of dielectric constant (ε) and loss tangent (tanδ) with temperature for Series A (Sm-substituted PZFNT) samples at different frequencies (continued).

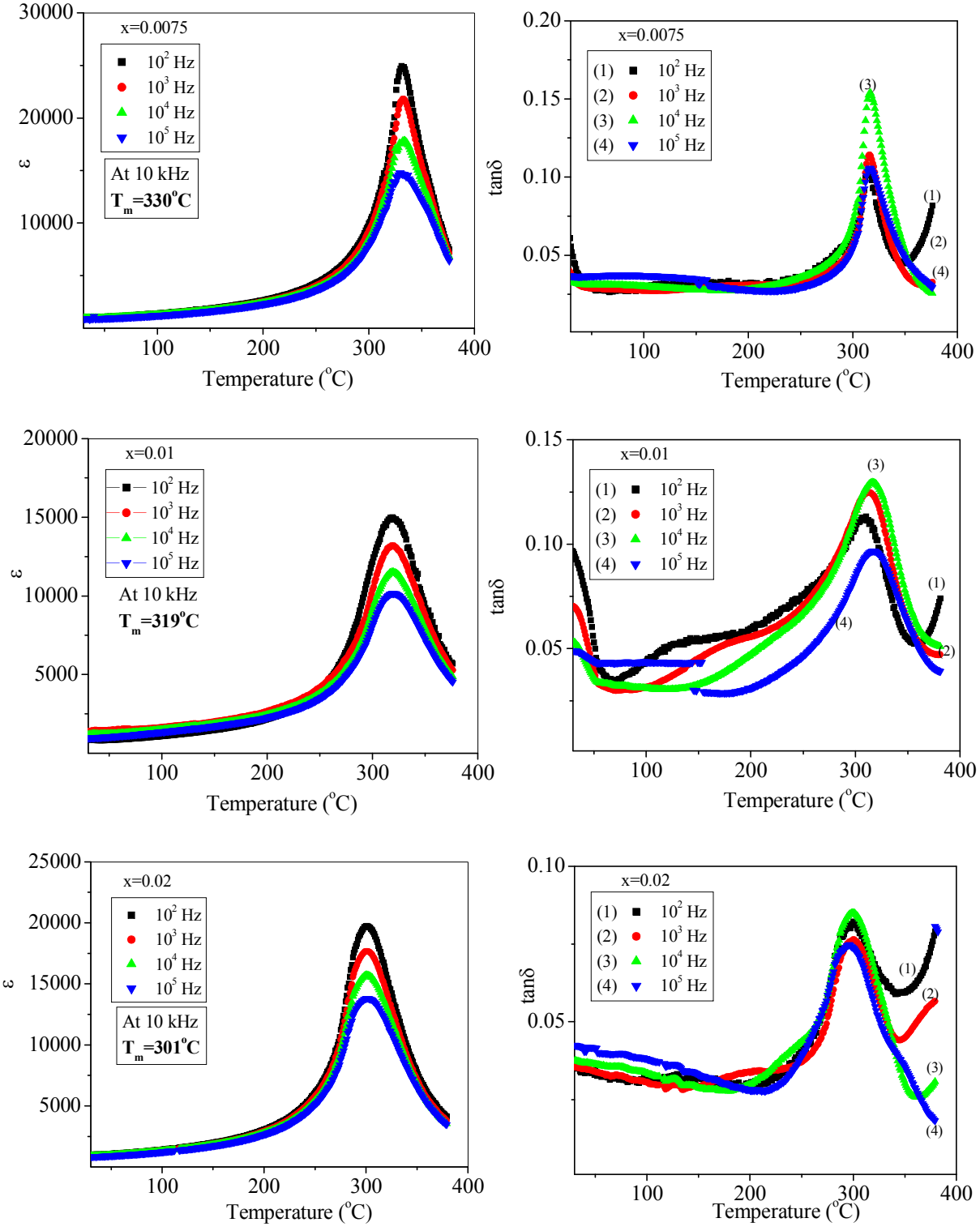

Fig. 4.4. Variation of dielectric constant (ε) and loss tangent (tanδ) with temperature for Series A (Sm-substituted PZFNT) samples at different frequencies (continued).

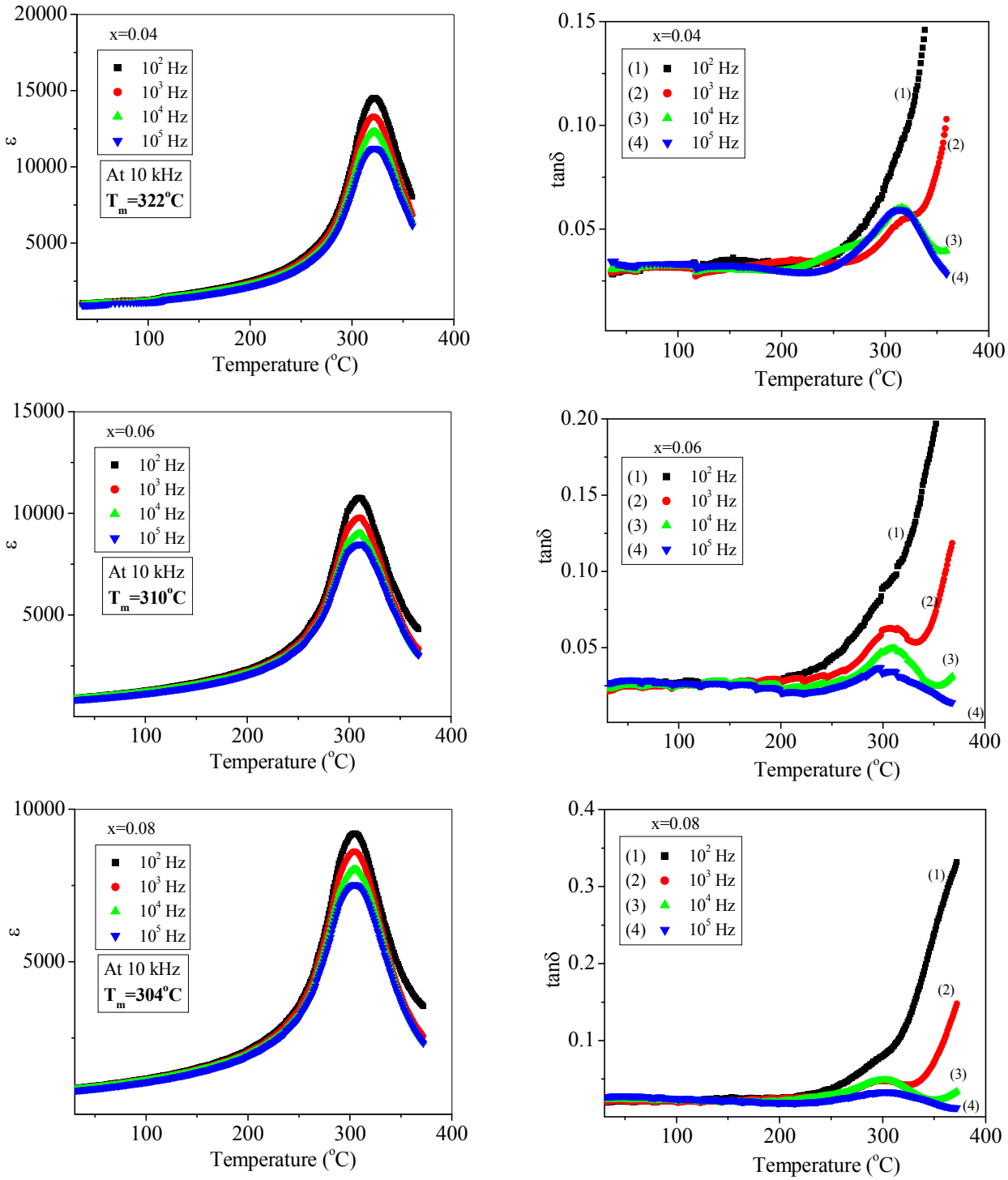

Fig. 4.4. Variation of dielectric constant (ε) and loss tangent (tanδ) with temperature for Series A (Sm-substituted PZFNT) samples at different frequencies.

Table 4.1.
Variation of dielectric parameters of Series A ceramics at different frequencies.

Sm (x)	ε_{RT}			ε_{max} at T_m			$\tan\delta_{RT}$			$\tan\delta_{max}$ at T_m		
	10^3 Hz	10^4 Hz	10^5 Hz	10^3 Hz	10^4 Hz	10^5 Hz	10^3 Hz	10^4 Hz	10^5 Hz	10^3 Hz	10^4 Hz	10^5 Hz
0	448	437	428	14327	11096	9232	0.023	0.017	0.018	0.414	0.181	0.106
0.0025	632	611	592	18280	15261	13916	0.023	0.024	0.028	0.517	0.139	0.055
0.0050	1398	842	630	18371	16681	15408	0.138	0.056	0.039	0.049	0.039	0.025
0.0075	1042	994	947	21792	17867	14439	0.038	0.033	0.037	0.074	0.109	0.081
0.01	1198	1171	966	13169	11523	10175	0.070	0.053	0.049	0.121	0.129	0.097
0.02	969	919	868	17676	15725	13826	0.036	0.037	0.042	0.076	0.085	0.073
0.04	1054	1014	971	13276	12321	11239	0.029	0.031	0.034	0.055	0.058	0.057
0.06	918	889	858	9789	9024	8493	0.022	0.023	0.026	0.062	0.049	0.034
0.08	879	854	827	8609	8035	7533	0.020	0.023	0.027	0.047	0.049	0.033

Table 4.2.
Variation of dielectric parameters of Series B ceramics at different frequencies.

La (x)	ε_{RT}			ε_{max} at T_m			$\tan\delta_{RT}$			$\tan\delta_{max}$ at T_m		
	10^3 Hz	10^4 Hz	10^5 Hz	10^3 Hz	10^4 Hz	10^5 Hz	10^3 Hz	10^4 Hz	10^5 Hz	10^3 Hz	10^4 Hz	10^5 Hz
0	448	437	428	14327	11096	9232	0.023	0.017	0.018	0.414	0.181	0.106
0.0025	890	864	836	32734	25402	22711	0.032	0.038	0.043	0.187	0.099	0.053
0.0050	990	944	891	44599	40841	38504	0.036	0.041	0.042	0.094	0.055	0.044
0.0075	1152	1091	1031	40604	37508	35657	0.037	0.039	0.044	0.087	0.048	0.033
0.01	1283	1219	1156	39905	36271	34374	0.033	0.037	0.043	0.083	0.050	0.037
0.02	1229	1157	1090	14266	13479	12167	0.044	0.041	0.043	0.034	0.052	0.084
0.04	2265	2158	2046	11091	10001	9738	0.034	0.035	0.039	0.085	0.042	0.017
0.06	6301	5588	4899	8118	7798	7508	0.049	0.064	0.083	0.028	0.029	0.039

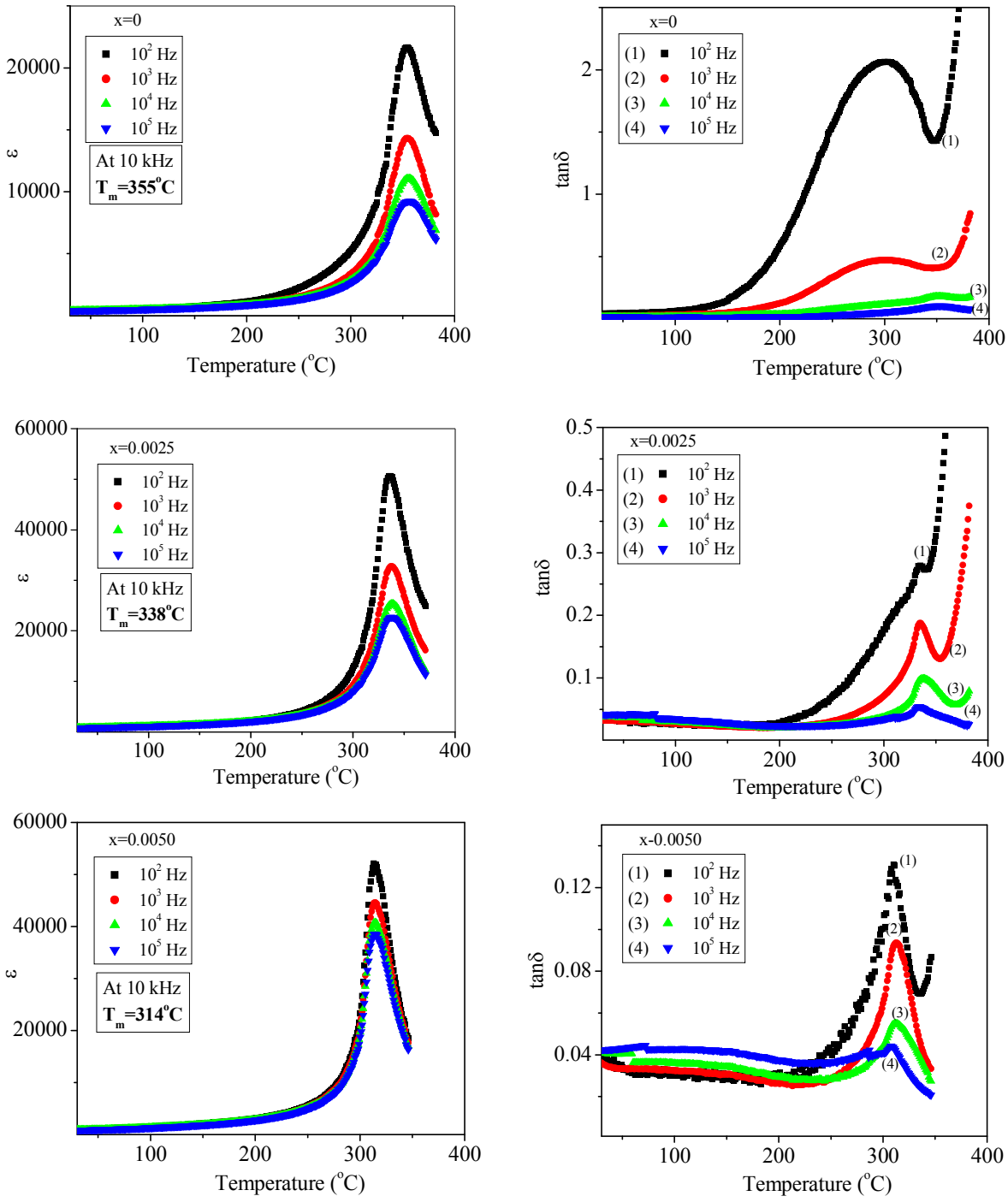

Fig. 4.5. Variation of dielectric constant (ε) and loss tangent (tanδ) with temperature for Series B (La-substituted PZFNT) samples at different frequencies (continued).

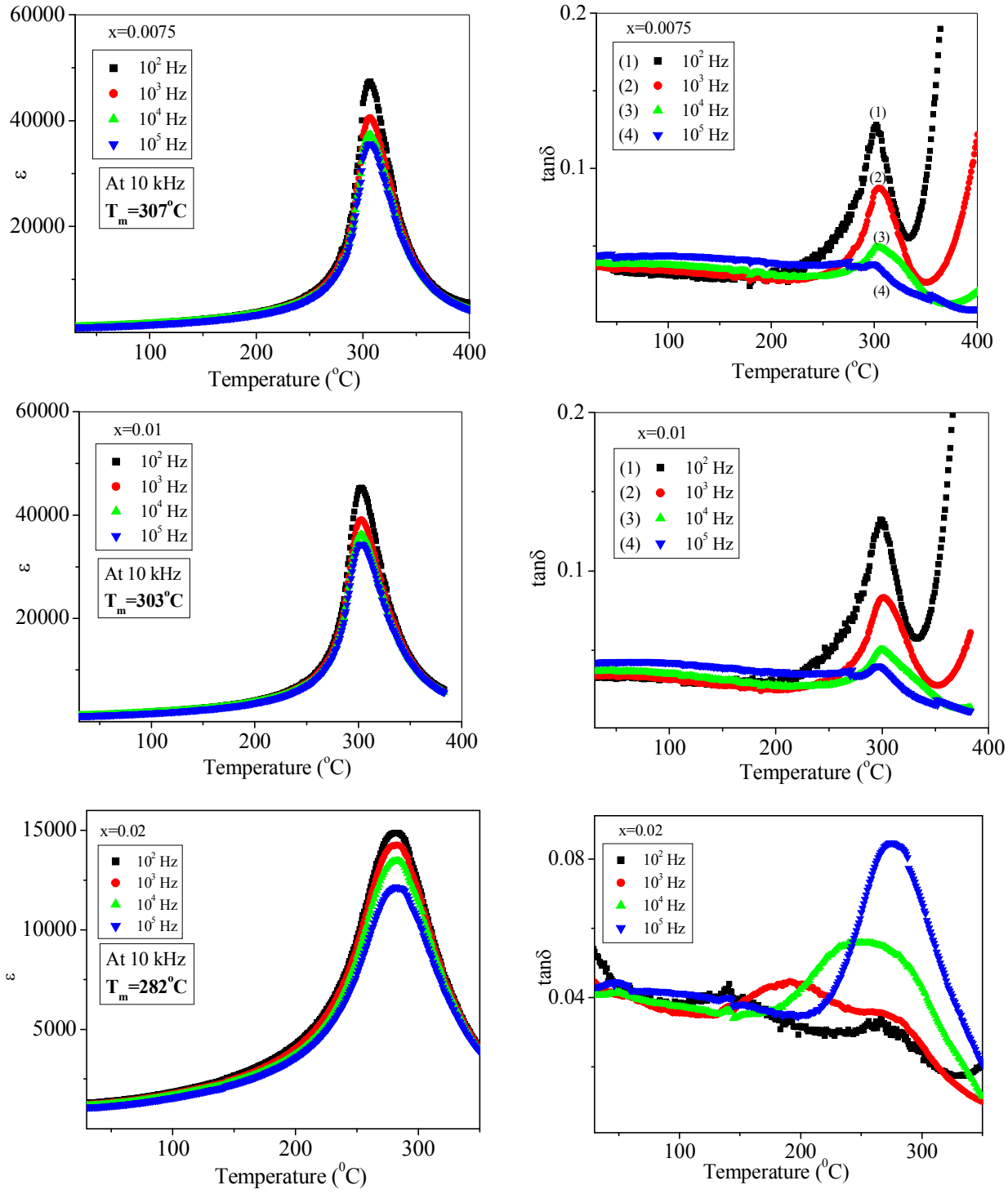

Fig. 4.5. Variation of dielectric constant (ε) and loss tangent (tanδ) with temperature for Series B (La-substituted PZFNT) samples at different frequencies (continued).

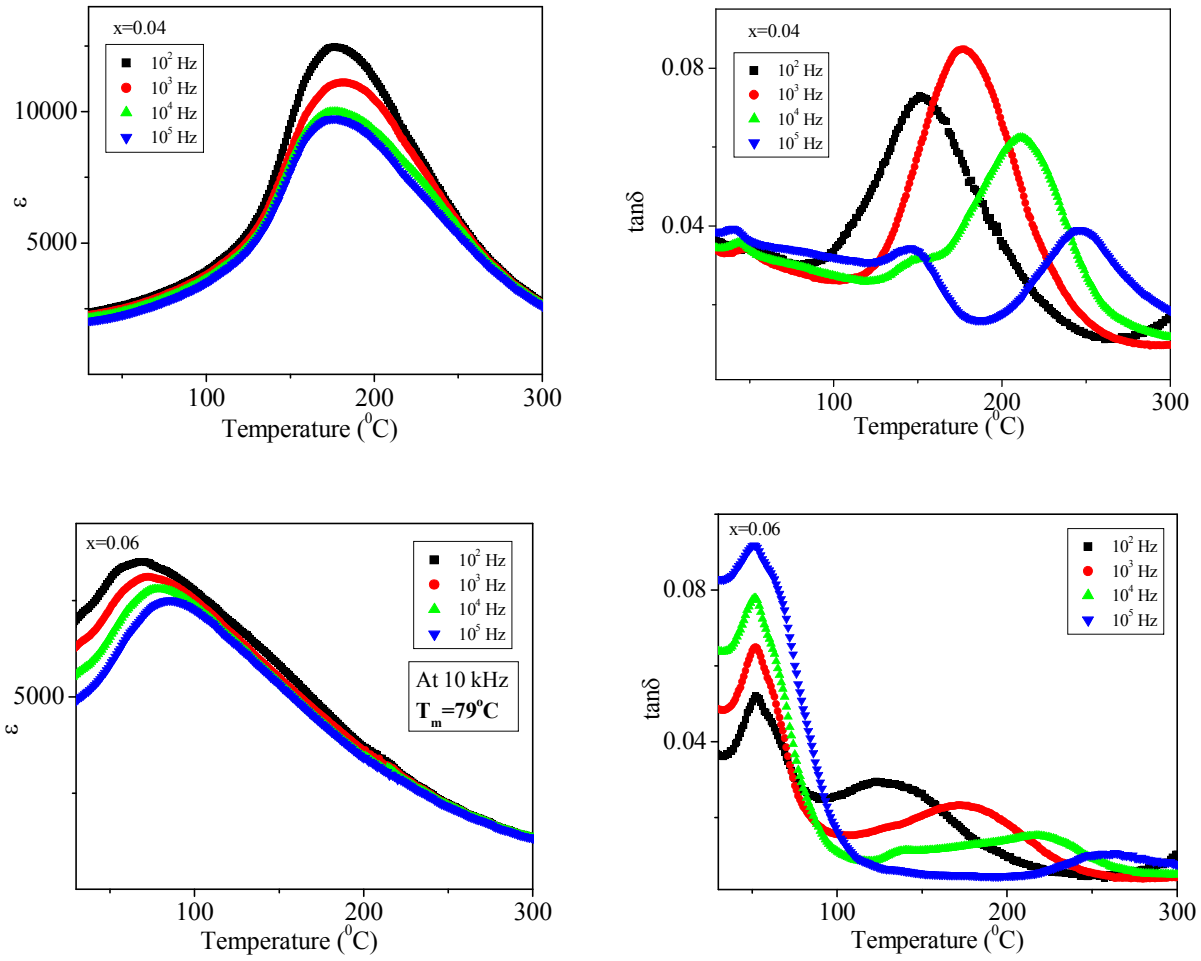

Fig. 4.5. Variation of dielectric constant (ε) and loss tangent (tanδ) with temperature for Series B (La-substituted PZFNT) samples at different frequencies.

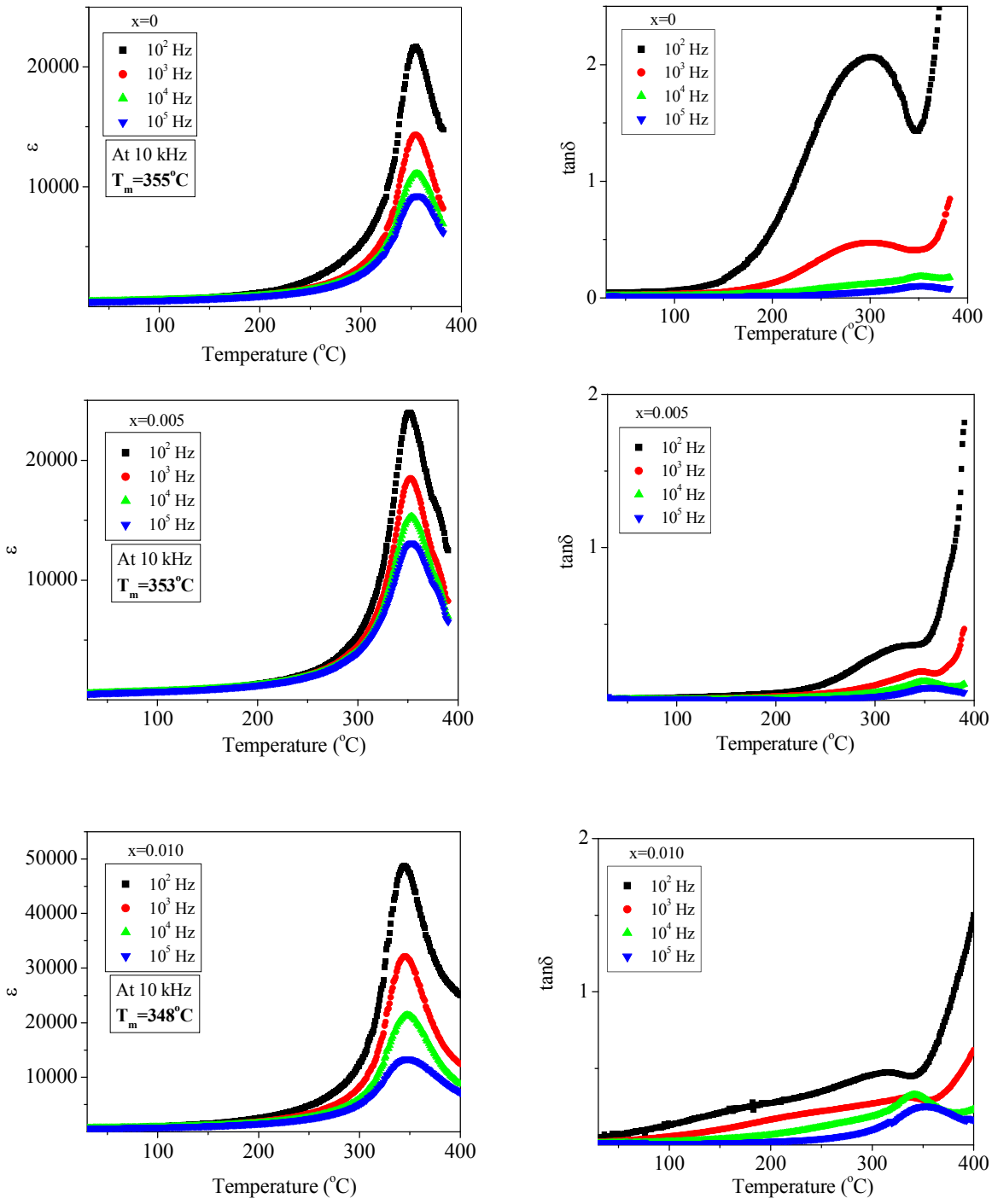

Fig. 4.6. Variation of dielectric constant (ε) and loss tangent (tanδ) with temperature for Series C (Mn-substituted PZFMNT) samples at different frequencies (continued).

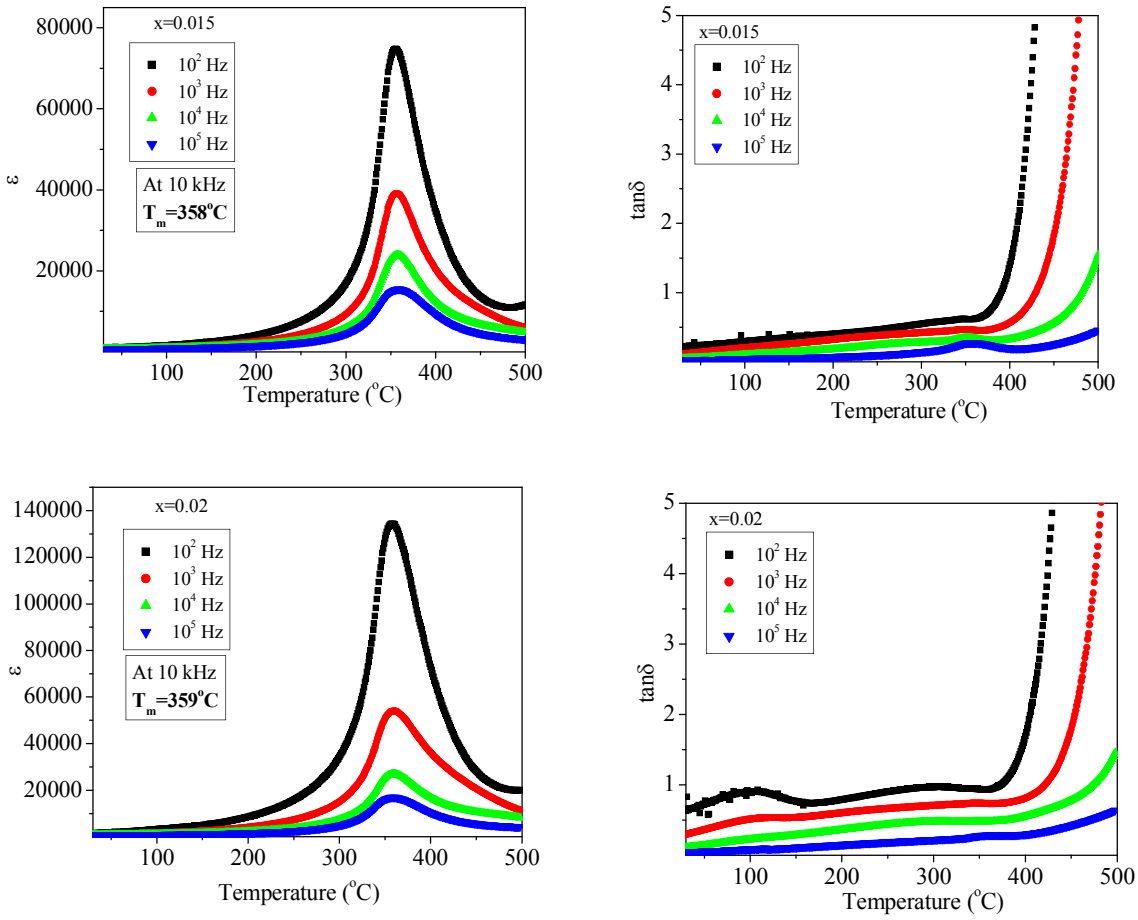

Fig. 4.6. Variation of dielectric constant (ε) and loss tangent (tanδ) with temperature for Series C (Mn-substituted PZFMNT) samples at different frequencies.

Table 4.3.
Variation of dielectric parameters of series C at different frequencies.

Mn (x)	ε_{RT}			ε_{max} at T_m			$\tan\delta_{RT}$			$\tan\delta_{max}$ at T_m		
	10^3 Hz	10^4 Hz	10^5 Hz	10^3 Hz	10^4 Hz	10^5 Hz	10^3 Hz	10^4 Hz	10^5 Hz	10^3 Hz	10^4 Hz	10^5 Hz
0	448	437	428	14327	11096	9232	0.023	0.017	0.018	0.414	0.181	0.106
0.005	539	536	533	18483	15301	13093	0.005	0.007	0.023	0.183	0.122	0.086
0.010	710	700	692	31889	21392	13369	0.020	0.013	0.016	0.029	0.317	0.252
0.015	746	685	664	39023	23945	15452	0.114	0.046	0.026	0.457	0.337	0.275
0.02	892	728	680	53912	26959	16943	0.295	0.108	0.047	0.734	0.482	0.287

Table 4.4.
Variation of curie temperature (T_m) with amount of substitution (x) in PZFNT samples.

Series A		**Series B**		**Series C**	
x	**T_m (^oC)**	**x**	**T_m (^oC)**	**x**	**T_m (^oC)**
0	355	0	355	0	355
0.0025	343	0.0025	338	0.005	353
0.0050	336	0.0050	314	0.010	348
0.0075	330	0.0075	307	0.015	358
0.01	319	0.01	303	0.02	359
0.02	301	0.02	282	-	-
0.04	322	0.04	178	-	-
0.06	310	0.06	79	-	-
0.08	304	0.08	-	-	-

The peak dielectric constant shows a significant dispersion with frequency in La substituted samples. The nature of transition is seen to change from normal (sharp-like dielectric peak) to diffuse (broad-like dielectric peak) when La^{3+} content increases up to 6 mol%. This dispersion suggests that the PLZFNT compounds become more disordered with increase of La amount at the Pb site confirming the diffuse phase transition in the materials.

Relaxor behavior is observed for PLZFNT compositions when La content reaches to x=0.06. A closer observation of peak at dielectric maxima reveals that the peaks are shifting towards higher temperature side with increase in frequency which is a typical behavior of a relaxor material and is considered to be useful for capacitor applications. All other compositions do not exhibit such kind of dielectric relaxation. This is due to the reason that normal micrometer-size ferroelectric domains cannot be sustained when the lanthanum content is higher than a critical value [75]. The relaxor behaviour is attributed to the presence of ions with different valence state at the B site of $A(B_1B_2)O_3$ perovskite structure [76-77]. However, in perovskite materials, such relaxor behaviour was mainly observed in lead-based and its derived compositions such as $Pb(Mg_{1/3}Nb_{2/3})O_3$(PMN), $Pb(Sc_{1/2},Ta_{1/2})O_3$ (PST), and $(Pb,La)(Zr,Ti)O_3$(PLZT) [72-73]. The main features of relaxor behaviour are linked to structural and compositional inhomogeneity occurring due to random site disorder giving rise to occurrence of polar nano-domains resulting in diffuse phase transition.

4.3. Ferroelectric Properties of Substituted Modified PZFNT

PZT based ferroelectric materials have tremendous potential to be used as ferroelectric memory devices. The success of material for this particular usage depends on the values of its remnant polarization and coercivity. A material with moderate coercivity, high remanant polarization and square/rectangular hysteresis loop is preferred for this purpose [78]. Materials with high coercivity are difficult to be made to reach their saturation polarization and are not suitable for memory devices. Squareness increases the probability of retention in a definite state of polarization until a reverse electric field equal to its coercivity is applied. The switching voltage from positive to negative bias (usually represented as 0 and 1 in the binary digital system) of the memory device is determined by the coercivity of the material. Ferroelectric materials have been considered for use in non-volatile ferroelectric random access memories (NVFRAM). These devices use the switchable spontaneous polarization which is the defining characteristic of a ferroelectric material [79-81].

4.3.1. Room Temperature Hysteresis Behavior

The typical polarization versus electric field (P-E) curves for Sm and La substituted PZFNT samples of Series A and B are shown in *Fig. 4.7-4.8.* at different electric fields. It is observed that as the applied field is increased the polarization increases and reaches to saturation at a substantial applied field. A high electric field (~20-25 kV/cm) was required to obtain saturation polarization (P_s). The samples show well-defined ferroelectric behaviour. The saturation and remnant polarizations (P_r and P_s) were found to increase with increase in electric field. A relatively higher value of remanant polarization is measured at low value of x ($0 \leq x \leq 0.01$) and with increase in rare earth ions (Sm, La) substitution ($0.02 \leq x \leq 0.08$) the remnant polarization decreases considerably. P_r was found to increase from ~13 $\mu C/cm^2$ to 35 $\mu C/cm^2$ and ~13 $\mu C/cm^2$ to 37 $\mu C/cm^2$ as x increases from 0 to 0.01 in Sm and La substituted PZFNT series. However, at higher value of $x \geq 0.02$, the P_r decreases from ~33 $\mu C/cm^2$ to ~9 $\mu C/cm^2$ and ~36 $\mu C/cm^2$ to ~0.4 $\mu C/cm^2$ with increase in Sm and La substitution. The Sm and La addition results in increase in tetragonality. Domain switching becomes easier because

La^{3+} and Sm^{3+} ions substitute Pb^{2+} ions at A-site and the presence of multiple ions (Pb^{2+}, Sm^{3+} and La^{3+}) resulted in higher multi-domain polarization as is evident by increase in P_r and P_s. These results are consistent with the literature [82-88]. Hence P_r/P_s was found to increase with increase in amount of Sm and La doping which indicates that squareness of the P-E loop increases. The measured ferroelectric properties of these bulk compositions seem to be very attractive for potential application in memory devices (NVRAM) in the form of thin films. The coercive field (E_c) increases with increase in Sm up to 8 mol% and La up to 4 mol%. Such behaviour can be correlated with the average grain size variation, which exhibits the decrease in grain size for 8 mol% Sm and La. It is reported in literature that when grain size decreases then E_c increases. This is due to the fact that each grain is mechanically clamped by its surroundings. There are mechanical stresses which accompany the 90^o domain rotations. Both factors have a combined effect which tends to impede the polarization reversal process [89]. Coercive field (E_c), remanent polarization (P_r), saturation polarization (P_s) and P_r/P_s (remanance ratio) determined from the hysteresis loops are listed in *Table 4.5-4.6*. The loop becomes slimmer for 6 mol% exhibiting relaxor behaviour and only a straight line is observed for 8 mol% La substitution in PZFNT. The material is in a paraelectric state at room temperature and therefore it was not possible to obtain a clear P-E hysteresis loop.

Fig. 4.9. depicts the hysteresis loops of Mn-substituted modified PZT (series C) samples. The larger the electric field applied, the more saturated the hysteresis loop appeared. The area of loop increases with increase in electric field. This is due to the fact that with increase in electric field, the motion of domains becomes easier and as a result P_r and E_c both increase. It can also be observed that polarization decreases from ~13 $\mu C/cm^2$ to ~9 $\mu C/cm^2$ while coercive field increases from ~7 kV/cm to ~9 kV/cm with the increase of Mn content from 0 to 2 mol%. The variation of P_r, P_s, E_c and P_r/P_s is tabulated in *Table 4.7*. This reduction in polarization is probably due to the fact that Mn ions, acting as 'hard' dopant in the PZT lattice, create oxygen vacancies, which eventually pin the domains, and thereby polarization is reduced. Mn doping in PZT introduces oxygen vacancies which act as grain growth inhibitors and limit further grain growth in PZT. The oxygen vacancy concentration increases when content of Mn increases in PZT which inhibit the movement of the ferroelectric domain walls, thereby leading to a decrease in the polarization. The results are

consistent with the literature [90-93]. The asymmetric P-E hysteresis loops for x≥0.015 indicate that there is an internal electric bias field in the polycrystalline grains caused by the space charge produced by the multivalence Mn ions in the lattice [68].

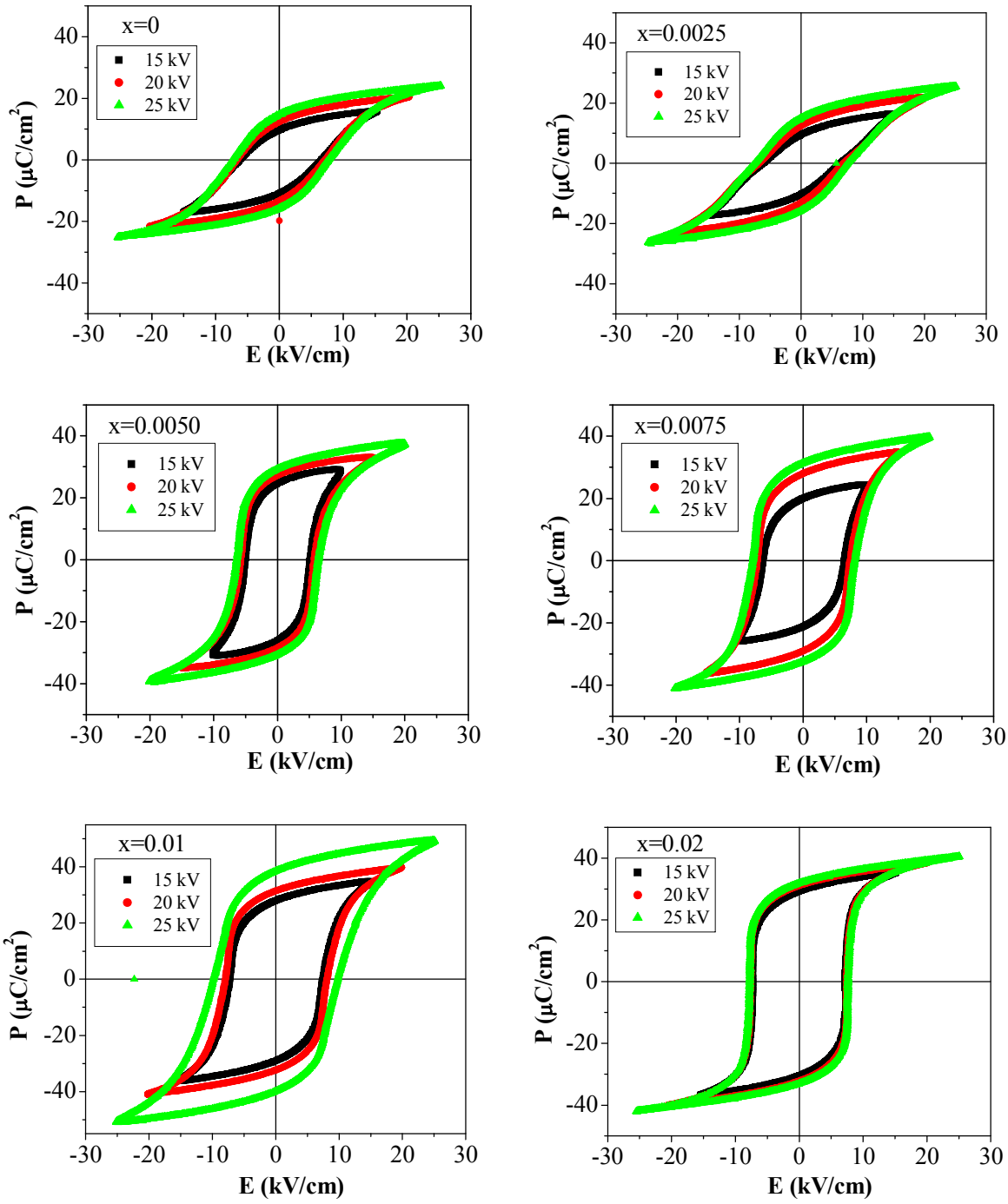

Fig.4.7. Hysteresis curves of Series A compositions at different maximum electric fields (continued).

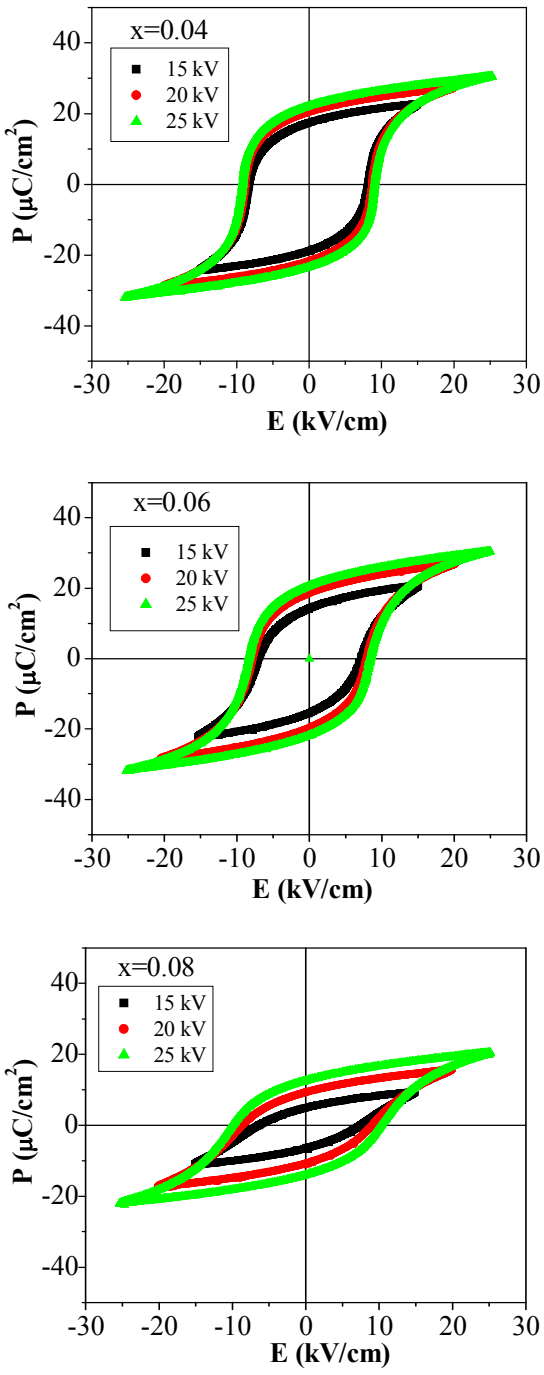

Fig.4.7. Hysteresis curves of Series A compositions at different maximum electric fields.

Table 4.5.
Variation of ferroelectric parameters of Series A samples.

Sm (x)	**0**	**0.0025**	**0.0050**	**0.0075**	**0.01**	**0.02**	**0.04**	**0.06**	**0.08**
E_c (kV/cm)	6.9	6.8	5.9	7.3	7.8	7.7	8.6	8.7	10.0
P_r ($\mu C/cm^2$)	13	14	27	29	35	33	21	18	9
P_s ($\mu C/cm^2$)	21	22	34	36	40	39	28	28	17
P_r/P_s	0.619	0.509	0.794	0.806	0.875	0.846	0.750	0.643	0.529

Table 4.6.
Variation of ferroelectric parameters of Series B ceramics.

La (x)	**0**	**0.0025**	**0.0050**	**0.0075**	**0.01**	**0.02**	**0.04**	**0.06**	**0.08**
E_c (kV/cm)	6.9	6.3	6.8	5.6	6.8	7.5	8.8	1.9	0.6
P_r ($\mu C/cm^2$)	13	19	23	26	37	36	31	6	0.4
P_s ($\mu C/cm^2$)	21	27	29	35	47	48	37	38	14
P_r/P_s	0.619	0.703	0.793	0.743	0.787	0.750	0.830	0.158	0.028

Table 4.7.
Variation of ferroelectric parameters of Series C ceramics.

Mn (x)	**0**	**0.005**	**0.010**	**0.015**	**0.02**
E_c (kV/cm)	6.9	6.8	7.5	7.6	8.7
P_r ($\mu C/cm^2$)	13	10.1	9.4	9.2	8.7
P_s ($\mu C/cm^2$)	21	20	19	19.5	17.1
P_r/P_s	0.619	0.505	0.495	0.472	0.508

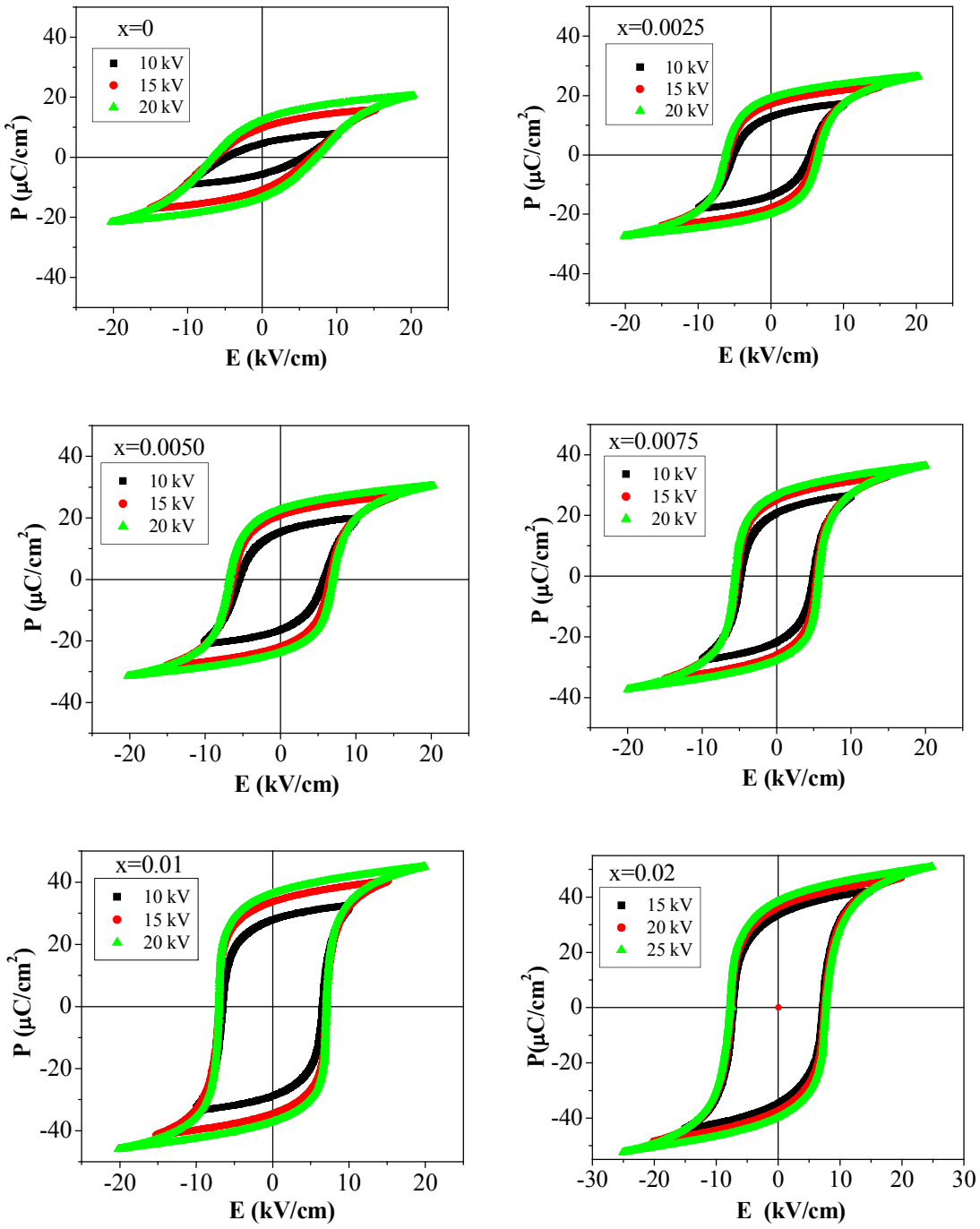

Fig. 4.8. Hysteresis curves of Series B samples at different maximum electric fields (continued).

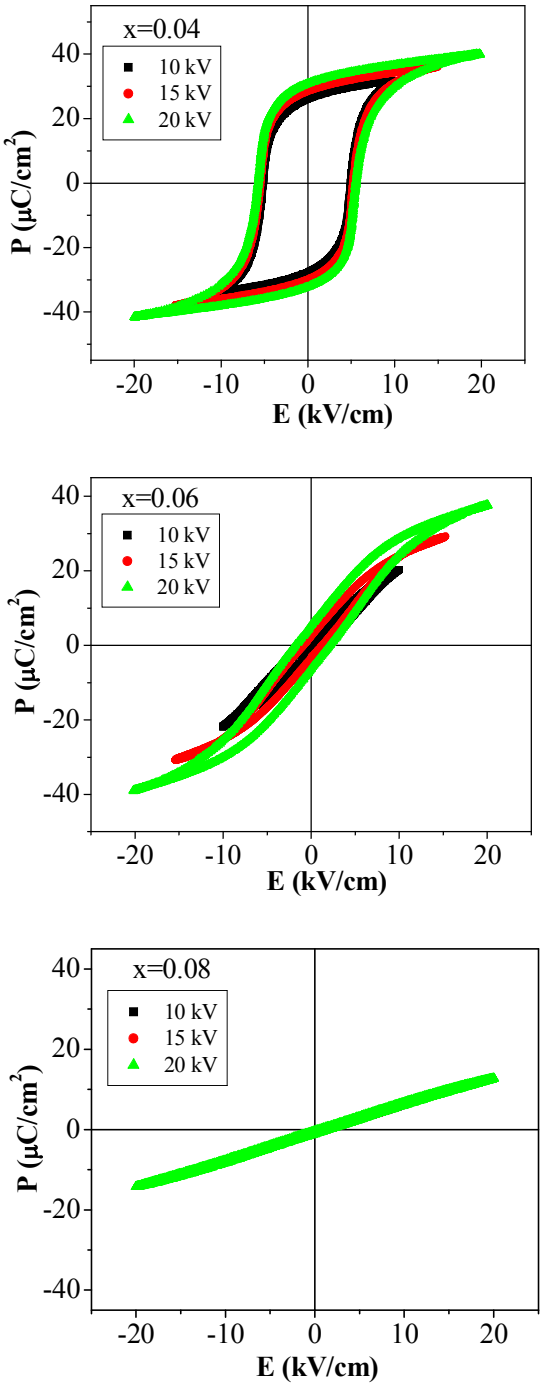

Fig. 4.8. Hysteresis curves of Series B samples at different maximum electric fields.

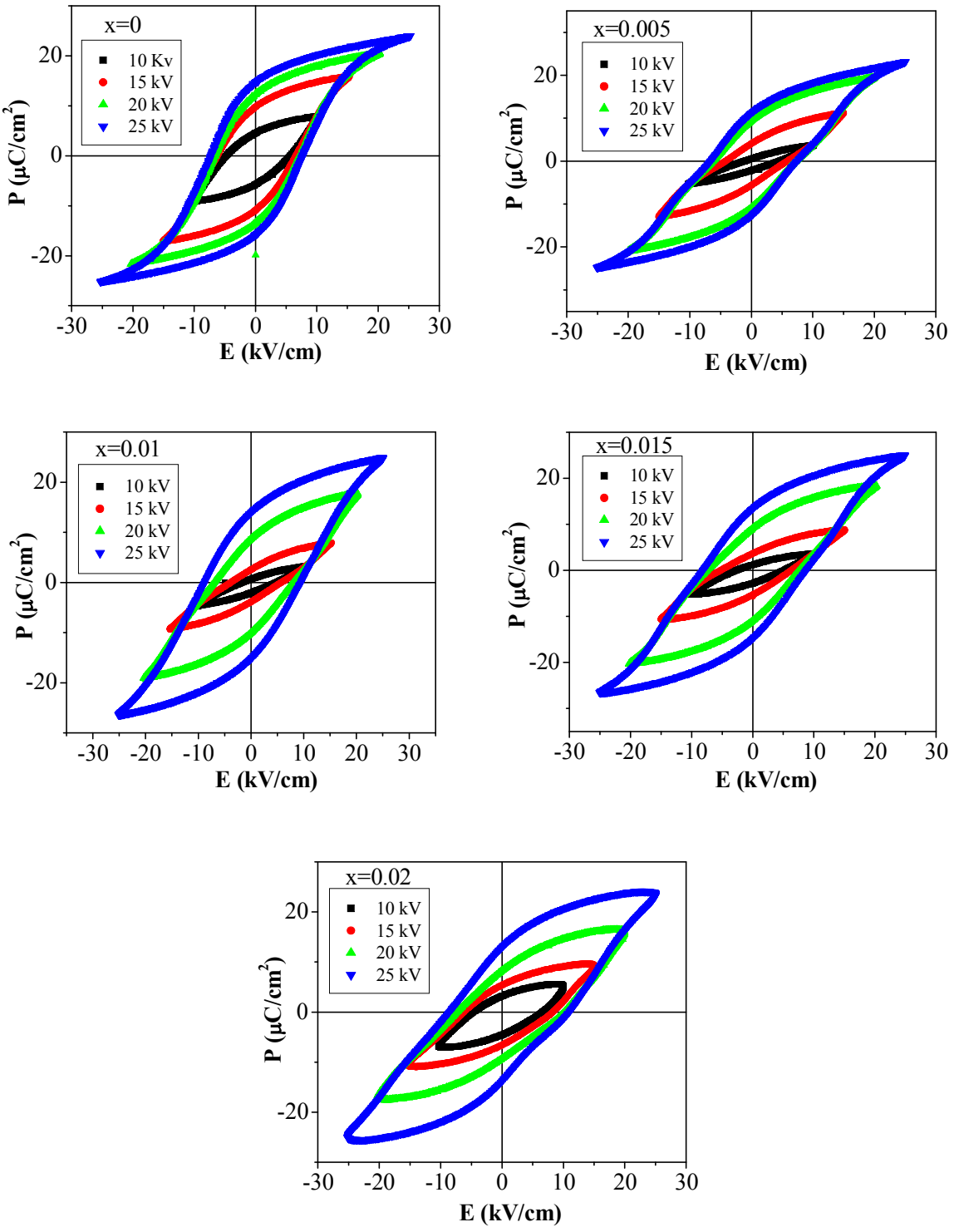

Fig. 4.9. Hysteresis loops of Series C compositions at different maximum electric fields.

4.3.2. Hysteresis Behaviour versus Temperature

Figs. 4.10, 4.12 and *4.14*. show the hysteresis behavior of substituted modified PZT compositions with temperature (30-100^{o}C) at 20 Hz. In substituted PZFNT samples of series A and B for x=0, remnant polarization (P_r) increases with increase in temperature but for Sm and La content $0.0025 \leq x \leq 0.08$, it decreases. As the temperature of ceramic is raised the spontaneous polarization and remanent polarization which are expected to remain either static or fall at a slow rate actually exhibits gradual enhancement. This increase in P_r and P_s can be visualized and explained by recognizing the fact that in addition to a decrease in atomic displacements resulting in decrease in P_r or P_s, a reverse influence due to increase in thermal energy of the domains is also in competition. As temperature increases, the domains pointing in a direction different to applied electric field obtain an additional energetic surge to orient themselves and switch along the direction of macroscopic polarization resulting in rise in remanent and spontaneous polarization of undoped PZFNT composition. As content of Sm and La increases in PZFNT, P_r or P_s decreases because of smaller dipole alignment due to decrease in internal energy caused by thermal excitation [94]. This decrease in area of hysteresis loop with rise in temperature is a characteristic feature of ferroelectric materials.

Hysteresis loops of series C samples are affected by increase in temperature. For all Mn-substituted PZFMNT compositions, loop area increases with rise in temperature. The hysteresis loops are somewhat constricted at room temperature. This is due to insufficient energy for removal of all factors contributing to the hysteresis loop pinching and slow kinetics of defects at low temperature and ferroelectric fatigue. This increase in P_r and P_s can be visualized and explained by recognizing the fact that in addition to a decrease in atomic displacements resulting in decrease in P_r or P_s, a reverse influence due to increase in thermal energy of the domains is also effective. As temperature increases, the domains pointing in a direction different from applied electric field obtain an additional energetic surge to orient themselves and switch along the direction of macroscopic polarization resulting in rise in remanent and spontaneous polarization of undoped and Mn doped PZFNT composition. Increase in temperature favours greater domain alignment and switching, and hence increases net polarization. The temperature dependence of E_c and P_r of substituted PZTFN materials at 20 Hz is exhibited in *Figs. 4.11, 4.13* and *4.15.*

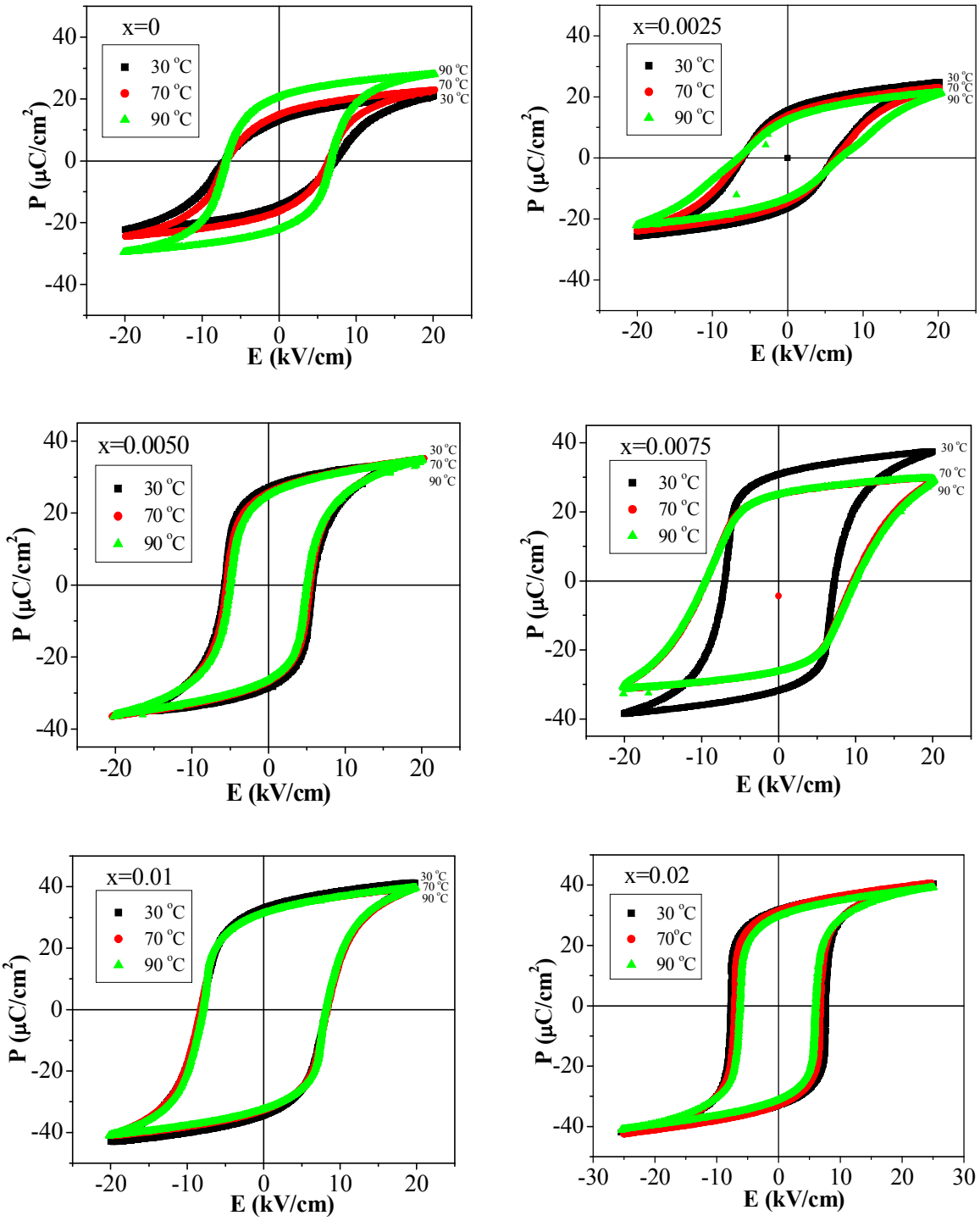

Fig. 4.10. Hysteresis loops of Series A ceramics for varying concentrations of Sm as a function of temperature (continued).

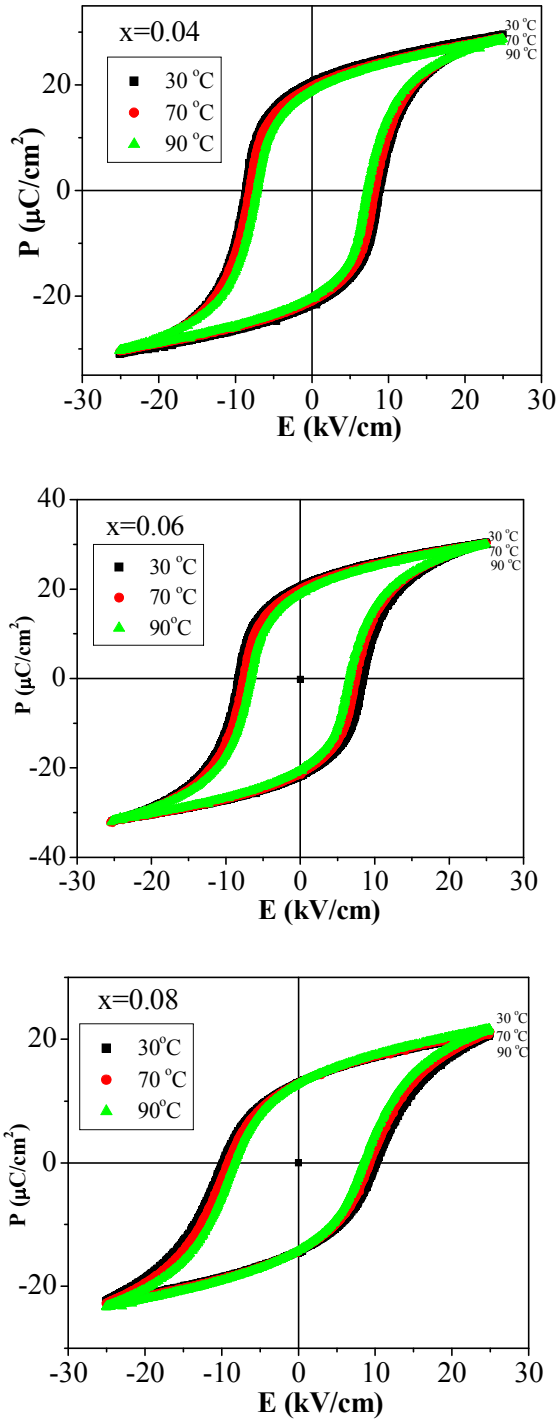

Fig. 4.10. Hysteresis loops of Series A ceramics for varying concentrations of Sm as a function of temperature.

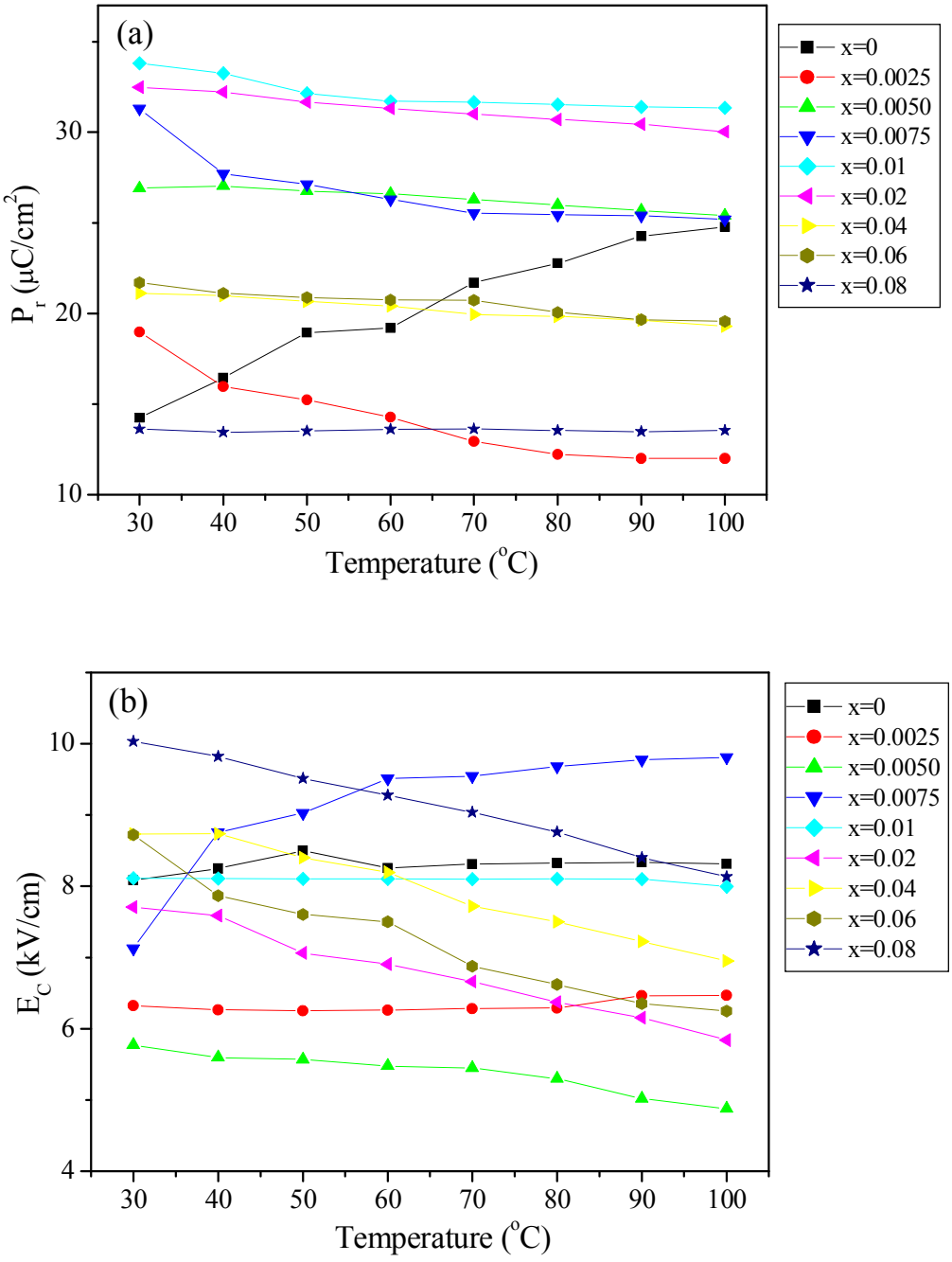

Fig. 4.11. Temperature dependence of (a) P_r (b) E_c of Series A samples.

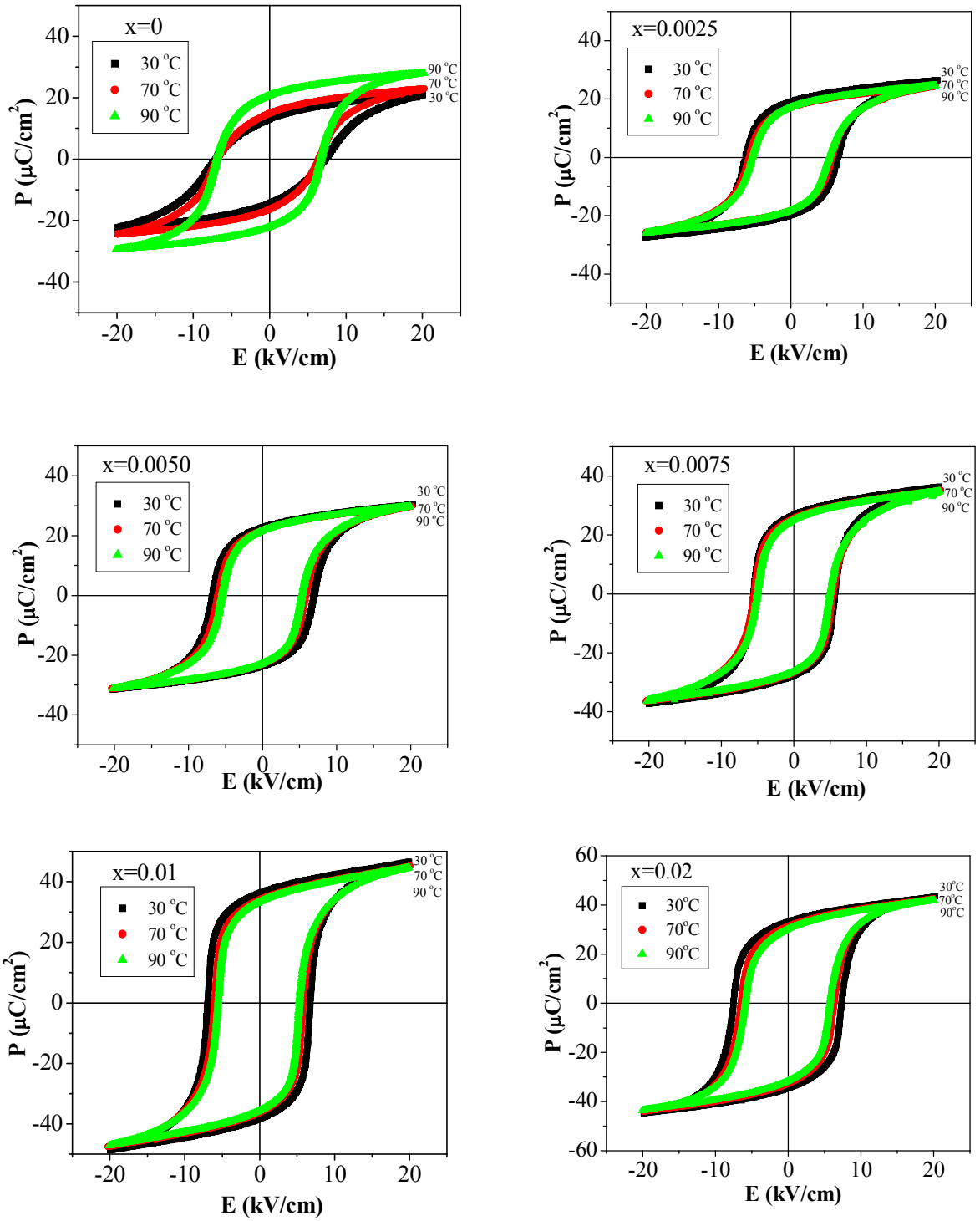

Fig. 4.12. Hysteresis loops of Series B ceramics for varying concentrations of La as a function of temperature (continued).

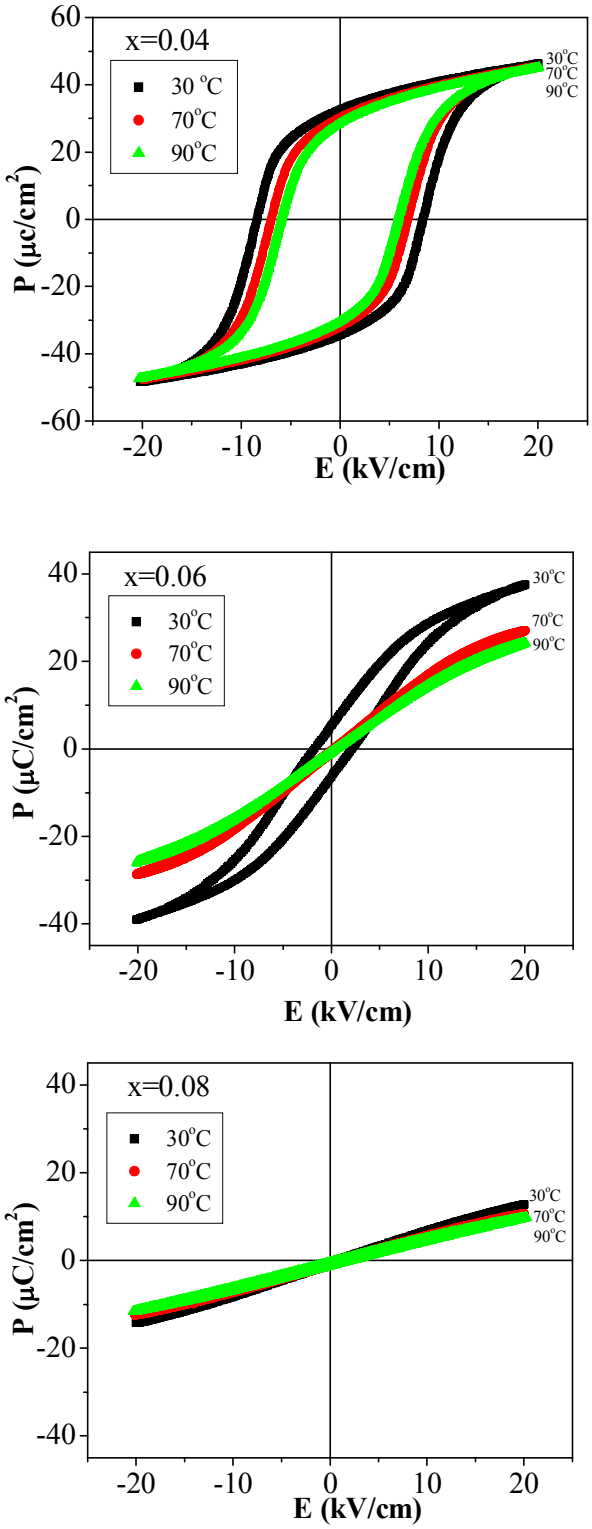

Fig. 4.12. Hysteresis loops of Series B ceramics for varying concentrations of La as a function of temperature.

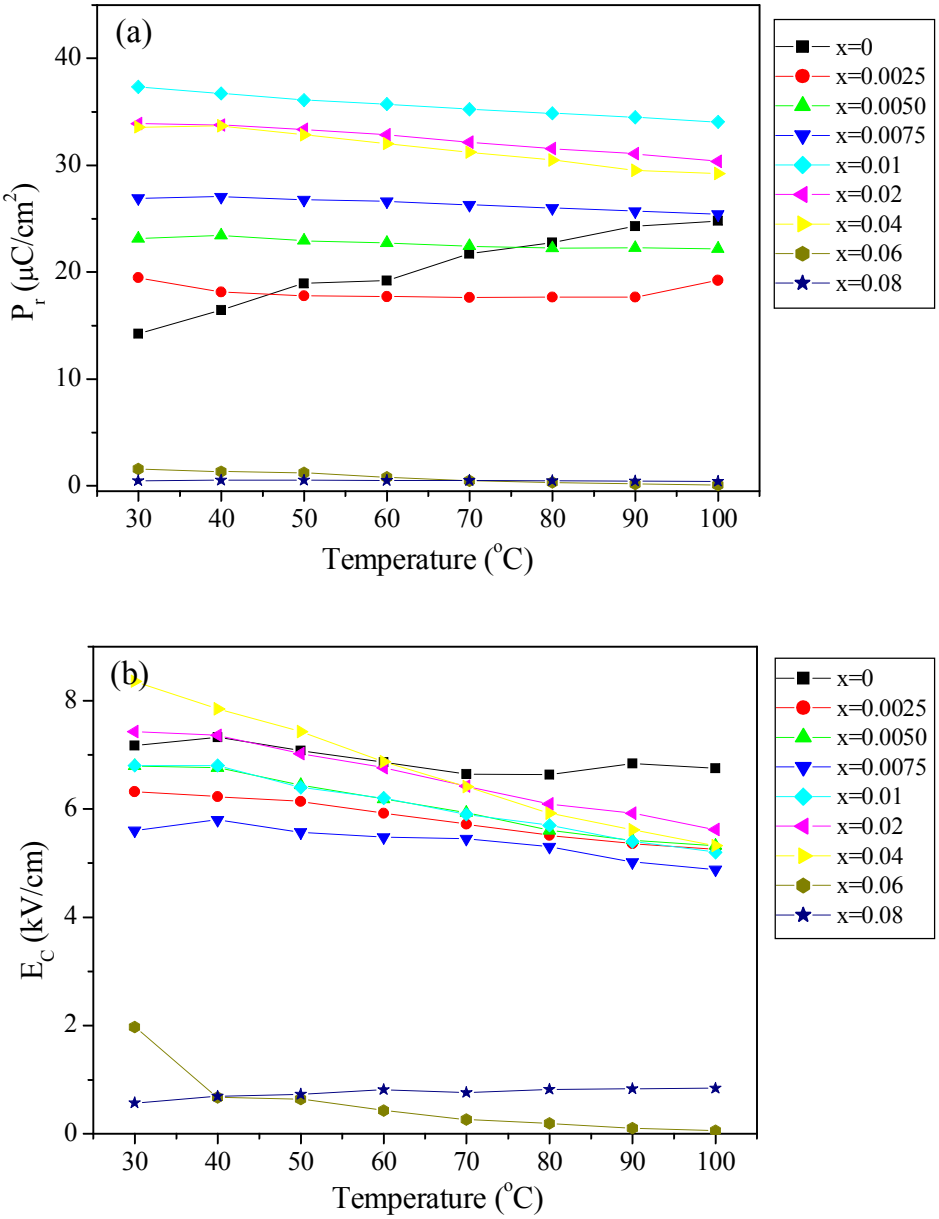

Fig. 4.13. Temperature dependence of (a) P_r and (b) E_c of Series B samples.

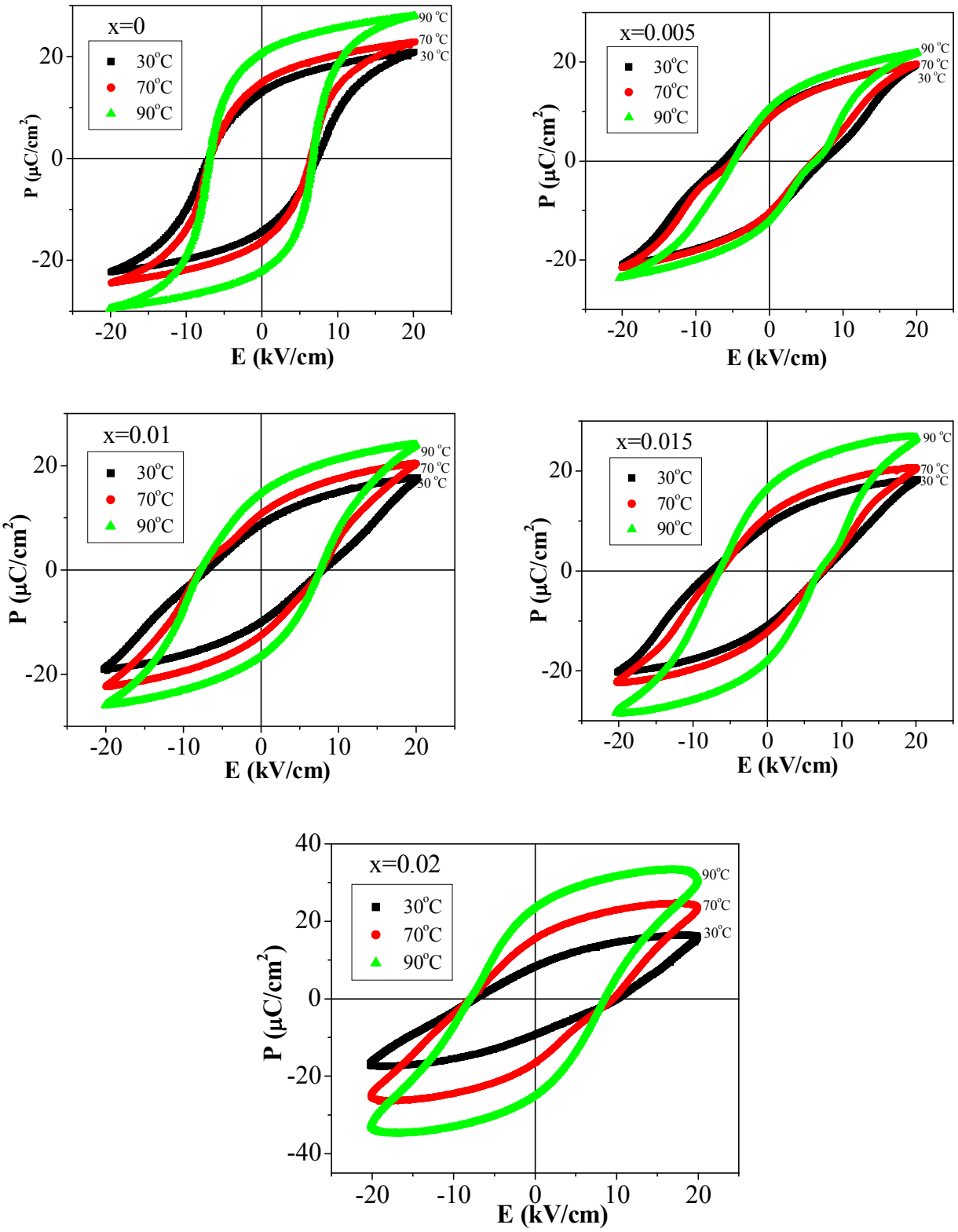

Fig. 4.14. Temperature dependence of hysteresis behavior of Series C samples.

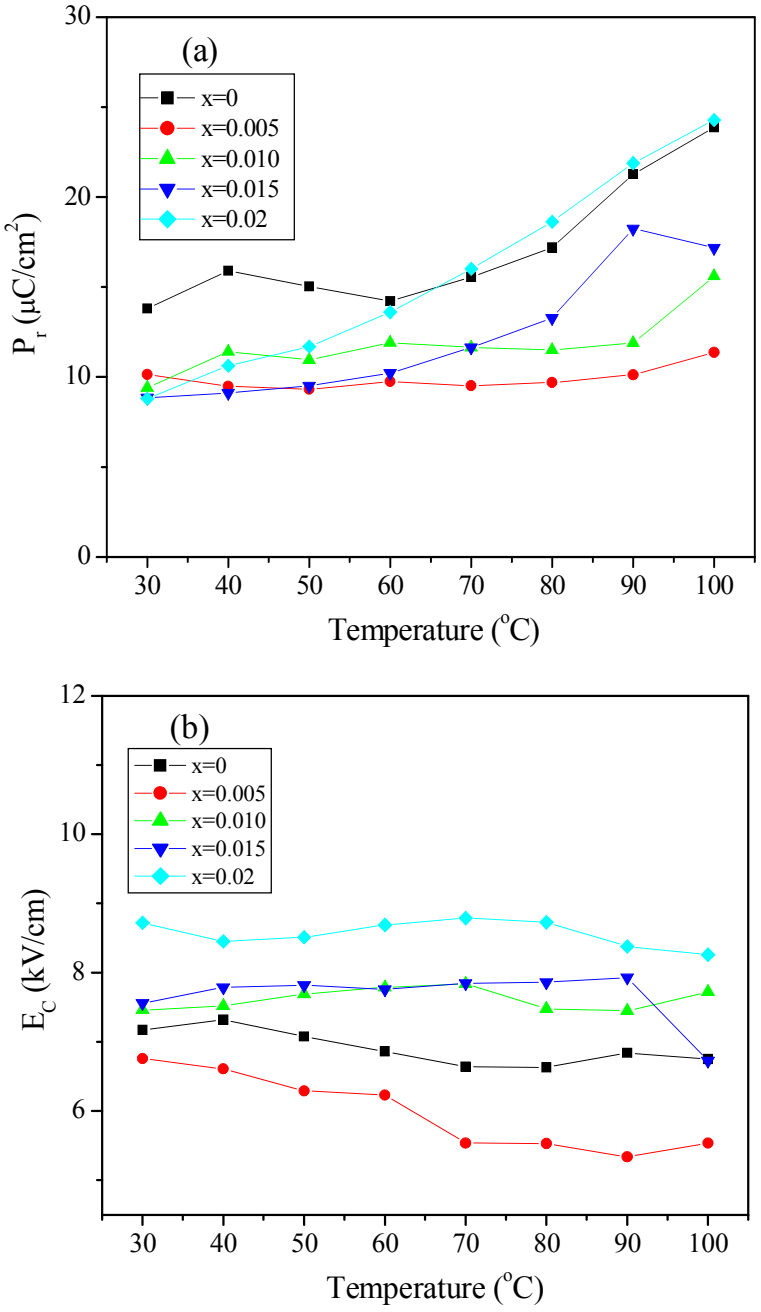

Fig. 4.15. Temperature dependence of (a) P_r and (b) E_c for Series C samples.

4.4. Piezoelectric Properties of Substituted Modified PZFNT

The piezoelectric charge coefficient (d_{33}) depends on composition and sintering temperature also plays a role [95]. Apart from the intrinsic parameters, extrinsic parameters including domain wall motion, electronic and ionic objects and grain size also play a part in determining the piezo-coefficients [96]. Other parameters like electrostrictive constants, dielectric permittivities, spontaneous polarization etc. are directly related to the d_{33} and d_{31} coefficients [97]. The piezoelectric charge coefficient (d_{33}) and electromechanical coupling coefficients (k_p) for Series A, B, C are shown in *Table 4.8.* The typical plot of admittance vs. frequency for calculation of planar electromechanical coupling factor is shown in *Fig. 4.16.* The gradual increase has been observed in d_{33} for lower Sm and La content but sharp increase is observed with increasing Sm and La amount in PZFNT lattice and d_{33} attains a maximum value of ~211 pC/N and ~285 pC/N for 4 mol% Sm and La substitution respectively, thereafter d_{33} value exhibits a diminishing trend. A similar trend is observed for k_p as well. The highest value of k_p ~0.48 and ~0.49 for the 1 mol% PSZFNT and PLZFNT sample is only due to better densification and high polarization of ~37μC/cm^2. This suggests that domain wall contribution is the maximum for 1 mol% Sm and La substituted sample. In general, piezoelectric properties of ceramics increase approximately linearly with increasing grain size. K.Okazaki et al. investigated dependence of piezoelectric properties on average grain size [98]. The grain size is increasing with increase in Sm^{3+}, La^{3+} ions in PZFNT lattice up to 0.5 mol% and decreasing afterwards. In PZFMNT compositions, maximum value of d_{33} ~122 pC/N for pure PZFNT (x=0) while it decreases to ~63 pC/N in 2 mol% Mn substituted sample. This suggests that domain wall contribution is the maximum for undoped sample whereas when concentration of MnO_2 increases domain wall contribution decreases [99]. The grain size is decreasing with increase in Mn ions in PZFNT lattice. With decreasing grain size, the domain rotation contribution to the d_{33} decreases resulting in continuous fall in d_{33}. The value k_p is observed to be maximum for 1 mol% Mn substituted sample and it decreases with further addition of Mn.

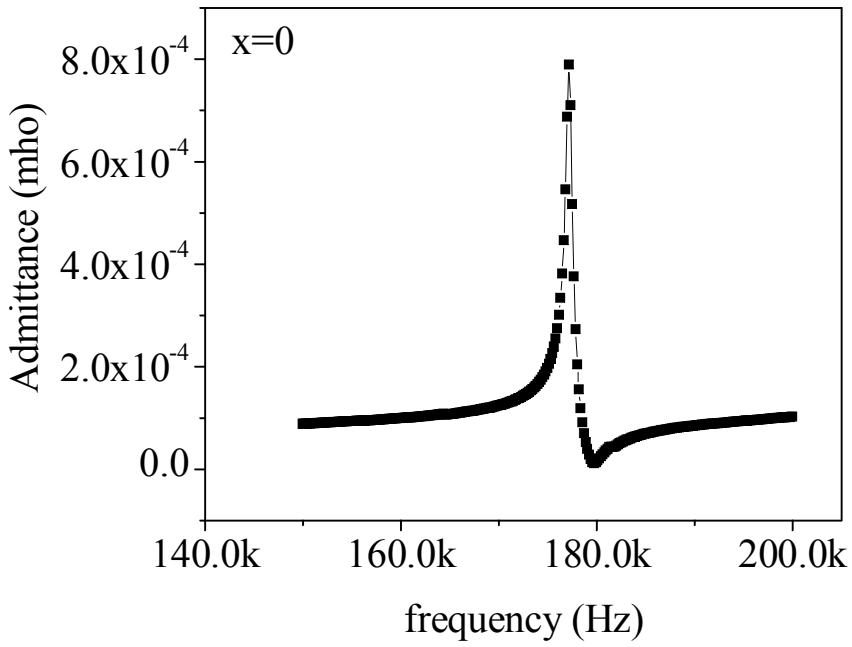

Fig. 4.16. Typical admittance spectra for the calculation of k_p for PZFNT sample (x=0).

Table 4.8.

Variation of piezo-coefficients in substituted modified PZT ceramics.

Series A			Series B			Series C		
x	**d_{33}**	**k_p**	**x**	**d_{33}**	**k_p**	**x**	**d_{33}**	**k_p**
0	143	0.18	0	143	0.18	0	143	0.18
0.0025	148	0.44	0.0025	154	0.40	0.005	111	0.20
0.0050	156	0.46	0.0050	136	0.42	0.010	96	0.27
0.0075	173	0.44	0.0075	162	0.46	0.015	71	0.16
0.01	174	0.48	0.01	168	0.49	0.02	63	0.17
0.02	207	0.24	0.02	253	0.28	-	-	-
0.04	211	0.23	0.04	285	0.27	-	-	-
0.06	154	0.24	0.06	54	-	-	-	-
0.08	161	0.22	0.08	8	-	-	-	-

References

[1]. T. Ikeda and T. Okano, Jpn. J. Appl. Phys. **3** (1964) 263.

[2]. B. Jaffe, W. R. Cook and H. Jaffe, *Piezoelectric Ceramics*, Academic Press; New York (1971)

[3]. P. R. Choudhary and S. B. Deshpandey, Ind. J. Pure and Appl. Phys **22** (1984) 708.

[4]. S. L. Fu, S.Y. Cheng and C. C. Wei, Ferroelectrics **67** (1986) 93.

[5]. R. Lal, S. C. Sharma and R. Dayal, Ferroelectrics **100** (1989) 43.

[6]. K. V. R. Murty, S. N. Murty, K. Umakantham, A. Bhanumati and K. Lingamurty, Ferroelectrics **19** (1991) 119.

[7]. T. B. Weston, A. H. Webster and V. M. McNamara, J. Am. Ceram. Soc. **52** (1969) 253.

[8]. R. Koduri and K. Chandramouli, Ceramics – Silikáty **53** (2009) 189.

[9]. K. H. Hardtl and D. Hennings, J. Am. Ceram. Soc. **55** (1972) 230.

[10]. S. Miga and K. Wojcik, Ferroelectrics **100** (1989) 167.

[11]. K. Fukai, K. Hidaka, M. Aoki and K. Abe, Ceram. Int. **16** (1990) 285.

[12]. D. Hennings, A. Schnell and G. Simon, J. Am. Ceram. Soc. **65** (1982) 539.

[13]. K.Y. Oh, K. Uchino and L. E. Cross, J. Am. Ceram. Soc. **77** (1994) 2809.

[14]. K. Oshima and K. Tsuzuki, Jpn. J. Appl. Phys. **33** (1994) 5389.

[15]. G. H. Haertling, Ferroelectrics **75** (1987) 25.

[16]. K. H. Hardtl and D. Hennings, J. Am. Ceram. Soc. **55** (1972) 230.

[17]. R. Lal, S. C. Sharma and R. Dayal, Ferroelectrics **100** (1989) 43.

[18]. I. A. Santos, C. Endo, A. L. Zanin, M. H. Lente, J. A. Eiras and D. Garcia, Mater. Res. **4** (2001) 291.

[19]. A. Garg and D. C. Agrawal, Mater. Sci. Eng. B **86** (2001) 134.

[20]. G. H. Haertling, J. Am. Ceram. Soc. **82** (1999) 797.

[21]. L. M. Brown and K. S. Mazadiyasni, J. Am. Ceram. Soc. **55** (11) (1999) 541.

[22]. Y. Yoshikawa and K. Tsuzuki, J. Am. Ceram. Soc. **75** (1992) 9.

[23]. M. A. Akbas and W. E. Lee, J. Euro. Ceram. Soc. **15** (1995) 57.

[24]. G. H. Heartling and C. E. Land, Ferroelectrics **3** (1972) 269.

[25]. Q. Y. Jiang, E. C. Subbarao and L. E. Cross, J. Appl. Phys. **75** (1994) 7433.

[26]. R. Rai, S. Sharma and R. N. P. Choudhary, Mater. Lett. **59** (2005) 3921.

[27]. B. S. Chiou, J. N. Kuo and H. T. Dai, J. Elec. Mater. **19** (1990) 393.

[28]. X. Dai, Z. Xu, J. F. Li and D. Viehland, J. Mater. Res. **11** (1996) 618.

[29]. A. Krumins, T. Shiosaki and S. Koizumi, Jpn. J. Appl. Phys. **33** (1994) 4940

[30]. K. L. Yadav, R. N. P. Choudhary and T. K. Chaki, J. Mater. Sci. **27** (1992) 524.

[31]. C. G. F. Stenger and A. J. Burggraaff, J. Phys. Chem. Solids **41** (1980) 25.

[32]. S. R. Shannigrahi, F. E. H. Tay, K. Yao and R. N. P. Choudhary, J. Euro. Ceram. Soc. **24** (2004) 163.

[33]. P. Goel, K. L. Yadav, J. Mater. Sci. **42** (2007) 3928.

[34]. X. Dai, A. Digiovanni and D. Viehland, J. Appl. Phys. **74** (1993) 3399.

[35]. A. Krumins, T. Shiosaki and S. Koizumi, Jpn. J. Appl. Phys. **33** (1994) 4940.

[36]. J. F. Li, X. Dai, A. Chow and D. Viehland, J. Mater. Res. **10** (1995) 926.

[37]. M. E. Marssi, R. Farhi and D. Viehland, J. Appl. Phys. **81** (1997) 355.

[38]. Q. Tan and D. Viehland, J. Appl. Phys. **81** (1997) 361.

[39]. P. H. Xiang, N. Zhong, X. L. Dong, R. H. Liang, H. Yang, C. D. Feng, Mater. Lett. **58** (2004) 2675**.**

[40]. N. W. Thomas, J. Phys. Chem. Solids **51** (1983) 1419.

[41]. C. Galassi, D. Piazza, F. Craciun and P. Verardi, J. Eur. Ceram. Soc. **24** (2004) 1525.

[42]. S. Dutta, R. N. P. Choudhary and P. K. Sinha, Mater. Lett. **58** (2004) 2735.

[43]. N. X. Zhang, L. T. Long and Z. L. Gui, J. Eur. Ceram. Soc. **21** (2001) 677.

[44]. D. Y. Kim, J. J. Choi and H. E. Kim, Appl. Phys. Lett**. 81** (2002) 706.

[45]. G. H. Haertling and C. E. Land, Ferroelectrics **3** (1972) 269.

[46]. G. S. Snow, J. Am. Ceram. Soc. **56** (1973) 479.

[47]. D. Viehland, X. Dai, J. F. Li and Z. Xu, J. Appl. Phys. **84** (1998) 458.

[48]. Y. Chen and K. Uchino, J. Electroceram. **6** (2001) 13.

[49]. X. Wang, M. Gu, B. Yang, S. N. Zhu and W. W. Cao, Microelectron. Eng. **66** (2003) 855.

[50]. H. Ouhi, M. Nishida and S. H. Akawa, J. Am. Ceram. Soc. **49** (1966) 577.

[51]. G. E. Savenkova, *Prediction, Preparation, and Characterization of New Piezoelectric Materials*, Cand. Sci. (Chem.) Dissertation, Moscow: Karpov Res. Inst. of Physical Chemistry, (1972).

[52]. L. A. Reznichenko, O. N. Razumovskaya and S.V. Gavrilenko, (Proc. Int. Conf. on the Fundamental Aspects of Piezoelectric Instrument Making, Rostov-on-Don) **1** (1999) 98.

[53]. J. P. Bykov, M. D. Glinchuk, V. V. Skorokhod and V. M. Kurland, Ferroelectrics **127** (1992) 89.

[54]. V. V. Klimov, N. I. Selikova, V. V. Dorofeeva and A. N. Bronikov, Inorg. Mater. **40** (2004) 1526.

[55]. Q. Zhang and R. W. Whatmore, Integrated Ferroelectrics **41** (2001) 43.

[56]. Q. Zhang and R. W. Whatmore, J. Appl. Phys. **94** (2003) 5228.

[57]. B. Tiwari and R. N. P. Chaudhary, Solid State Sciences **11** (2009) 219.

[58]. P. R. Chowdhary and S. B. Deshpandey, J. Mater. Sci. **22** (1987) 2209.

[59]. Y. D. Hou, M. K. Zhu, J. L. Tang, X. M. Song, C. S. Tian, H. Yan, Mater. Chem. Phys. **99** (2006) 66.

[60]. V. V. Klimov, N. I. Selikova and A. N. Bronnikov, Inorg. Mater. **42** (2006) 573.

[61]. B. Cherdhirunkorn and D. A. Hall, Integrated Ferroelectrics **62** (2004) 61.

[62]. J. H. Park, B. K. Kim, K. H. Song and S. J. Park, J. Mater. Sci.: Mater. Electron. **6** (1995) 97.

[63]. R. Koduri and M. Lopez, J. Mater. Sci: Mater. Electron. **19** (2008) 669.

[64]. M. Zivkovic, D. Stojanovic, C. R. Foschini, V. Paunovic and D. Mancic, Science of Sintering **35** (2003) 133.

[65]. S. B. Narang and D. Kaur, Ferroelectric Letters **36** (2009) 20.

[66]. S. Singh, O. P. Thakur, C. Prakash and K. K. Raina, Phase Transitions **78** (2005) 655.

[67]. L. I. Maissel and R. Glang, *Handbook of Thin Film Technology*, McGraw-Hill, New York; (1970).

[68]. Y. Xu , *Ferroelectric Materials and Their Application*, North-Holland, Amsterdam, (1991).

[69]. T. Kamiya, T. Suziki, T. Tsurumi and M. Daimon, Jpn. J. Appl. Phys. **31** (1992) 3058.

[70]. L. X. He and C. E. Li, J. Mater. Sci. **35** (2000) 2477.

[71]. R. Tipakontitikul, Y. Suwan and A. Niyompan, Ferroelectrics **381** (2009) 144.

[72]. D. Lin, K. W. Kwok and H. L. W. Chan, Mater. Chem. Phys. **109** (2008) 455.

[73]. C. Prakash, O. P. Thakur, Mater. Lett. **57** (2003) 2310.

[74]. B. N. Rolov and F. T. Tela **6** (1964) 2128 (in Russian). For translation see Sov. Phys. Solid State **69** (1976).

[75]. J. Mal and R. N. P. Choudhary, Phase Transitions **62** (1997) 19.

[76]. L. E. Cross, Ferroelectrics **76** (1987) 241.

[77]. L. E. Cross, Ferroelectrics **151** (1994) 305.

[78]. A. R. West, *Solid State Chemistry and its Applications,* Wiley; New York (2003).

[79]. J. T. Evans and R. Womack, IEEE J. Solid State Circuits **23** (1988) 1171.

[80]. A. Kingon, Nature **401** (1999) 658.

[81]. J. F. Scott, *Ferroelectric Memories*, Springer, New York, (2000).

[82]. S. R. Shannigrahi, R. N. P. Choudhary, H. N. Acharaya,J. Mater. Sci 35 (2000) 1737.

[83]. H. Ouchi, J. Am. Ceram. Soc. **51** (1968) 169.

[84]. M. D. Durruthy-Rodríguez, L. D. Pérez-Fernández, A. P. Barranco, F. C. Pinar, Appl. Phys. A **95** 423.

[85]. L. E. Cross, Ferroelectrics **76** (1987) 241.

[86]. S. Li, J. A. Eastman, R. E. Newnham and L. E. Cross, Phys. Rev. B. **55** (1997) 12067.

[87]. R. Yimnirun, S. Ananta and P. Loaratanakul, Mater. Sci. Eng. B **112** (2004) 79.

[88]. S. L. Swartz, T. R. Shrout, W. A. Schulze and L. E. Cross, J. Am. Ceram. Soc**. 67** (1984) 311.

[89]. K.Carl, Ferroelectrics **9** (1975) 23.

[90]. Q. Zhang and R.W. Whatmore, Integrated Ferroelectrics **41** (2001) 43.

[91]. K.L. Yadav, P. Sharma, Ind. J. Engg. Mater. Sci. **15** (2008) 61.

[92]. Q. Zhang and R.W. Whatmore, Mater. Sci. Engg. B **109** (2004) 136.

[93]. S. M. Lee, S. H. Lee, C. B. Yoon, H. E. Kim and K. W. Lee, J. Electroceram. **18** (2007) 311.

[94]. S. Singh, O. P. Thakur, C. Prakash, Def. Sci. J. **55** (2005) 349.

[95]. W. Wersing, K. Lubitz and J. Mohaupt, IEEE Trans. on Ultrasonics, Ferroelectrics and Frequency Control **36** (1989) 424.

[96]. D. Damjonvic, T. R. Gururaja and L. E. Cross, Am. Ceram. Soc. Bull. **66** (1987) 699.

[97]. M. J. Haun, E. Furman, S. J. Jang and L. E. Cross, IEEE Trans. On Ultrasonics, Ferroelectrics and Frequency Control **36** (1989) 393.

[98]. K. Okazaki and K. Nagata, J. Electron. Commun. Soc. Jpn. C **53** (1970) 815.

[99]. K. Uchino, *Ferroelectric Devices*, Marcel Dekker; New York, (2000).

CHAPTER V

Conclusions & Recommendations for Future Work

This chapter reviews, the key conclusions drawn from the present work which justify the selection of modified PZT as the base matrix and highlights the most technologically significant results. The marked effect of samarium, lanthanum and manganese substitution on dielectric, ferroelectric and piezoelectric properties of modified PZT is concluded. The chapter also includes some suggestions related to future investigations for basic and applied research point of view.

5.1. Conclusions

This chapter summarizes the accomplishments demonstrated in this thesis and provides recommendations for future work on ferroelectric materials and devices. The ultimate, long term aim of the present work initiated in this thesis is the realization of ferroelectric material showcasing excellent ferroelectric, dielectric and piezoelectric properties. A literature review of the fundamentals of ferroelectric devices was undertaken, as elucidated in Chapter 1 of this thesis and PZT was identified as the potential material for initiating a study on ferroelectric materials. The criterion for selecting PZT, as the base material is its excellent ferroelectric properties, i.e., its high dielectric constant and remnant polarization. Abundance of literature on modified PZT gives insight to its phenomenal properties. The modification of these ceramics was carried out by complex doping by substituting Sm^{3+}, La^{3+} ions at A site and Mn^{4+}, Fe^{3+}, Nb^{5+} ions at B site in PZT. The complex substitution combines the properties of donor doped and/or acceptor doped PZT which exhibit better stability and improved dielectric, ferroelectric and piezoelectric properties than those of the single element doped PZT. This substitution was undertaken in a view to understand the suitability of the substituting elements for the enhancement of various structural, dielectric, ferroelectric and piezoelectric properties of PZFNT ceramics. The samples in bulk form were synthesized by conventional mixed oxide route. In view of results and discussion of the substituted PZFNT compositions the following conclusions can be drawn at:

1. The modified lead zirconate titanate ceramic compositions with 0-8 mol% Sm and La content form single phase perovskite structure except the composition with 2 mol% of Sm. A small amount of pyrochlore phase (4%) is present in PSZFNT. In Mn-substituted PZFNT composition single phase perovskite structure is observed upto Mn content 1 mol% while an extra phase (Mn_2O_3) is depicted in XRD patterns of 1.5 and 2 mol% Mn-substituted PZFNT.

2. X-ray diffraction spectra were indexed and crystal structures have been determined. The Sm and La modified PZT composition is tetragonal upto 8 mol% and 6 mol% respectively. While for Mn substituted PZFNT samples rhombohedral phase is

observed. With Sm, La and Mn substitution, the main peak with highest intensity is shifting towards higher angle side indicating the decrease in lattice parameters. The variation in lattice parameters with substitutional level is explained in terms of different ionic radii of substituent cations.

3. The relative density increases to ~92% and ~94% with 1 mol% Sm and La substitution in PZFNT from ~90% for x=0 and decreases afterwards with donor substitution. The same trend is observed with Mn substitution in modified PZT. The relative density increases to ~92% for 1 mol% of Mn content and decreases afterwards.

4. La, Sm and Mn substitution in PZFNT provides many interesting features of the materials, such as the shift in transition temperature, diffuse phase transition and modification of dielectric properties. Temperature dependence of dielectric constant (ε) measured at different frequencies (100 Hz-100 kHz) reveals that for Sm and Mn substitution, the diffuse type behavior is observed. For lower La substitutions ($0 \leq x \leq 0.04$) it follows normal or first order phase transition while for higher La content (x=0.06), it gets converted into relaxor ferroelectric material. The relaxor behavior is explained in terms of compositional fluctuations/structural order that arise due to disturbance in the composition because of different sized substituted cations at A and B site.

5. Room temperature dielectric constant of ~1170 is obtained for 1 mol% Sm substituted sample. A high value of room temperature dielectric constant (~6000) is observed for 6 mol% La substitution as compared to pure PZFNT where x=0 (~440). This shows appreciable relaxor behavior at around room temperature which can be exploited for multilayer capacitor applications.

6. Dielectric loss was found to be reduced from 0.18 of pure PZFNT to 0.007 on Mn substitution (x=0.005) which render Mn-substituted compositions suitable for power devices (hydrophone systems, piezoelectric motors, piezoelectric transformers etc.)

7. The Sm, La and Mn substituted samples are ferroelectric in nature. 1 mol% Sm and La substituted sample can be exploited for NVRAM memory application if thin films of this composition can be made as their retention behavior is as high as 35 $\mu C/cm^2$ and 37$\mu C/cm^2$ respectively.

8. The results indicated that for bulk modified PZT ceramics (modified with both the soft ions (Sm, La and Nb) and hard ions (Fe, Mn)) the piezoelectric properties are stable with the compositional variations which makes it possible to establish the higher reliability and reproducibility of the piezoelectric performance as soft PZT. The highest value of d_{33} measured for 4 mol% Sm and La substituted sample is 211 pC/N and 285 pC/N respectively which is significantly higher than 143 pC/N, for pure PZFNT composition (x=0) so these compositions can be utilized in sensors and actuators.

9. The value of electromechanical coupling coefficient, k_p, is 0.48 and 0.49, maximum for 1 mol% Sm and La substituted sample in La and Sm modified PZT compositions and hence these compositions are potential candidates for MEMS applications.

5.2. Recommendations for Future Work

The thesis explored several aspects of ferroelectric materials in modified PZT system. This material has potential for NVRAMs, multilayer capacitors, sensors, actuators and power devices. The modified PZT compositions needed to be investigated for other applications as well. Accordingly, it is quite interesting to explore the ways and means to improve the dielectric and ferroelectric properties in our future research work. The studies suggested for these materials for future work are as follows:

1. The modified PZT composition selected for investigation can be studied systematically for their sintering temperature and sintering time behaviour based on their DTA/TGA analysis. The shrinkage characteristics can be studied systematically with different compositions and with different temperature and time schedule.

2. The microwave sintering is an innovating technique in today's time which not only improves the performance of the material and it is considered to be efficient and cost effective. The other mechano-chemical alloying technique is advantageous over the conventional solid-state reaction process as it skips calcination and greatly lowers sintering temperature. Hence effect of microwave sintering and mechano-chemical alloying on various properties of modified PZT compositions can be studied in near future. These techniques may be adopted to investigate improvements in dielectric, ferroelectric and piezoelectric properties due to enhanced densification and better microstructure.

3. In the present study, the fine structural changes observed in modified PZT compositions may further be studied using more sophisticated characterization methods. These include EDAX, XPS and EPMA techniques and correlations can be made between structural, dielectric, ferroelectric and piezoelectric properties.

4. The investigated La and Sm modified compositions have potential for NVRAM applications. The thin films of the selected compositions may be made adopting Sol-gel, RF sputtering, metal organic deposition and pulsed laser deposition techniques as the method of preparation of ferroelectric materials have a major role in determining the properties of the materials.